University of Southampton

University of Southampton Research Repository

Copyright © and Moral Rights for this thesis and, where applicable, any accompanying data are retained by the author and/or other copyright owners. A copy can be downloaded for personal non-commercial research or study, without prior permission or charge. This thesis and the accompanying data cannot be reproduced or quoted extensively from without first obtaining permission in writing from the copyright holder/s. The content of the thesis and accompanying research data (where applicable) must not be changed in any way or sold commercially in any format or medium without the formal permission of the copyright holder/s.

When referring to this thesis and any accompanying data, full bibliographic details must be given, e.g.

Thesis: Author (Year of Submission) "Full thesis title", University of Southampton, name of the University Faculty or School or Department, PhD Thesis, pagination.

Data: Author (Year) Title. URI [dataset]

University of Southampton

Faculty of Environmental and Life Science

Ocean and Earth Science

Optimising ICP-MS performance for the measurement of very low levels of radioisotopes in food and environmental matrices

by

Mariusz Huk

Thesis for the degree of PhD Ocean and Earth Science

December 2023

University of Southampton

Abstract

Faculty of Environmental and Life Science

Ocean and Earth Science

Thesis for the degree of Doctor of Philosophy

Optimising ICP-MS performance for the measurement of very low levels of radioisotopes in food and environmental matrices

by

Mariusz Huk

The development of novel analytical methods for the determination of radioelements in diverse environmental samples using state-of-the-art ICPTQMS system started in the early 2010's with the introduction of the Agilent 8800 ICP-MS/MS system in 2012. A similar instrument, developed by Thermofisher (iCAP TQ ICP-MS) was used here for the first time for measuring a selection of radioelements in diverse marine matrices. This system is uniquely equipped with a 90° cylindrical ion lens named as Right Angular Positive Ion Deflection ('RAPID') ion optics that provides ion transmission across the entire mass range. By way of independent case studies, several instrumental parameters were tested, in particular the plasma condition, lens voltages and gas flow rates as well as the use of an additional desolvation system, manufactured by Teledyne Cetac Technologies - Aridus 3) and connected upstream to the ICAP TQMS system.

First, these parameters were optimised for measuring low levels of ^{90}Sr in milk and seawater samples. A significant reduction in dihydrate formation from the natural content of strontium ($^{88}Sr^{1}H^{1}H$ – peak tail) was observed after successfully removing the main isobaric interferences (i.e., ^{90}Y, ^{90}Zr) using a recent chromatographic Sr-resin manufactured by Triskem International. To achieve an even lower limit of detection, samples were first introduced in the Aridus 3 desolvation system, using tested and optimised He, N_2 gas flow rates. A good agreement was observed between the results obtained from ICPTQMS analysis and liquid scintillation counting. This novel radioanalytical method was found to be suitable for food and environmental samples presenting a ^{90}Sr concentration of at least 50 Bq L^{-1} (equivalent to 0.01 pg g^{-1} approximately) and therefore for monitoring ^{90}Sr more efficiently following an emergency incident or as part of ongoing nuclear decommissioning operations.

Instrumental optimisation tests were also undertaken for measuring ^{129}I in seawater and seaweed materials. The two European nuclear fuel reprocessing facilities, Sellafield and La Hague, are known to be the largest sources of iodine-129 is known to be mainly discharged from in the UK

marine environment. The main challenge associated with its measurement by mass is related to the presence of ^{129}Xe impurities in the argon plasma gas and the tailing effect from stable ^{127}I. To remove this isobaric interference, different O_2 gas flow rates were tested in the collision/reaction cell of the ICPTQMS instrument. Once optimised parameters were retained, this technique was found to be approaching the performance that can be achieved via traditional LSC. A detection limit of 1.53×10^{-5} Bq g^{-1} (equivalent to 2.34 pg g^{-1}) was achieved for ^{129}I, which would be suitable for environmental monitoring purposes.

Finally, the performance of the instrument was also investigated for direct analysis of ^{226}Ra in seawater samples and solid certified reference materials provided by the IAEA (two marine sediments and one NORM waste). The same operating parameters were evaluated. A chromatographic separation, an anion exchange resin and Sr-resin, were also used prior to the ICPTQMS to attempt the removal of potential interferences prior to analysis. Although the sensitivity for measuring ^{226}Ra was improved by using the desolvating system – Aridus 3. The retained chromatographic separative approach could not remove the main polyatomic interference composed of ^{138}Ba and ^{88}Sr, two chemical analogues of elemental radium. Further chemical work would then be required to validate the use of this analytical tool for measuring low levels of ^{226}Ra in diverse marine matrices.

Table of Contents

Table of Tables

Table of Tables

Table of Tables

Table of Figures

Table of Figures

Table of Figures

Table of Figures

Research Thesis: Declaration of Authorship

Print name: Mariusz Huk

Title of thesis: Optimising ICP-MS performance for the measurement of very low levels of radioisotopes in food and environmental matrices

I declare that this thesis and the work presented in it are my own and has been generated by me as the result of my own original research.

I confirm that:

1. This work was done wholly or mainly while in candidature for a research degree at this University;
2. Where any part of this thesis has previously been submitted for a degree or any other qualification at this University or any other institution, this has been clearly stated;
3. Where I have consulted the published work of others, this is always clearly attributed;
4. Where I have quoted from the work of others, the source is always given. With the exception of such quotations, this thesis is entirely my own work;
5. I have acknowledged all main sources of help;
6. Where the thesis is based on work done by myself jointly with others, I have made clear exactly what was done by others and what I have contributed myself;
7. None of this work has been published before submission.

Signature: ..... Date:.....

Acknowledgements

First of all, thank you to Cefas Seedcorn office for funding this project.

I would like to express my appreciation and thanks to my Cefas supervisors Kinson Leonard, Nick Evans, Gordon Copp (R.I.P.) and Franck dal Mollin. Also, I would like to thank my academic supervisors: Phillip Warwick, Andrew Cundy and Ian Croudace.

Finally, very special thanks to my wife, Anna, who always encouraged and supported me through my life.

This work I dedicated for her and our three sons: Mikolaj, Antoni and Adam.

Definitions and Abbreviations

ICP-MS – Inductively Coupled Plasma Mass Spectrometry

MS/MS – Tandem Mass Spectrometry

QQQ – Triple Quadrupole

ICP – Inductively Coupled Plasma

RF – Radio Frequency

MHz – Megahertz Frequency

CRC – Collision/Reaction Cell

TQ ICP-MS – Triple Quadrupole Inductively Coupled Plasma Mass Spectrometry

W – Watt Unit

Bq – Becquerel

m/z – Mass to-charge ratio

amu – Atomic Mass Unit

LOD – Limit of Detection

LSC – Liquid Scintillation Counting

CRM – Certified Reference Material

ppq – parts per quadrillion

ppt – parts per trillion

ppb – part per billion

ppm – parts per million

IAEA – International Atomic Energy Agency

Chapter 1 Introduction

Radioactivity in the environment presents a risk to humans and the environment that requires attention and accurate evaluation. When assessing a radiological risk and dose received from exposure situations, it is essential to be able to determine accurately the concentration of the most radiologically significant elements in diverse matrices of interest, in particular food matrices routinely consumed when dealing with general public exposure investigations. In addition, the use of some of these radioelements can also be a powerful tool for studying environmental processes or mechanisms. For example, in environmental tracing applications, the radiochemical analyses combined with precise detection and data interpretation can determine a sample's origin, aga and transformation history. This information not only clarifies the pathways and rates of radionuclide transport in natural system, such as soil, groundwater, and the atmosphere, but also helps assess their potential uptake, accumulation, and effects within the human body.

Over the last decades, several methodologies using radiation counting instruments have been developed and utilised to characterise a wide range of matrices. Many of these traditional radiometric methodologies suffer from lengthy counting times, especially when dealing with matrices that contain very low or low level of radioactivity. This procedural limitation can indirectly affect the commercial viability of important routine radiological and environmental monitoring programmes in the long term.

In the last thirty years[1-4], the inductively coupled plasma mass spectrometry (ICP-MS) has emerged as a highly promising analytical technique for the detection and quantification of radioelements. One of the key advantages of ICP-MS lies in its ability to significantly reduce counting times compared to traditional radiometric methods, making it an efficient tool for routine and high-throughput analysis. Initially, ICP-MS was primary applied to long-lived heavy radionuclides, which typically exhibit low specific activities and are challenging to quantify accurately using conventional techniques. However, recent advantages in ICP-MS instrumentation – such as improvements in sensitivity, signal stability, and interference reduction – combined with the development of novel engineering materials, have greatly expanded its analytical capabilities. These innovations now allow for the measurement of a broader spectrum of radionuclides, including those present at trace levels, with much greater precision and sensitivity than previously possible.

As a result, ICP-MS now offers significant potential for the development of more efficient and innovative radioanalytical methodologies capable of detecting very low levels of radioactivity.

These advanced methods enable rapid and accurate radiological risk assessment which are essential for ensuring public safety and informing evidence-based regulatory decisions. Moreover, the versality of ICP-MS based approaches allows their application across a wide spectrum of environmental studies, including the monitoring of radionuclide transport and distribution within soil, water, and atmospheric systems.

Beyond environmental monitoring, these advancements in ICP-MS methodologies also play crucial role in supporting nuclear and industrial decommissioning activities. They facilitate the precise characterisation and clearance of contamination materials, thereby contributing to safer and more cost-effective decontamination and waste management processes. Furthermore, ICP-MS serves a s a powerful analytical tool in nuclear emergency response scenarios, where rapid, sensitive, and accurate measurements are vital for effective intervention and mitigation strategies.

In addition, the high specificity and sensitivity of ICP-MS for tracing radioelements provide valuable insights into environmental tracing studies. These capabilities enhance the understanding of fundamental processes such as pollutant migration, sedimentation, and the biogeochemical cycling radionuclides[5-7].

The integration of modern ICP-MS technology with emerging analytical and preparatory techniques is revolutionizing the field of radiochemistry. This synergy enables scientist to achieve unprecedented levels of sensitivity, precision, and isotopic resolution in the detection and quantification of radioactive and trace elements. As a result, research can now explore complex nuclear processes with greater accuracy, enhance environmental monitoring of radionuclide, and improve safety protocols within the nuclear industry. Collectively, these advancements are reshaping the landscape of radiochemical analysis, paving the way for innovative applications in research, environmental protection, and nuclear safety applications.

1.1 Inductively Coupled Plasma Mass Spectrometry - ICP-MS

Over the past three decades, ICP-MS equipped with collision/reaction cell has become the preferred technique for the rapid and accurate determination of many radioisotopes in several matrices because of low sample consumption, high sensitivity, excellent precision, and potential for multi-elemental analysis[2, 8, 9]. In 2012, Triple Quadrupole ICP-MS (ICPQQQ) technology was first introduced in the market. This novel system is also equipped with a collision/reaction cell, but two additional quadrupole mass filters are also present before and after the collision cell (Figure 1). This new configuration with quadrupole in front and back of collision/reaction cell (instrument operating in MS/MS mode) has significantly expanded the scope of application and

improved the performance. This front quadrupole can be used to accurately controls the analytes that enter the cell before reactions occur, resulted into precise control of the reaction chemistry in collision/reaction cell. The use of MS/MS mode with ICP-QQQ enables the reaction chemistry to be applied to the most complex and challenging interference problems in comparison to single quadrupole mode. The Triple Quadrupole it is powerful tool and starts to play a significant role in radiological analysis, and it has now the potential for replacing traditional radiometric instruments in some applications. For example, for trace detection of actinides (uranium, plutonium) in environmental samples[10, 11], rapid screening of radionuclides in food and water[12, 13], and monitoring radionuclides in biological fluids[14].

Modern inductively coupled plasma mass spectrometers are at the leading edge of the analytical instrumentation market, driven by their exceptional sensitivity, multielement detection capabilities, and their ability to perform ultra-trace analysis across a variety of industries. Improvements in hardware design, collision/reaction technology (CRC), and software automation have made contemporary ICP-MS systems faster, more reliable, and easy to use. Their applications range from environmental monitoring, food and pharmaceutical safety testing to semiconductor manufacturing, clinical research, and geochemical analysis, contributing to a steady global demand.

Major manufactures such as ThermoScientific, Agilent Technologies, and PerkinElmer are firmly established as leaders in the global ICP-MS market. The ThermoScientific iCAP TQ ICP-MS, Agilent 8900 ICP-MS, and PerkinElmer NexION 2000 represent three prominent systems in inductively coupled plasma mass spectrometry. Each one specifically designed to meet various analytical requirements.

The iCAP TQ is a triple quadrupole device engineered for superior interference elimination using reaction gases, making it well suited for regulatory testing, environmental monitoring, and speciation studies [ThermoScientific].

The Agilent 8900 is recognized as the most sophisticated ICP-MS available, integrating dual quadrupoles with highly efficient collision/reaction cell to achieve ultra-trace detection limits and exceptional durability, which is especially appreciated in the semiconductor, geochemical, and nuclear sector [Agilent Technologies].

The PerkinElmer NexION 2000 is quadrupole system equipped with Universal Cell Technology (UCT), enabling flexible modes; standard, collision, and reaction to adeptly handle diverse matrices and interferences, ideal for routine applications such as environmental, food safety, and clinical testing [PerkinElmer].

Collectively, these three instruments have unique strengths and is designed for different application, from high-throughput routine analyses to the most rigorous ultra-trace research. Summary of technical specification of these three instruments collected in Table 1.

Table 1. Technical specifications of ICP-MS systems

System	iCAP TQ ICP-MS	Agilent 8900 ICP-MS	NexION 2000 ICP-MS
Mass Analyser	Triple Quadrupole (Q1 mass analyser; Q2 Collision/Reaction Cell; Q3 mass analyser)	Triple Quadrupole (Q1 mass analyser; Q2 Collision/Reaction Cell; Q3 mass analyser)	Triple Quadrupole (Q0 ion deflector (QID); Q1 collision/reaction cell; Q2 mass analyser)
Ion Deflection System	90 degrees ion beam via cylindrical ion optic	Omega lens system deflects the ion beam off the central axis	90 degrees ion beam via quadrupole fields
Ion Detection	Electron multiplier with pulse/analog switching	Electron multiplier with pulse/analog auto-switch	Electron multiplier with fast switching pulse/analog
Mass Range	Q1: 2-240 amu Q3: 2-290 amu	Q1: 2-260 amu Q3: 2-275 amu	Q2: 1-285 amu
Mass Resolution	≈0.7 amu	≈0.7 amu	<0.7 amu
Abundance Sensitivity	10^{-13}	10^{-14}	10^{-13} to 10^{-14}
Collision/Reaction Cell (CRC)	Flatapole Collision/Reaction Cell	Octopole Collision/ Reaction Cell with axial acceleration	Hexapole Collision/Reaction cell with dynamic bandpass tuning
Gas Switching (CRC)	Moderate (≈30 seconds)	Ultra-fast (<5 seconds)	Dynamic on-the-fly gas mixing and blending
Gass Lines	4 gas lines, extendable up to 15 additional gases	4 gas lines, extendable up to 12 additional gases	3 gas lines, extendable up to 5 additional gases
Dynamic Range	10 orders of magnitude	11 orders of magnitude	Up to 14 orders of magnitude (extended dynamic range)
Detection Limits	Sub-ppt (parts per trillion)	Sub-ppt	Low ppt to sub-ppt depending on element

These instruments are primarily designed to analyse samples in liquid form, however solid samples can be also analysed. Indeed, solid matrices can be diluted in solvent or can be analysed directly using an electrothermal vaporisation or laser-ablation technique[15-18].

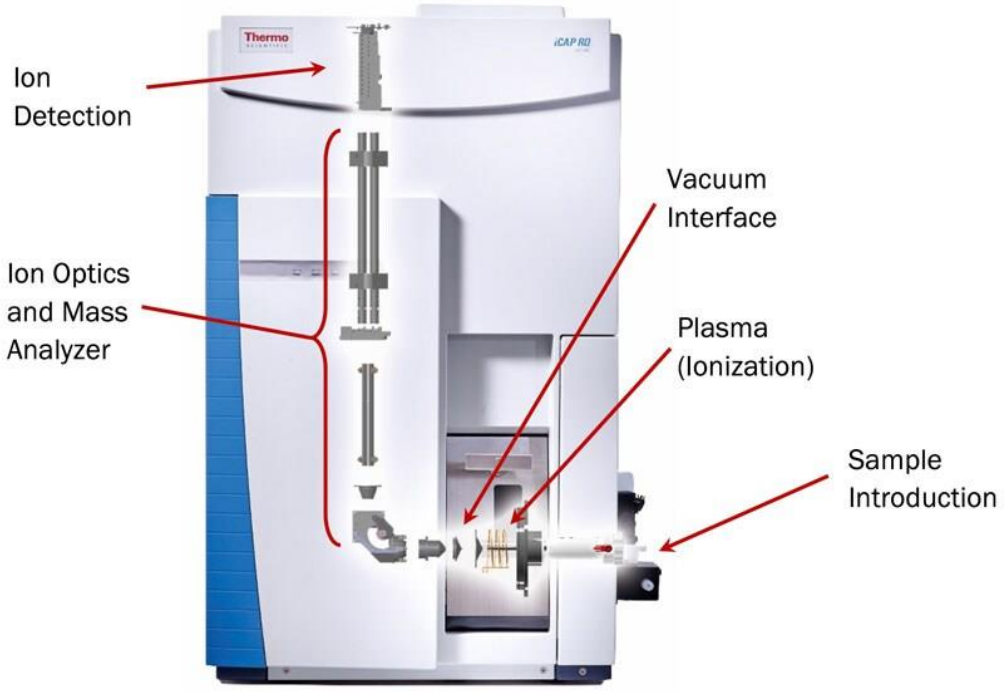

Figure 1. Schematic representation of iCAP TQ ICP-MS [ThermoScientific]

There are five fundamental compartments of ICP-MS system: 1) the sample introduction (nebuliser and spay chamber); 2) plasma (ionisation); 3) the vacuum interface (sample cone and skimmer cone); 4) the ion optics and mass analyser; and 5) the ion detection.

1.1.1 The sample introduction system

The sample induction system serves two purposes: the conversion of the sample into an aerosol and guiding a representative part of the sample into plasma. But first, the liquid samples are aerosolised by a nebuliser. The most used in inductively coupled plasma spectrometry is the pneumatic nebuliser[19]. However, a number of different nebulisers are available such as ultrasonic, the thermospray (superheated liquid), electrostatic, and jet impact, have also been used[20, 21]. After being aerosolised by the nebuliser, the sample enters the spray chamber. The spray chamber has a simple design but serves a few important purposes; it selectively filters out the larger aerosol droplets that are generated by the nebuliser and acts to smooth out nebulisation 'pulses' produced by the peristaltic pump[22]. In the baffled cyclonic spray chamber (Figure 2), the larger droplets are efficiently filtered out by turbulent deposition on the inner walls of the spray chamber, and by gravity. In addition, the spray chambers are externally cooled for thermal stability of the sample, minimise the amount of solvent going into the plasma and the formation of oxides.

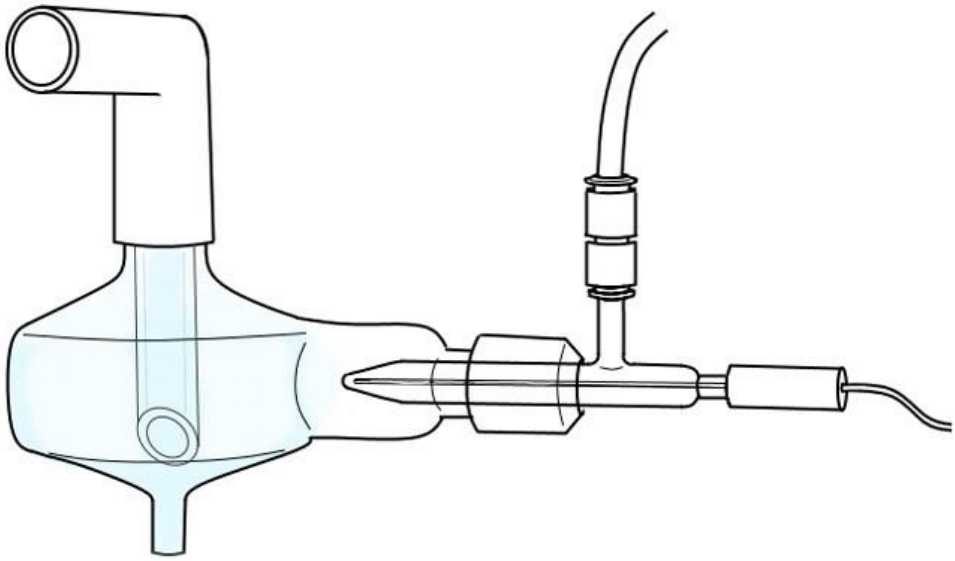

Figure 2. Baffled cyclonic spray chamber with attached pneumatic nebuliser [ThermoScientific]

1.1.2 Plasma (ionisation) – Inductively coupled plasma (ICP)

A plasma is an ionised gas that contains electron, ions, and neutral atoms/molecules. All particles acquire or lose energy through collisions with one another or through contact with solid objects. This energy is in the form of kinetic energy (E_K), related to the mass (M) and velocity (v) of the molecule by the expression (Eq.1):

$$E_K = \frac{1}{2}Mv^2 \quad (1)$$

The energy distribution of such a collection of molecules is statistical and is described by a function known as a Maxwell–Boltzmann distribution. The mean kinetic energy of molecules, and mean square speed c^2, for a Maxwell–Boltzmann distribution is expressed as Eq. 2:

$$\overline{c^2} = \frac{3kT}{M} \quad (2)$$

therefore, the mean kinetic energy of the molecules is related to the gas temperature by the expression (Eq. 3):

$$E_K = \frac{1}{2}M\overline{c^2} = \frac{3}{2}kT \quad (3)$$

where:

k is Boltzmann's constant,

T is temperature in Kelvin,

M is the mass of the molecule in kg.

Thus, as the temperature increases, the particle velocity increases and therefore increasing the collision frequency.

The inductively coupled plasma is generated at the end of plasma torch, manufactured from quartz. The instrument use an argon plasma, although helium plasmas have been described[23, 24]. When argon gas passes through a quartz torch placed in an induction coil, radio frequency (RF) power between 500 and 1600 W is applied, an alternating current oscillates within the field (the frequency of oscillation is governed by the type of RF generator used, usually 27 or 40 MHz, megahertz or million cycles per second). These oscillations set up electrical and magnetic fields at the top of the torch. If a spark is then applied to the argon gas via a Tesla coil[25], then electrons are stripped from some of the argon atoms. These electrons then become trapped in the magnetic field and are accelerated in closed circular paths. As these rapidly moving electrons collide with neutral argon atoms, further electrons are stripped from the atoms and hence a chain reaction is established. Because of their kinetic energy and collisions with other atoms, a large amount of heat is generated, that is sufficient to generate and sustain a plasma at temperatures up to 10,000 K.

The amount of energy required to generate argon ions in this process is approximately 15.8 eV (first ionisation potential, i.e. the energy required to remove a single electron from an atom), which is high enough to ionise the majority of the elements in the periodic table. In an argon inductively coupled plasma, the degree of ionization (the fraction of atoms that are ionized) depends strongly on the element's ionization potential and the plasma temperature. Energy transfer from plasma to sample aerosol results in the dissolution of the aerosol, followed by the atomisation of the molecules and ionisation/excitation of the atoms[26]. The latter process can occur via different mechanisms, the most important mechanisms being[27]:

- Thermal ionisation/excitation; collisions between atoms, ions and electrons as shown in Eqs. 4 and 5:

$$M + e^- \rightarrow M^+ + 2e^- \quad (4)$$

$$M + Ar \rightarrow M^+ + Ar + e^- \quad (5)$$

- Penning ionisation/excitation; collisions between atoms in ground state and metastable argon species shown in Eqs. 6 and 7:

$$Ar^m + M \rightarrow Ar + M^+ + e^- \quad (6)$$

$$Ar^m + M \rightarrow Ar + M^{+*} + e^- \quad (7)$$

- Ionisation/excitation by charge transfer; charge transfer between atoms and ions, as shown in Eqs. 8 and 9:

$$Ar^+ + M \rightarrow Ar + M^+ \quad (8)$$

$$Ar_2^+ + M \rightarrow 2Ar + M^{+*} \quad (9)$$

where:

Ar is the argon atom; M is molecule; e is electron; $*$ is the exited state[28].

The level of ionisation is proportional to the plasma temperature and is described by the Saha equation (Eq. 10)[29, 30]:

$$\varepsilon(\%) = \frac{[X^+]}{[X]} = \frac{(2m_e kT_i\pi)^{3/2}}{n_e h^3}\frac{2Z_{X^+}}{Z_X}e^{\frac{\varphi_X}{kT_i}} \quad (10)$$

where:

$([X^+]/X)$ is the degree of ionisation of the atoms of element X,

n_e is the electron density,

m_e is the electron mass,

φ_X is the ionisation potential of an atom of element X,

k is Boltzmann's constant,

h is Plank's constant,

T is the ionisation temperature,

Z_{X^+} and Z_X are defined as the statistical weights weight of ions and atoms, respectively (assumed to be 0.5)[31].

Table 2. Ionisation potential, ionisation energy and degree of ionisation in the plasma for some selected radioisotopes at 7500 K[30]

Element	Ionisation potential (E_i, eV)	Ionisation Energy $(\varphi_x, 10^{-18}J)$	Degree of ionisation $(\varepsilon, \%)$
Se	9.75238	1.563	30
Sr	5.69484	0.9124	100
Zr	6.63390	1.063	98
Tc	7.28	1.166	95
I	10.45126	1.674	13
Cs	3.89390	0.624	100
Pb	7.41666	1.188	94
Ra	5.27842	0.846	100
Th	6.3067	1.010	99
Pa	5.89	0.943	99
U	6.19405	0.992	99
Np	6.2657	1.004	99
Pu	6.0260	0.965	99
Am	5.9738	0.957	99
Cm	5.9914	0.959	99

From equation 21, it is possible to calculate the degree of ionisation for all the isotopes (stable or radioactive) of a specific element (Table 2). Also, the level of ionisation is proportional to the plasma temperature. Elevated plasma temperature facilitates a greater level of ionization for the elements of interest, thereby increasing analyte sensitivity and enhancing detection efficiency.

Nevertheless, in situation where analytical sensitivity is not the primary concern, colder plasma condition may be utilized. Reduced plasma temperatures lead to decrease matrix effect (signal suppression) or analyte volatilization, providing a balance between performance and operation stability for routine or less rigorous analyses. Colder plasma stabilizes the sample introduction and ionization process[32, 33].

1.1.3 Vacuum Interface

Ions, photons and neutral atoms or molecules are extracted from the plasma into the interface region via a small orifice at the tip of the sample cone (Figure 3). A mechanical roughing pump is used to maintain an interface pressure between the cones. As ions enter this interface region, the dramatic reduction in pressure causes a supersonic expansion of the ions, generating a so-called

free jet[34]. Ions are subsequently extracted through an even smaller orifice in the skimmer cone and into the main vacuum chamber which is held under high vacuum by a turbomolecular pump. Ions can be subsequently be guided effectively by charged surfaces called electrostatic lenses.

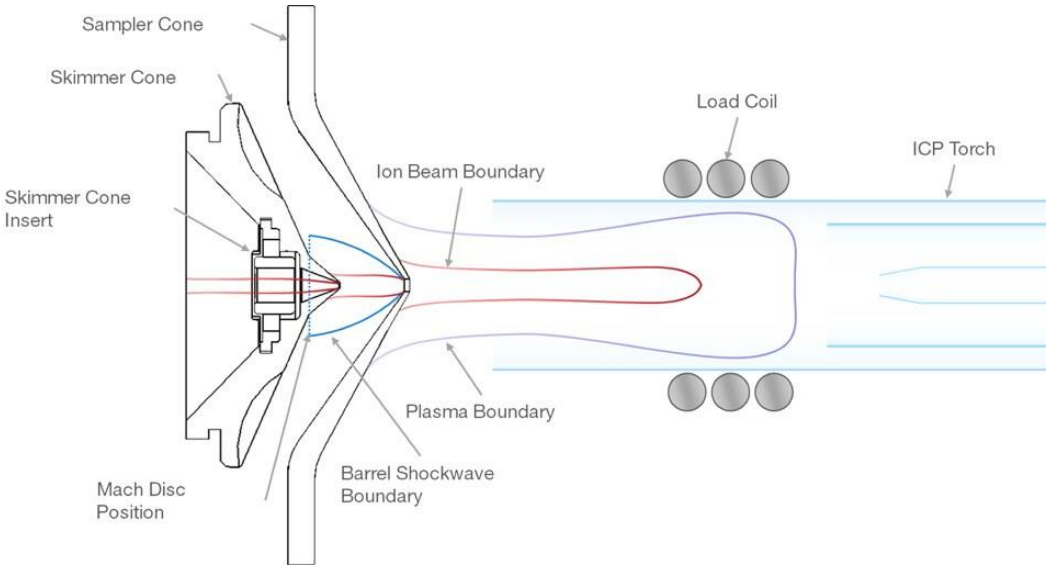

Figure 3. Interface region [ThermoScientific]

1.1.4 Ion optics and mass analyser

An ion lens system is used to transfer positive ions from the supersonic jet of sampled gas while neutral particles were pumped away and guide the ions beam toward the reaction/collision cell. Also prevent photons from reaching the detector. The ion optic system then separates electrons from analyte ions, resulting in a positive ion beam that is then transmitted into the mass spectrometer where ions are separated according to their mass-to-charge ratios (m/z) and then counted[35].

The iCAP TQ ICP-MS is equipped with 90° cylindrical ion lens (Figure 4) – the RAPID (Right Angular Positive Ion Deflection). Providing ion transmission across the mass rage – Table 1.

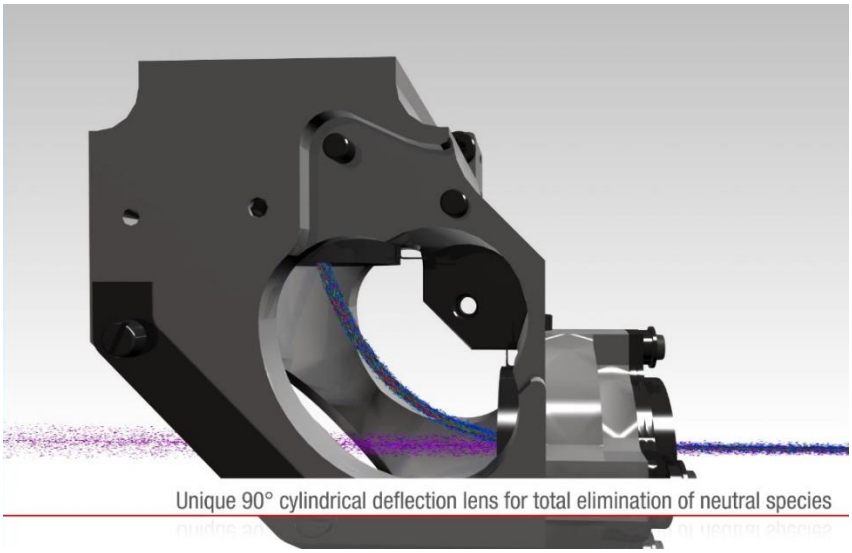

Figure 4. Ion optics – Right Angular Positive Ion Deflection (RAPID) [ThermoScientific]

While the ion beam progresses through the skimmer positive ions are drawn toward the ion lenses while the electrons are repelled. The electrostatic repulsion between ions result in a radial expansion or defocussing of the ions. This defocusing phenomenon is referred to as the space charge effect. Ion transmission under the space charge is also a function of ion kinetic energy (Equation 12). Ions with higher masses, i.e. higher kinetic energies, tend to stay more focused and are transmitted more efficiently through the defocusing space charge than lighter ions. Thus, the electrostatic field applied to ion lenses guiding the ion beam off-axis.

1.1.5 Collision/reaction cell (CRC)

Over the past decades, collision/reaction cells have been developed and applied in analytical plasma mass spectrometry[36, 37]. A gas filled multipole (quadrupole, hexapole or octopole – more information in the next section) is located before the mass analyser and the gas phase ion/molecule interactions are responsible for the removal of polyatomic interfering ions[38]. Choosing an appropriate reaction gas is critical and is dictated by whether or not the gas reacts efficiently enough with either the overlapping ion by removing it or with the analyte ion to move the analyte to a new mass that does not suffer from an overlap[39].

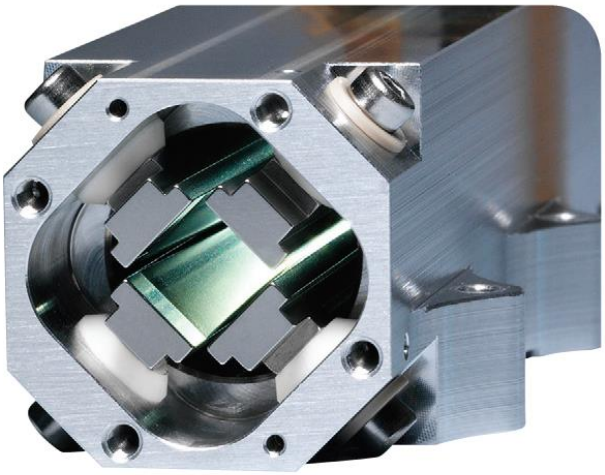

Figure 5. QCell collision/reaction cell (CRC) – flatapole rods in iCAP TQ ICP-MS [ThermoScientific]

The most useful reagent gases for ICP-MS can be classified as collision gas (e.g. He – inert gas), charge-exchange reagent gases (e.g. H_2, NH_3, Xe, CH_4, and N_2), oxidation gas reagents (e.g. O_2, N_2O, NO, and CO_2), relatively few adduction gases (e.g. H_2 and CO), and other reagent gases (e.g. CH_4, C_2H_6, C_2H_4, CH_3F, SF_6, and CH_3OH). Several reaction mechanisms have been described in literature and these are:

- Charge transfer reactions[40], for example (Eq. 11):

$$M^+ + H_2 \rightarrow H_2^+ + M \quad (11)$$

- Proton transfer[41], for example (Eq.12):

$$MH^+ + H_2 \rightarrow H_3^+ + M \quad (12)$$

- Hydrogen atom transfer[42], for example (Eq.13):

$$M^+ + H_2 \rightarrow MH^+ + H \quad (13)$$

- Atom transfer[37], for example (Eq. 14):

$$M^+ + O_2 \rightarrow MO^+ + O \quad (14)$$

Also, collision/reaction cell can selectively attenuate all polyatomic interferences based on their size by use of a potential barrier between the cell and mass analyser. Kinetic energy discrimination exploits the fact that all polyatomic ions are larger than analyte ions of the same mass, so they collide with the cell gas more often as they pass through the cell, emerging with lower residual energy. The lower energy ions formed in the cell are unable to overcome the potential barrier and are thus prevented from passing through. For example, the monatomic ion (^{210}Pb) and polyatomic ion (^{208}PbHH) enter the cell with the same energy and collide with the inert gas (He) (Figure 6). The molecular ion (^{208}PbHH) has a larger cross section than the analyte at the same mass to charge (^{210}Pb) and experiences more frequent collisions with He. Consequently,

^{208}PbHH undergoes a significant reduction in kinetic energy relative to the analyte (^{210}Pb). Energy filtering can be used to ensure only the analyte of interest pass through collision/reaction cell.

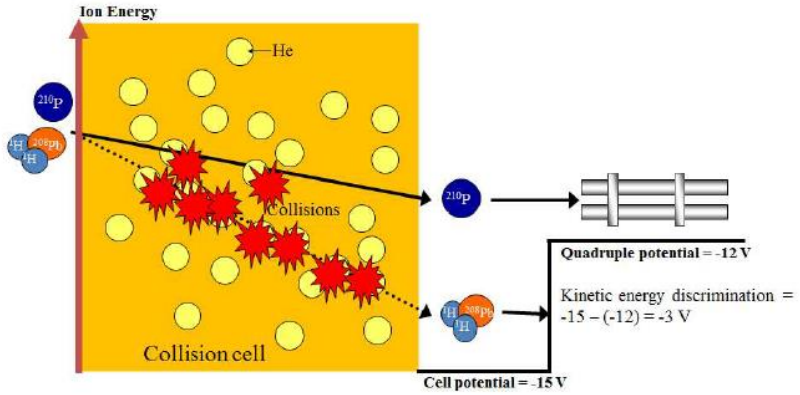

Figure 6. Energy discrimination between 210Pb and 208PbHH in the collision/reaction cell when He is used as the collision gas[43]

1.1.6 Mass analyser – quadrupole mass filter

Quadrupole mass filter are made up of four rods (e.g. circular, hyperbolic). The rods must be perfectly parallel positioned at the corners of a square[44]. The diagonally opposed rods are electrically connected, so that two pairs of electrodes are formed. Each pair is supplied with a combination of a direct current (DC) and a radio-frequency (RF) voltage (active current).

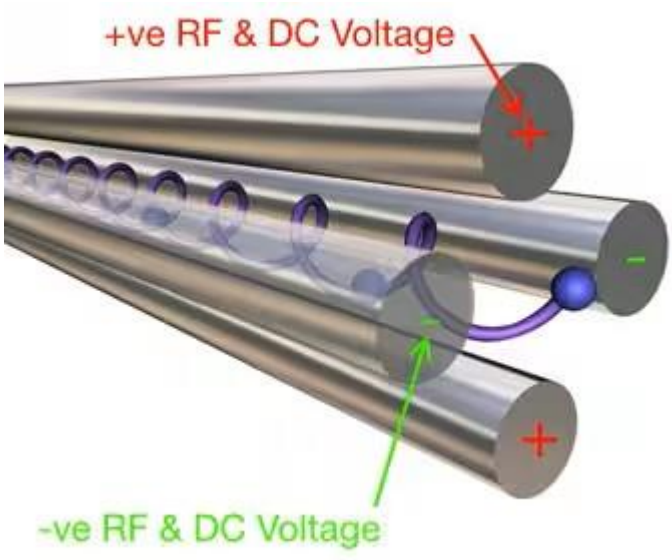

Figure 7. Quadrupole mass filter [ThermoScientific]

The RF voltage on both electrode pairs is the same. Ions entering the quadrupole can either traverse according to a stable trajectory and finally reach the detector, or they can follow an

unstable trajectory and be removed from the quadrupole prior to arrival at the detector (Figure 7). The operation of quadrupole mass filter is best visualised by trajectory of a charge particle after applied potential in the X-Z and Y-Z planes separately[45] (Figure 8).

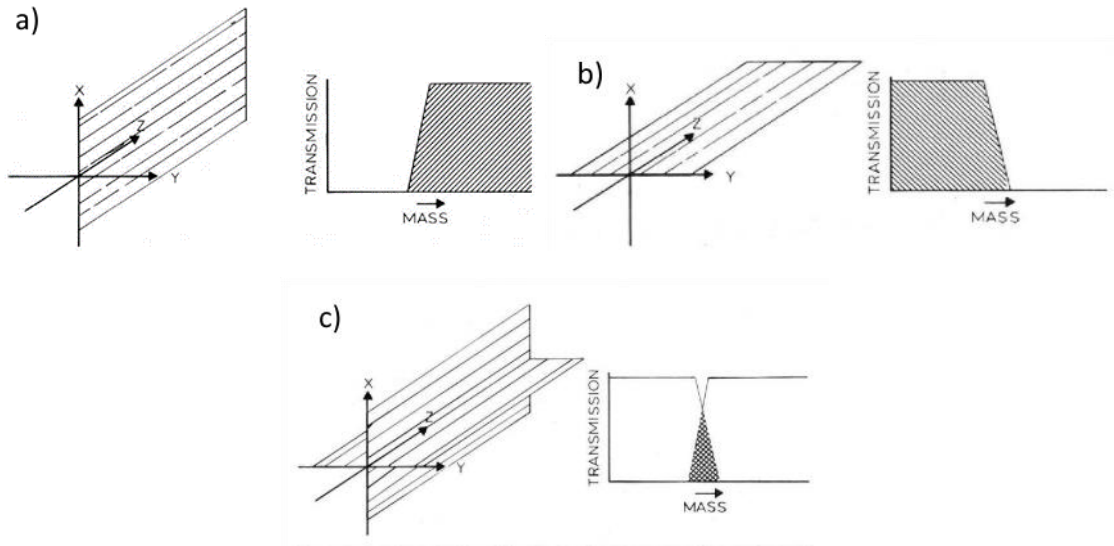

Figure 8. The quadrupole acts as: a) a high pass mass filter in the in x-z plane, b) a low pass mass filter in the y-z plane, c) operation of the quadrupole as a bandpass mass filter results from overlap of the high pass mass filter and the low pass mass filter[45]

In the X-Z plane, combined direct current and active current have mass dependent effect on trajectories of ions. If an ion is very heavy and/or the RF of the active current potential is very rapid, then an ion is influenced by the mean potential applied to the electrode structure. Thus, are only influenced by the DC component, leading to focusing of the ion towards the central axis of the quadrupole. The small period of time when electrodes have a negative potential (rapid RF) the effect on the trajectories of heavy ions are negligible. In the Y-Z plane, DC potential applied to lying electrodes is negative, whereas in the X-Z plane, DC potential is positive. As the heavy ion tend to be influenced by mean value of the applied potential and in this scenario heavy ions with negative charge are eliminated. Combining the effect of both the X-Z and Y-Z planes results in a mass bandpass filter; only ions with an m/z within a narrow range will pass through the quadrupole. These specific dynamics of this process will be governed by a number of factors; magnitude of the negative potential applied to the electrodes, the period of time during which the electrodes are held at a negative potential (e.g. the frequency of the ac waveform - RF), position, velocity, and mass-to charge ratio (m/z) of the particle[45]. Ions travelling along the *z* axis are subjected to the influence of a total electric field made up of a quadrupole field (Figure 9).

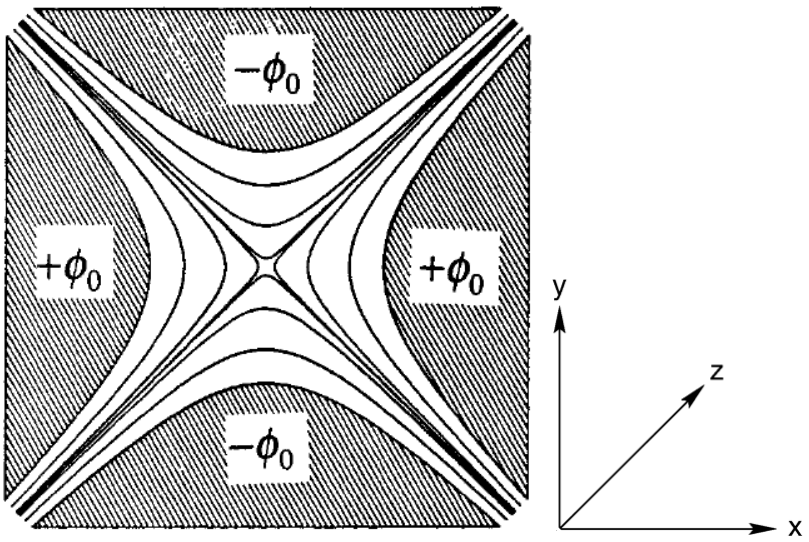

Figure 9. The quadrupole potential. The shaded regions are the ends of hyperbolic shaped rods. Lines are equipotentials (same potential) in the x, y plane. A potential $+\phi_0$ is applied to the electrodes in the x direction and a potential $-\phi_0$ to the electrodes in the y direction. Equipotential contours have hyperbolic shapes. The potential at the centre is zero[46]

The electric potential within the rods, $\Phi(x, y)$, is described (Eq. 15):

$$\Phi(x, y) = \frac{(x^2 - y^2)}{r_0^2}\phi_0 \tag{15}$$

where:

x, y is the distance to from the centreline, r_0 is the distance from centreline to an electrode (rod), ϕ_0 - the potential applied to electrode.

The x direction corresponds to the positive electrode and the y direction corresponds to the negative electrode for a positive ion[46]. The applied potential ϕ_0 has both a radiofrequency (RF) voltage, $V \cos \omega t$, and DC voltage, U, and is describe by (Eq. 27):

$$\phi_0 = U - V \cos \omega t \tag{16}$$

where:

V is the amplitude of RF voltage, ω is the RF frequency, t is time, U is the DC voltage.

Ion motion is determined by Newton's second law and the force by electrostatic field (Eq. 17):

$$m\frac{d^2x}{dt^2} = -e\vec{E} \tag{17}$$

where:

e is an ion that carries an electric charge (in coulombs), $\vec{E}$ is the electrostatic field as a unit vector (Figure 10).

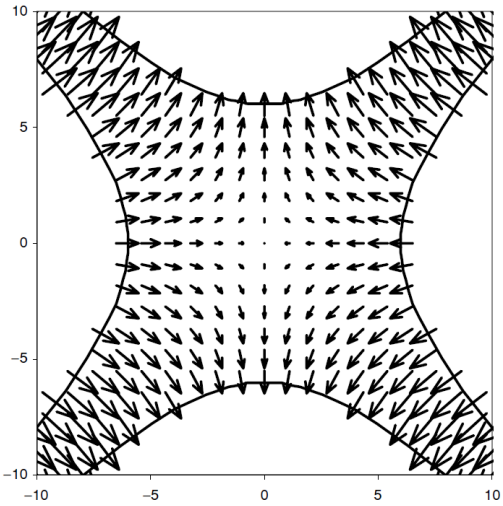

Figure 10. Electric field vector. Modified from reference[47].

Because, the electrostatic field is related to the potential and linked by Eq.18 [47]:

$$\vec{E} = -\nabla\Phi = \vec{x}\frac{d}{dx} + \vec{y}\frac{d}{dy} + \vec{z}\frac{d}{dz} \tag{18}$$

For the motion in the x direction force is given by Eq. 19:

$$m\frac{d^2x}{dt^2} = -e\frac{2x}{r_0^2}\phi_0 \tag{19}$$

The full equations (Eqs. 20, 21, 22) of motion along the x, y and z axes of the quadrupole are:

$$\frac{d^2x}{dt^2} - \frac{2e}{mr_0^2}[U + V\cos(\omega t)]x = 0 \tag{20}$$

$$\frac{d^2y}{dt^2} - \frac{2e}{mr_0^2}[U + V\cos(\omega t)]y = 0 \tag{21}$$

$$\frac{d^2z}{dt^2} = 0 \tag{22}$$

By the substitution (Eq. 23):

$$\omega t = 2\xi \tag{23}$$

And the introduction of the Mathieu parameters a and q (Eqs. 24, 25) where[45]:

$$a = a_x = -a_y = \frac{8eU}{m\omega^2 r_0^2} \tag{24}$$

$$q = q_x = -q_y = \frac{4eV}{m\omega^2 r_0^2} \tag{25}$$

the Mathieu equation becomes (Eq. 26):

$$\frac{d^2u}{d\xi^2} - [a + 2q\cos(2\xi)]u = 0 \quad (26)$$

where: $u = x$ or y.

The solutions of the Mathieu equation are classified in two categories:

- The 'stable' ion trajectories describe the paths of ions passing along the full length of the quadrupoles filter without hitting the rods;
- The 'unstable' ion trajectories represent the path of ions that hit the quadrupole rods and are therefore lost from the system.

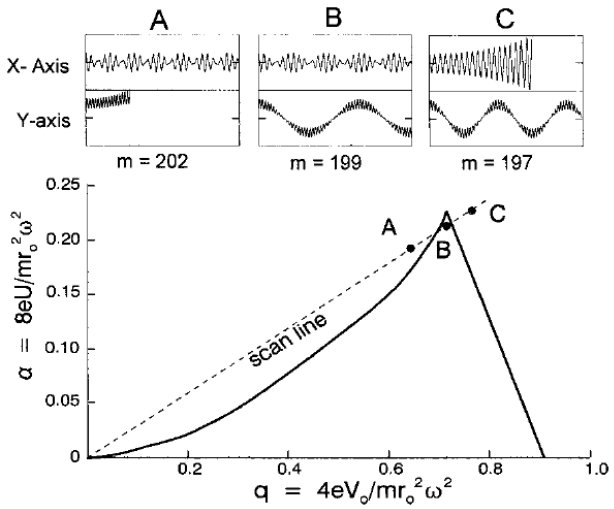

Figure 11. Stability diagramme in terms of parameters a and q. The three inset diagrammes show X and Y trajectories for $m/z = 202, m/z = 199$ and , $m/z = 197\ amu$ (atomic mass unit) in the regions exhibiting $(A)\ Y$ instability, (B) no instability and $(C)\ X$ instability[48]

A line representing the ratio $a/q = 2U/V$ can be drawn on the stability diagramme (Figure 11). The line represents the ratio of the amplitudes of the RF and DC components is held constant, while their absolute values are increased. Line is known as a mass scan line and consists of all the values of a and q occurring in the scan. When the parameters e, ω, r_0, U, V are kept constant, the mass scan line can be considered as a line of points, each representing a certain mass. The slope of the mass scan line can be adjusted by appropriate parameter settings so that only a small segment of the mass scan line intersects the stable region. As a consequence, only ions with an m/z corresponding to the masses in the stable region of the mass scan line will travel a stable trajectory through the quadrupole (Figure 12). A mass scan can be performed by a linear increase of the DC and RF components while their ratio is kept constant. When one point of the mass scan line, inside the stable region, is considered when U and V are increased, this point corresponds to an increasing m/z. The a versus q stability diagramme can be replaced by a U versus V diagramme (Figure 13).

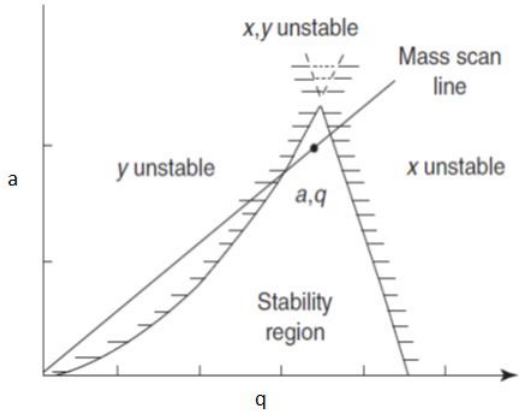

Figure 12. Stability diagramme for quadrupole mass filter[49]

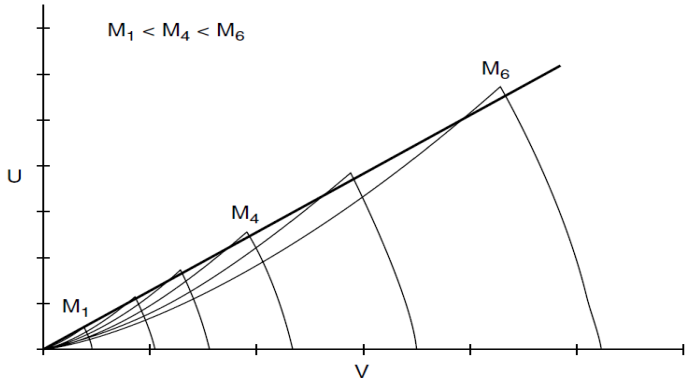

Figure 13. Stability diagrammes in U, V space for ions in order of increasing mass/charge ratio. By ramping the DC and RF potentials appropriately, only the peak of each individual stability diagramme will be intersected. Therefore, the ions will be transmitted selectively from the quadrupole mass filter, with the ions of lowest mass/charge ratio being transmitted first[50]

1.1.7 Detector

The ion beam must be detected and measured by an appropriate system. The magnitude of the signal to be detected is in the range of a few ions per second (sec.) for ultra-trace concentration up to 10^{10} ions/sec. for high concentration[51]. There are two mainly categories of detectors: electron multiplayer (continuous dynode electron multiplayer or discrete dynode electron multiplayer) and Faraday cup. – where each ion's charge produces a small electrical current. This current is then enhanced by high-gain electrometer, resulting in a measurable signal that corresponds to the number of ions.

Electron multipliers are capable of quantitatively measuring, with a very good reliability, a small ion current (<10^{-15} A), corresponding to a trace element and even a single-ion current from a small stream of ions. They, work on the principal of secondary electron emission. The electrons are multiplied using either continuous or discrete dynodes (Figure 14).

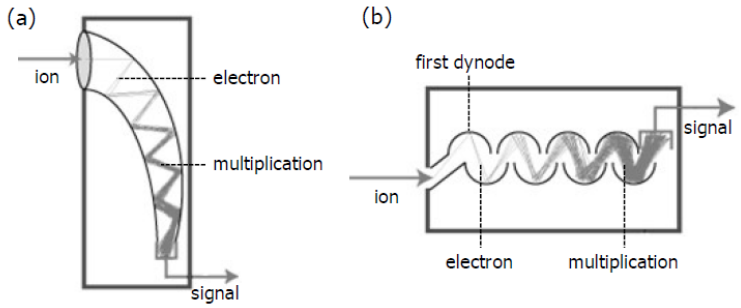

Figure 14. Electron multiplayer with (a) a continuous dynode and (b) several discrete dynodes

The multiplier can be operated in pulse counting mode, its most sensitive mode of operation, in which an exponential cascade of electrons caused by successive impacts against the dynodes coating results in a large electron pulse and a consequent gain of 10^7–10^8 over the original ion collision. Alternatively, the multiplier can be operated in analog mode with a gain of only 10^3–10^4. The pulsing counting mode is used for analytes present in low concentrations or a trace levels, where individual ions on the detector results in discrete pulses that are counted, thus ensuring high sensitivity. Nevertheless, when the analyte concentration is high, the ion flux may exceed the capacity for pulse counting, which can lead to pulse overlap. In these cases, the analog mode is preferred, as it allow the detector to measure the continuous current generated by ions. Through the integration of these detection modes, ICP-MS instruments achieved a wide dynamic range (Table 1), which supports the simultaneous quantification of trace and major concentration of elements in complex samples with high accuracy and linearity. This capability is a primary advantage of ICP-MS, facilitating thorough elemental analysis without the necessity for multiple sample dilution.

Alternatively, the ion beam may be directed into a Faraday collector (Faraday cup) (Figure 15). The Faraday cup detector is used for the measurement an analyte with an ion concentration of >10^4 ions/s where ultra-trace element analysis is not required[52]. With high ion's flux (>10^4 ions/s), the generated current is sufficiently robust to allow for precise measurement with minimal electric noise. The accurate Faraday cup detector must neutralize the incoming singly charged particle with exactly one electron. The Faraday cup is connected to ground via a high-ohm resistor ($10^8 - 10^{12}\Omega$). Current signal is created when a potential drop is created because of the ion current striking the metal electrode, which is balanced by electrons flowing from the ground - ions produce a current (I) resulting in a voltage drop (V) across the resistor (R) proportional to the

ion current incident at the collector by Ohm's law ($V = I * R$). Thus, measuring a single ion current is particularly beneficial for analyses that demand high precision. This approach provides stable and reproducible signals, which are crucial for accurate quantification and for determining isotope ratios with high accuracy. As such, it is well-suited for investigations related to isotopic composition, tracer experiments, or any other applications requiring precise isotopic measurements.

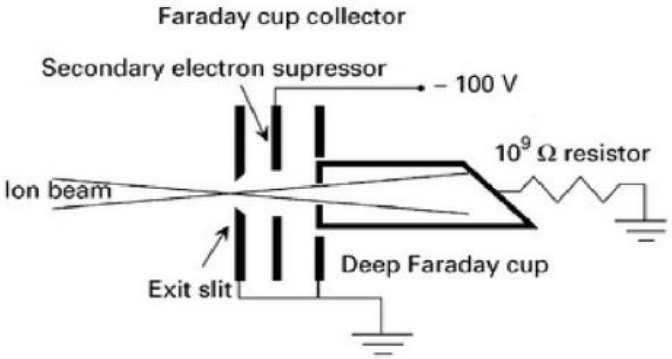

Figure 15. Schematic layout of a Faraday cup assembly. The cups are deep and have secondary electron suppression in order to precisely record one charge per incoming singly charged ion. Different resistor values are used depending on the ion current[53]

1.2 ICP-MS performance and challenges

Inductively Coupled Plasma Mass Spectrometry (ICP-MS) is widely acknowledged as one of the most effective methods for elemental and isotopic analysis due to remarkable sensitivity, accuracy, and capability to analyse multiple elements simultaneously. This technique can detect elements at trace and ultra-trace concentrations, with detection limits reaching the parts-per-trillion (ppt) level. A key advantage of ICP-MS is its extensive dynamic range (Table 1) which allow for the concurrent quantification of trace elements alongside major constituents within a single sample.

Additionally, ICP-MS delivers high throughput and rapid analysis, making it suitable for a range of application including environmental monitoring, clinical analysis, food safety, and geochemistry. Another significant benefit is its capacity to perform isotopic ratio measurements with high precision, which is crucial for tracer studies, radiogenic isotope analysis, and nuclear applications.

Although ICP-MS has notable strengths, it also faces several analytical challenges that can influence its curacy and reliability. There are four basic types of mass spectrometric interferences: isobaric spectral overlap; polyatomic molecular ion overlap; multiple charged species (usually doubly charged ions); and background contribution to the measurement of

analyte. To mitigate this issue, modern instruments often incorporate collision/reaction cell (CRC) or triple quadrupole technology, which utilize inert or reactive gases to reduce or eliminate these interferences. Another challenge is the matrix effects, where elements of the sample matrix can either suppress or enhance the signals of analytes, resulting in inaccurate quantification. To address these effects, sample preparation, extraction of element of interest, the use of internal standard(s), and optimised plasma condition are required.

The challenges outlined here focus on the optimisation process, which involves the careful adjustment of plasma parameters, ion optics and the use of collision/reaction cell to remove isobaric overlaps, polyatomic formation, and matrix signal suppression.

Complementing these instrumental strategies, rigorous sample clean-up procedures are implemented to reduce matrix load and eliminate any potential contaminants before the analysis takes place.

1.2.1 Ion-counting versus radiation counting

In mass spectrometry, the conventional unit of analyte quantity is the gram, whereas it quantity of radiation emitted reported in Becquerel (Bq) (number of nuclear rearrangements per unit of time) when using traditional radiometric techniques. Both units are related to each other, and the conversion is detailed below. Radioactive decay occurs at a contestant decay rate (A), specific for each radionuclide. The decay rate is a measure of the number of disintegrations per unit of time (t) and can be expressed as (Eq. 27):

$$A = N\lambda \tag{27}$$

where N represents the number of radioactive atoms and λ is the decay constant (t^{-1}), or fraction of atoms undergoing rearrangements per unit time.

The number of radioactive atoms (N) is proportional to the mass of analyte (m) with respect to molar mass (M) and Avogadro's number $(\mathcal{N}_A)$, thus can be expressed as (Eq.28):

$$N = \frac{\mathcal{N}_A * m}{M} \tag{28}$$

The decay constant (λ) is specific to a radionuclide and can be expressed as (Eq. 29):

$$\lambda = \frac{ln2}{t_{1/2}} \tag{29}$$

where $t_{1/2}$ is half-life of radionuclide.

By substituting (Eq. 28) into (Eq. 27), using information from (Eq.29) and rearranging the equations, the result) in grams can be calculated following (Eq.30):

$$m = \frac{A*M*t_{1/2}}{ln2*N_A} \quad (30)$$

In mass spectrometry methods, the atom numbers of the radioelement of interest are directly measured. As the half-life of the radionuclide decreases, the specific radioactivity (Bq/g) of the radionuclides increases in a clearly linear fashion (Figure 16). As such, relative to the mass spectrometric method, the shorter the half-life of the radionuclide, the more sensitive is the radiometric method. In the other words, radiometric methods are generally sensitive for short-lived radionuclides, whereas mass spectrometric methods are sensitive for long-lived radionuclides.

In addition, improvements in instrument sensitivity achieved through advances in sample introduction, mass spectrometry configuration and design, has opened up the possibility of using ICP-MS for quantification of shorter-lived radionuclides such as ^{90}Sr, significantly reducing the analytical time for such analyses[54].

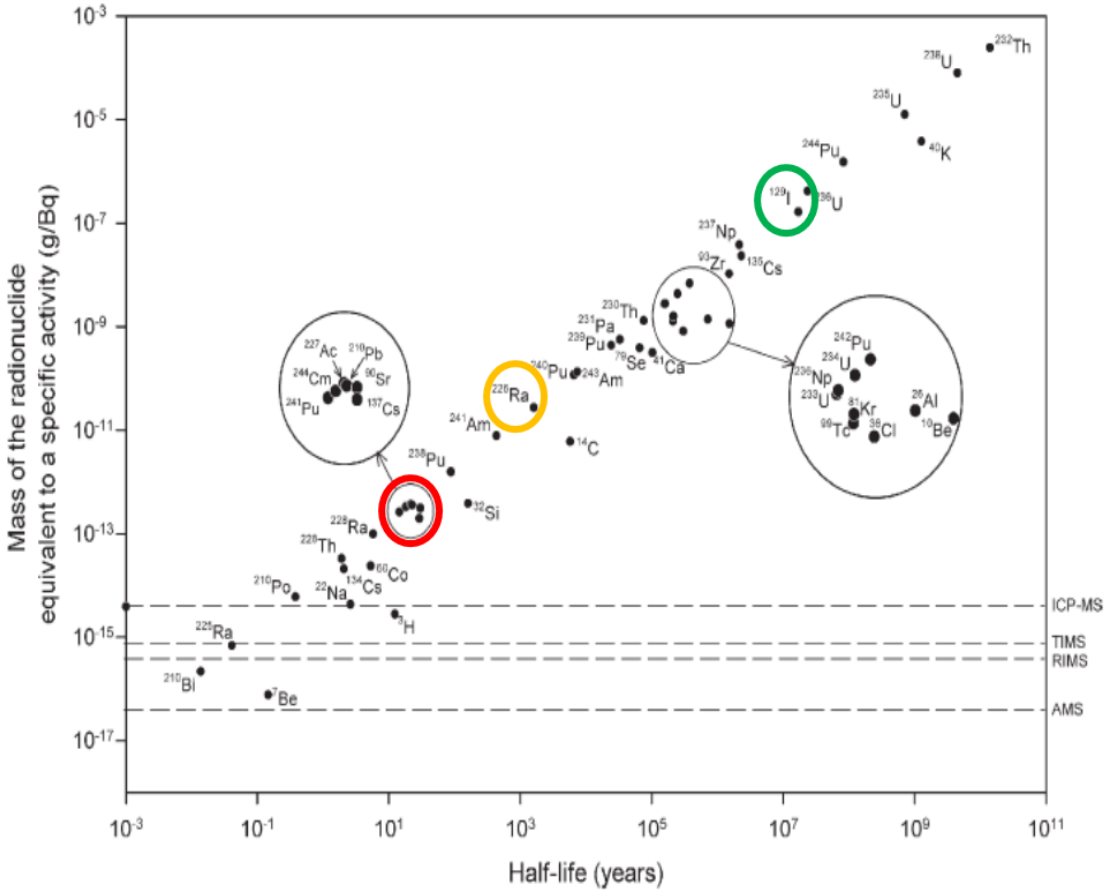

Figure 16. Relationship between the half-life and the mass equivalence for a specific activity (1 Bq) for the radioisotopes[30]

1.2.2 Isobaric and polyatomic spectral interferences

Spectral interference is a serious challenge to ICP-MS because it leads to inaccurate determination of the analyte concentration. Spectral interference refers to the signals generated by isobaric and polyatomic species which overlap with the mass to-charge (m/z) ratio of the analyte being monitored[55-60]. These overlapping signals result in an overestimated value compared to the analyte concentration. Isobaric overlap is because of the monoatomic species that have the same m/z ratio as the target analyte, e.g. ^{90}Sr and ^{90}Y, ^{90}Zr. Polyatomic interfering species may come from plasma gas, plasma-entrained atmospheric gas (forming the C, H, N, O, and Ar-containing species), acids or solvents (generating the oxide, hydroxide, C, Cl or S-based polyatomic species), or buffers and salts (yielding the S- and P-containing species) in the sample solution.

The most straightforward approach to remove this spectral interference is to monitor an element which is free from spectral overlap. However, the solution to the problem may not be advantageous because the interference-free element may have much lower abundance. A second non-instrumental approach is mathematical correction. For example, a correction factor can be used to the analyte of the interference-free isotope of the element[61, 62]. Also, spectral interference can arise from the species present in the solution and thus reduce the detection sensitivity. Different types of sample preparations could be used to isolate the elements of interest prior to instrumental analysis, which is the third non-instrumental approach to reduce interference.

Optimisation of instrumental parameters can also reduce spectral interferences. Changing the temperature of the plasma by optimising the radio-frequency power would result into a reduction in the interfering signal[63, 64]. Another approach to reduce interferences is introducing either collision gas or reaction gas into a pressurized cell. Collision gases such as Helium (He) and Hydrogen (H_2) will collide with both the interfering polyatomic species and the target analytes. However, the interfering elements are often larger in size than the target analytes, they will lose kinetic energy more readily after collision with gas and be expelled in the mass analyser without being detected. In case, when the reaction gas such as Oxygen (O_2)[65-72], Ammonia (NH_3)[37, 71-76], Methane (CH_4)[77-79], and Hydrogen (H_2)[71, 72, 80, 81] is introduced, the gas can either react with the target analyte to form another species which is interference-free for detection or react with the

interfering species and convert them to other species, such that they no longer overlap with the analyte of interest.

1.2.3 Multiple charged species (double charge)

In mass spectra obtained from ICP-MS not only single charge ions appear, but also double charge ions. These ions may lead to spectral overlap interferences. Doubly charged ions (M^{2+}) are formed from elements with a low second ionisation energy and for elements that have a high Ion-oxygen (MO) bond strength, oxide (MO^{+}) and hydroxide ions (MOH^{+}) are formed. By settings of the instrumental parameters the intensities of these species can be reduced[56].

1.2.4 Background

The background of the mass spectrum is the count rate in the absence of any specific species at the m/z value where an analyte ion is to be measured quantitatively. True background count rates generally result from unknow ions, which reach of the electron multiplier; photons, which result from stray light inside the mass spectrometer; and random electronic noise generated in the detector (usually as a function of temperature). Background measurements are often used in ICP-MS as a diagnostic tool but also a way to correct the instrumentation is performing property or requires maintenance to function reliably.

1.2.5 Chemical (matrix effect) interference and physical interference

High concentrations of a matrix constituent (chemical element) can cause a suppression of the ion analyte. Furthermore, matrix-induced space charge effects could occur if the contribution of a high concentration of matrix ions is significant. Based on space charge effects, heavy analyte ions (which have higher ion kinetic energies) should be less affected than light analyte ions (1.1.4. Ion optics and mass analyser). It means, the suppression is most severe for light analyte ions in the presence of higher mass matrix elements as a result of the defocusing nature of ions under the space charge effect. Matrix effects are the most challenging problem for ICP-MS analysis as

matrices are likely to be unavoidable ingredients in the analysis of real samples. This interference is not necessarily specific in nature and is usually not limited to a single interferent element. Therefore, by reducing the absolute concentration of the matrix components (by dilution), suppression effects can be reduced to an insignificant level [82, 83].

Also, matrix effects can be eliminated with chemical or physical separation prior to analysis. Precipitation and solvent extraction have been used successfully to remove the matrix from samples prior to analysis by ICPMS. However, chromatography has been the most popular. Chromatography using either ion-exchange or chelating resins for matrix removal has proved to be a very successful technique in eliminating the matrix for the analysis of real samples[33, 84-86].

One type of physical interference effect is that associated with a high dissolve solids content in the sample. As the concentration of the total solids in the sample increases, the possibility of drift in analyte ion current signals becomes more problematic. Internal standards can be used to correct for the depression of analyte signal caused by this build up on the sampler cone. This approach does not require sample dilution for correction of the drift. However, it can be used in conjunction with sample dilution to achieve optimal correction. Also, matrix matching of the calibration standards to the sample composition will improve this situation[87-89].

Other types of physical interference effects include those affecting the nebulization/sample introduction process. These sample transport effects, which result from differences in viscosity, surface tension, and volatility, can be minimized by dilution. The use of a delivery pump to transport the sample solution to the nebulizer will normalize these effects to a limited extent.

A serious problem can result from contamination of the analytical system (i.e. sample transport, nebulizer, spray chamber, plasma torch, and attendant tubing and fittings) by high concentrations of analytes originating from sample solutions. If care is not exercised when analysing multiple samples, then analyte carryover can mitigate the quality of the analytical determinations. After the ion measurement is made (i.e. signal integration is performed), the analytical system must be wash out before the next sample can be processed.

1.3 Expected benefits of ICP-QQQMS technology for measuring of radioisotopes in environmental matrices

Inductively coupled plasma mass spectrometry (ICP-MS) started to play wider role for measuring medium and long-lived radionuclides and became alternative to traditional alpha and beta counting techniques[2, 14, 90]. ICP-MS is increasingly growing and becoming a recognised technique for the measurement medium and long-lived radionuclides due to sensitivity, speed and sample preparation compared to traditional radiometric techniques: alpha and beta counting. Many of reviews, work have been published on the measurement of radionuclide by ICP-MS[54, 71, 72, 91].

The determination of radionuclides in environmental samples is important in relation to the protection of human health. Numerous sources of ionizing radiation can lead to human exposure: natural resources, nuclear explosions, nuclear power generation, the use of radiation in medical industrial and research purposes, and radiation-emitting consumer products[92].

The environmental samples, including biological, geological, and water samples, exhibit significant complexity and contain a wide range of analytes at various concentration levels. The biological samples consist of a complex mixture of carbohydrates, proteins, and lipids. The geological samples may consist of a combination of different materials, e.g., clay, organic material, silicanes, while water sample contain dissolved solids. Prior to analysis, it is necessary to decompose the organic matter or otherwise remove the matrix to release the compound of interest, e.g., radionuclide from the sample matrix. Sample pre-treatment is therefore a critical step, and in many cases is effectively supported by microwave-assisted digestion techniques. This technique involves a pressurised closed-vessel system where the sample (usually in acid) is heated by microwave. The boiling point of acid is raised by the pressure produced inside the vessel and the temperatures reached are higher than under normal pressure, thus the total digestion (decomposition of the matrices: organic matter, clay, silicanes, other minerals etc.) is completed in a shorter period of time. This technique is especially advantageous in emergency contexts, such as following accidental releases of radionuclides, where environmental concentrations are likely be high. In such scenarios, only minimal sample amounts are necessary for analysis to achieve accurate and reliable outcomes. The ability to work with smaller sample volumes is beneficial for several reasons. Firstly, it reduces the handing of radioactive materials, thereby mitigating health risks to laboratory personnel.

Secondly, smaller sample sizes allow for quicker preparation and analysis, which is critical for timely decision-making in emergency responses. Finally, minimizing sample sizes also decreases the production of radioactive waste, which is essential for safe laboratory operations and

subsequent waste management. Microwave-assisted digestion enhances this methodology by allowing for the swift and effective breakdown of organic materials and the release of radionuclides from complex matrices, ensuring precise quantification in a variety of environmental samples.

The varied types of sample induction, e.g., laser ablation, desolvation system, allow for customisation of techniques for specific sample matrix or form of analyte. Laser ablation (LA) is a tool for direct analysis of solid samples combined with ICP-MS. It allows for macroscopic analysis and/or mapping, with advantage of being fast and doable for routine analysis. With the desolvation system where the solvent is removed from analyte, the sensitivity of ICP-MS is improved by enhancing analyte transport efficiency, reducing solvent loading to the plasma and significant reducing of hydride generation. Compared with conventional pneumatic nebulization, injected water vapor causes oxide and hydride polyatomic ion interferences.

The Aridus 3 desolvating nebuliser system is a specialised liquid sample introduction for ICPMS instruments. Principle of operation based on introduction the liquid sample by self-aspirating C-Flow PFA (perfluoroalkoxy) nebulizer. The nebulizer aerosol is sprayed into heated PFA spray chamber to maintain the sample aerosol in a vapor phase. The sample vapor then enters a heated fluoropolymer membrane desolator module – Figure 17. Fluoropolymers such as perfluoroalkoxy (PFA) is used for lowest trace metal blanks and maximum chemical resistance.

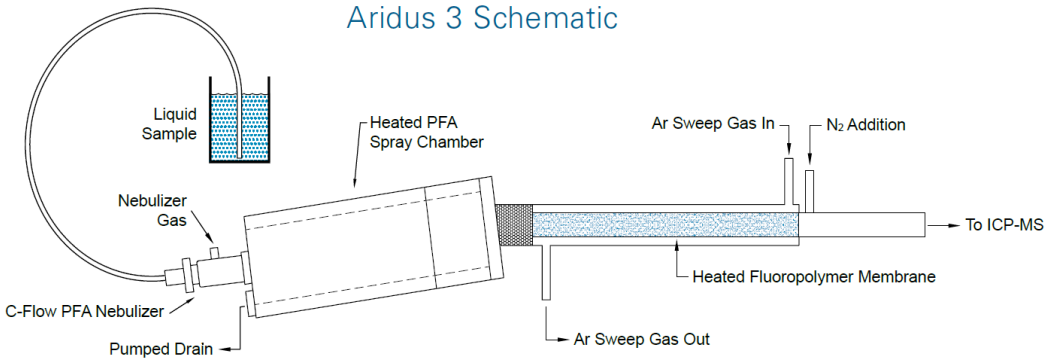

Figure 17. Schematic of Aridus 3 – desolvation nebuliser system [Teledyne Cetac Technologies]

The vapor from the spay chamber is transported to a heated fluoropolymer tubular membrane. Solvent vapor passes through the membrane and is removed by an exterior flow of argon gas (sweep gas) and additional nitrogen gas. The enhanced sensitivity reduced solvent loading to the plasma and significant reduced of hydride generation are advantageous of this system which be explore further in this work.

With introduction of triple quadrupole ICP-MS technology in 2012, the system has significantly

expanded the scope of application. It is powerful tool and starts to play a significant role in radiological analysis. With combination of different types of sample induction can be applied to more complexes matrices.

1.4 Aim and objectives of the project

The main aim of this research project is to evaluate the potential benefits of using the ThermoFisher iCAP Triple Quadrupole ICP Mass Spectrometer (iCAP TQ ICP-MS) for measuring a selection of radioelements present at very low levels in food and other environmental matrices. This system presents specific configurations in comparison to other ICP-TQMS technologies available on the market, by integrating a distinctive orthogonal deflection lens, referred to as the Right-Angle Positive-Ion Deflection (RAPID) system. The RAPID configuration implements a right-angle deflection that improves ion transmission efficiency while simultaneously minimizing the transmission of neutrals atoms and molecules, and photons. By way of independent case studies, several optimisation parameters will be tested included the use of an additional desolvation system (Aridus 3) and new analytical applications will be developed for different environmental matrices and three radioisotopes of high interest: strontium-90 (^{90}Sr), iodine-129 (^{129}I) and radium-226 (^{226}Ra).

The objectives of this project are:

1. Optimisation of the plasma condition, extraction lens and first quadrupole entry lens voltage for analysis of strontium-90 (^{90}Sr), iodine-129 (^{129}I) and radium-226 (^{226}Ra).
   The ionisation efficiency, robustness of the plasma, and transmission of analyte ions into mass spectrometer are strongly depended on these parameters. Utilizing the iCAP TQ ICP-MS, optimisation of these parameters enhances efficiency and ion transmission into the mass spectrometer while minimizing space-charge effect. Fine-tuning of the plasma power, extraction lens potential, and quadrupole entry lens voltage is essential to maximize sensitivity for target radionuclides and stable operation when analysing complex environmental matrices.
2. Optimisation of oxygen flow as a reaction gas and helium as a collision gas to remove interferences for qualitative and quantitative determination of ^{90}Sr in milk and seawater.
   In the iCAP TQ ICP-MS, oxygen gas can be used in the collision/reaction cell to convert analyte ions to mass-shifted product ions, thereby separating them from isobaric and polyatomic interferences. Helium used in collision mode, removes polyatomic species. Optimisation of the oxygen and helium flows is crucial to suppress major interferences such as ^{90}Zr, ^{90}Y, ^{1}H^{1}H^{88}Sr, ^{1}H^{89}Sr, ensuring accurate detection of ^{90}Sr in complex matrices like milk and seawater.

3. Development of novel method for quantifying low levels of ^{90}Sr in milk and seawater samples.

   Owing to the radiotoxicity of ^{90}Sr, achieving ultra-low detection limits is essential. This objective focuses on combining optimised the iCAP TQ ICP-MS condition with matrix separation/preconcentration strategies (e.g., extraction chromatography of Sr) to allow for accurate and reproducible quantification of ^{90}Sr at environmental relevant concentration.

4. Optimisation of oxygen flow as a reaction gas in order to remove ^{129}Xe interferences for quantitative determination of ^{129}I in seaweed and seawater materials.

   A major analytical challenge in ^{129}I determination is the interference from ^{129}Xe, which is present in the plasma gas (Ar - Argon) and instrument background. By controlling oxygen flow in the collision/reaction cell, selective ion-molecule reaction can be promoted to suppress ^{129}Xe signal, thereby enhancing the signal to background ration for ^{129}I.

5. Development of a novel method for the determination of ^{226}Ra in sediment and seawater samples.

   The accurate quantification of ^{226}Ra is analytically challenging due to isobaric overlaps and matrix interferences from alkaline earth elements commonly present in seawater and sediments. This objective involves developing of the iCAP TQ ICP-MS method that incorporates optimised reaction/collision cell conditions, as well as chemical separation steps to achieve precise and interference free measurements of ^{226}Ra in environmental matrices.

Chapter 2 Optimised removal of interferences for the measurement of ^{90}Sr in milk and seawater samples

2.1 Strontium in the environment

Strontium - symbol Sr, atomic no. 38; is a natural occurring alkaline earth metal (lying in group IIa, period 5, between calcium and barium in the periodic table). The mineral was discovered in 1790 by Adair Crawford and William Cruickshank at Strontian (Scotland) and was first isolated in 1808. Strontium occurs naturally as strontium sulfate (Celestine - $SrSO_4$) and strontium carbonate (strontianite - $SrCO_3$) and is mined from these minerals. Strontium concentrations and isotope ratios in rock, groundwater, soil, plants, and animals thus depend on local geology [93, 94]. Strontium accounts for 0.02–0.03% of the Earth's crust [95, 96]. This element has four stable, naturally occurring isotopes: ^{84}Sr (0.56%), ^{86}Sr (9.86%), ^{87}Sr (7.0%) and ^{88}Sr (82.58%). Only ^{87}Sr is radiogenic since it is produced by decay from the radioactive alkali metal ^{87}Rb, which has a half-life of 48.8 billion years [97].

The ratio $^{87}Sr/^{86}Sr$ is the parameter typically reported in geological investigations (age of rocks - older rocks will in general have higher $^{87}Sr/^{86}Sr$ ratios than younger ones) [97, 98]; to study migration patterns of ancient populations (e.g., Vikings in Iceland, African slaves in colonial Mexico, migrants in Roman London) [99-101]; food authentication (origin of products, e.g., wine, olive oil, cereals, mineral water, cheese, rice, honey) [102-106] and forensic sciences (mostly narcotics, e.g., heroin) [107].

Strontium in the Earth's crust/rocks is released into the atmosphere as a result of natural weathering of rocks and soils, entrainment (lifting) of dust particles, resuspension of soil by wind and sea spray – aerosol mechanically produced from the interaction of wind at the sea surface [97, 108, 109]. Human activities play a crucial role in the contamination of the environment with strontium. The milling and processing of compounds that contain strontium, along with the burning of coal, release strontium into the air. The quantity emitted from coal-fired power plants is influenced by the strontium content in the coal, the amount of coal that is burned, and the effectiveness of fly ash capture. During the combustion process, around 90% of the coal mass is utilized, resulting in approximately 10% remaining as non-volatile material (fly-ash), which may contain strontium levels ranging from 100-4,000 ppm (or mg/kg) of strontium[110]. Other contributors to atmospheric strontium include the application of phosphate fertilizers sourced from rocks[111] and the use of pyrotechnic devices, such as fireworks and flares, which emit red colour due to strontium compounds[112-115]. Wet and dry deposition moves strontium into soil,

groundwater, rivers, seas and into food chain [116, 117]. Plants do not discriminate between strontium and calcium during uptake and metabolic utilisation [118-120], leading to its accumulation in vegetation. Aquatic organisms, particularly fish, also strongly accumulate strontium [121, 122], which can pose a potential risk to human health through dietary ingestion. A study led by *Bronner et al*. found that strontium and calcium followed the same metabolic pathway in human qualitatively, but with significant quantitative differences in how the body handled these two elements [123]. The major difference was in the urine, with the fraction of strontium excreted in the urine three times that of calcium, on the average [116, 124, 125]. Although strontium is a bone-seeking element, easily absorbed and incorporated into bone and tooth enamel in place of calcium [96, 126].

There are 35 known isotopes of strontium [127] – 4 stable, natural (^{84}Sr, ^{86}Sr, ^{87}Sr, ^{88}Sr) and 31 unstable, anthropogenic (^{73}Sr, ^{74}Sr, ^{75}Sr, ^{76}Sr, ^{77}Sr, ^{78}Sr, ^{79}Sr, ^{80}Sr, ^{81}Sr, ^{82}Sr, ^{83}Sr, ^{85}Sr, ^{89}Sr, ^{90}Sr, ^{91}Sr, ^{92}Sr, ^{93}Sr, ^{94}Sr, ^{95}Sr, ^{96}Sr, ^{97}Sr, ^{98}Sr, ^{99}Sr, ^{100}Sr, ^{101}Sr, ^{102}Sr, ^{103}Sr, ^{104}Sr, ^{105}Sr, ^{106}Sr, ^{107}Sr). Only four radioactive isotopes of strontium, ^{82}Sr, ^{85}Sr, ^{89}Sr and ^{90}Sr, have found practical applications [128].

Strontium-82 (^{82}Sr) is used to produce rubidium-82 (^{82}Rb) [129, 130] which the main field of its application is positron emission tomography (PET) of the cordial system [131-133]. Rubidium behaves like potassium in the body and very quickly transfer to the blood stream. The radionuclide (^{82}Rb) decays by emission of positrons (positive charge particle). The positron is emitted from the nucleus and rapidly loses kinetic energy before colliding with an electron (negative charge particle). Both particles annihilate and emit 2 gamma rays with energies of 511 keV. The two gamma rays travel in opposite directions with an angle very close to 180 degrees. Thus, a PET instrument detects a coincidence pair of 511 keV gamma rays [134].

Strontium-85 (^{85}Sr) and strontium-89 (^{89}Sr) are used in medicine for palliative therapy of bone tumours [135-142]. Strontium is preferentially incorporated into bone at sites of increased disease[143, 144]. This localisation focuses the radiation exposure on the cancerous lesion.

Strontium-90 (^{90}Sr) is not used in nuclear medicine because of its long half-life (28.8 years); however, its short-lived daughter (half-life: 64.04 hours) Yttrium-90 (^{90}Y) is utilised in therapy of various tumours – liver [145], brain [146], breast cancer and prostate cancer [147]. This radionuclide is also used as a power source for radioisotope thermoelectric generators (RTG or RITEG) where heat energy is transformed into electricity by the Seebeck effect. In the Seebeck effect, the electromotive force is created in the presence of a temperature difference between two different metals or semiconductors, which creates a continuous current in the conductors if they form a complete loop. RTGs have been used as power sources in lighthouses and navigation systems such as those built by the former USSR (Union of Soviet Socialist Republics) inside the Arctic Circle [148], in space probes, and satellites [149, 150].

However, ^{90}Sr is one of the by-products generated from the nuclear fission of uranium-235 (^{235}U) in a nuclear reactor (see Figure 18). Its production yield is more than 5% [151].

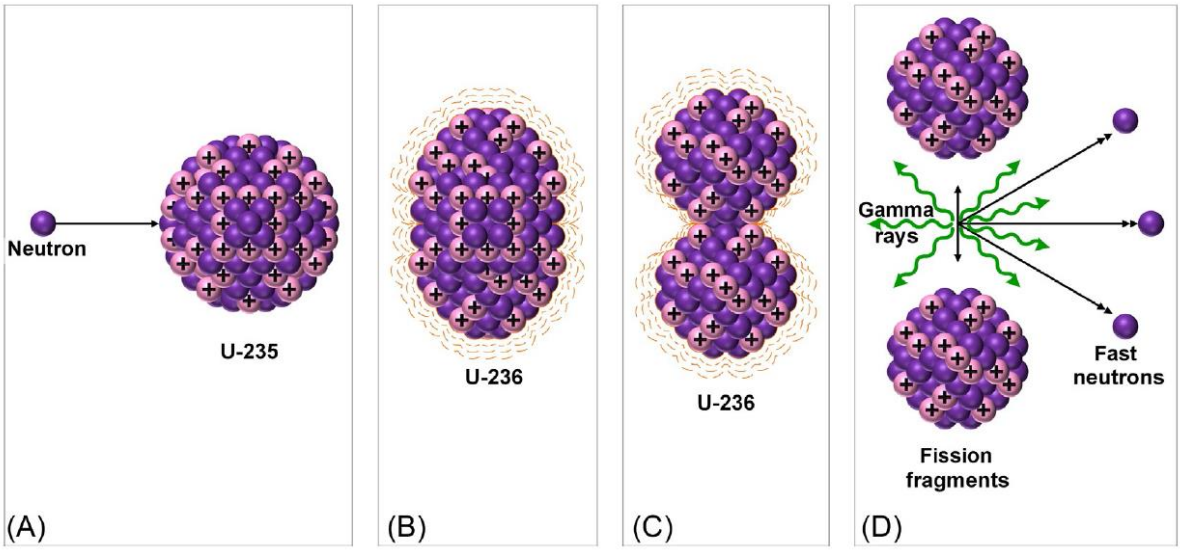

Figure 18. The fission process. (A) A neutron approaches a U-235 nucleus; (B) the U-236 compound nucleus is formed in an excited state and elongated; (C) the nucleus further distorts into the shape of a dumbbell; and (D) the nucleus separates into fission fragments, fast neutrons, and gamma rays [152]

The nuclear reaction equation for fission resulting from neutron absorption in ^{235}U may be written in general form (1):

$$^{235}_{92}U + {}^{1}_{0}n \rightarrow {}^{A_1}_{Z_1}F_1 + {}^{A_2}_{Z_2}F_2 + \vartheta\,{}^{1}_{0}n + energy \quad (1)$$

Where:

F_1, F_2 – two fragments (fission products).

An example of fission products showed in equations 2 to 5:

$$^{235}_{92}U + {}^{1}_{0}n \rightarrow {}^{90}_{36}Kr + {}^{144}_{56}Ba + 2\,{}^{1}_{0}n + energy \quad (2)$$

$$^{90}_{36}Kr \xrightarrow{32.3\ seconds} {}^{90}_{37}Rb \xrightarrow{2.6\ minutes} {}^{90}_{38}Sr \xrightarrow{28.8\ years} {}^{90}_{39}Y \xrightarrow{64\ hours} {}^{90}_{40}Zr\ (stable) \quad (3)$$

$$^{235}_{92}U + {}^{1}_{0}n \rightarrow {}^{89}_{36}Kr + {}^{144}_{56}Ba + 3\,{}^{1}_{0}n + energy \quad (4)$$

$$^{89}_{36}Kr \xrightarrow{3.2\ minutes} {}^{89}_{37}Rb \xrightarrow{15.4\ minutes} {}^{89}_{38}Sr \xrightarrow{50.5\ days} {}^{89}_{39}Y\ (stable) \quad (5)$$

Equations 3 and 5 showed decay of krypton nuclides and that strontium is the longest-live nuclide in the chain. The decay processes of ^{90}Sr and ^{89}Sr are shown Figures 19 and 20, respectively.

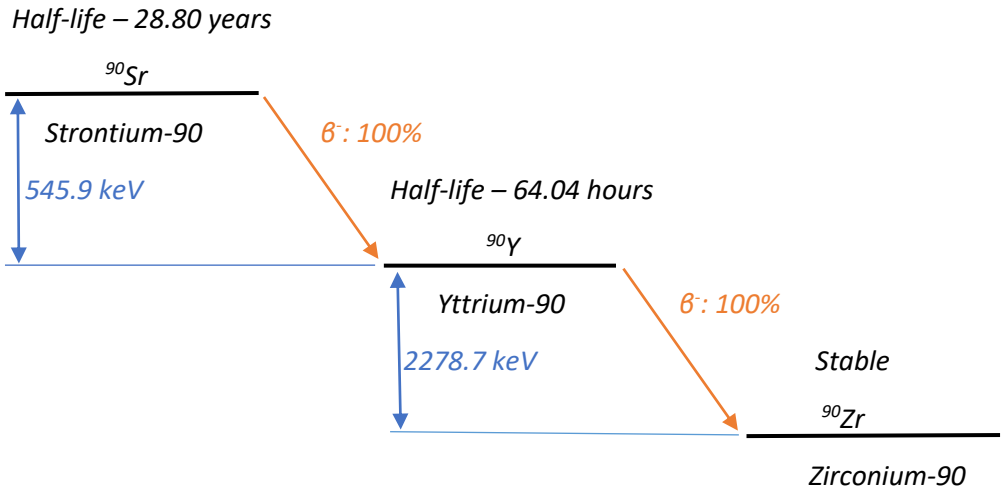

Figure 19. Strontium-90 decay diagram

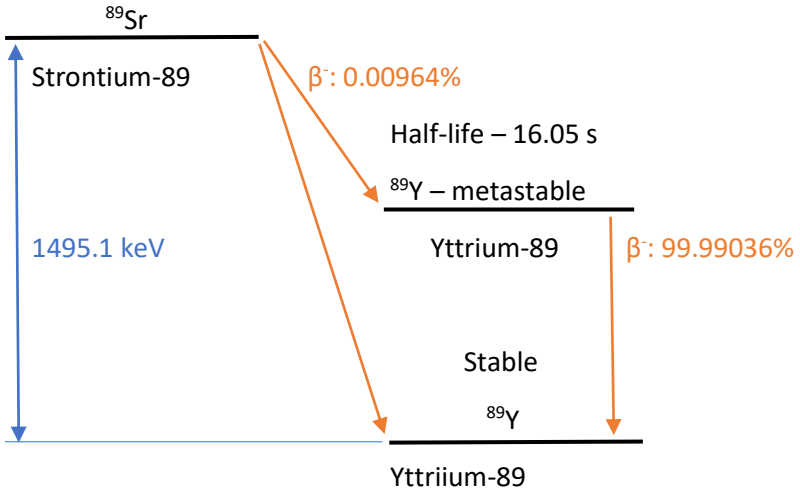

Figure 20. Strontium-89 decay diagram

Radioactive strontium was mainly released into the atmosphere from aboveground testing of nuclear weapons during the period in 1950 – 1963, a severe accident in 1957 at Sellafield, formerly known as Windscale Works, and the nuclear power plant accident at Chernobyl in 1986. At that point, the determination of anthropogenic radionuclides, as e.g., ^{90}Sr started to be studied extensively.

^{90}Sr is one of the most hazardous fission products due to its chemical similarity with calcium and its relatively uniform distribution within the bone volume, where it exchanges with calcium in hydroxyapatite [153] – a major component and an essential ingredient of bones and teeth. Its accumulation to bone tissue may cause damages to the bone marrow [154, 155].

The first measurements of ^{90}Sr in the environment has been routinely undertaken as part of the Project Sunshine [156] in the United States following nuclear weapon tests [157, 158]. The aim of this project was to analyse samples of soil, plants, animals, dairy products, human bone, and other materials from the United States and other parts of the world for levels of ^{90}Sr [159].

At Windscale (currently known as Sellafield, UK), two nuclear reactors were constructed between 1947 and 1951 to produce plutonium and other materials for the United Kingdom's weapons program. The reactors were cooled by air, that was supplied by blowers, filtered and discharged to the atmosphere via 120m stacks [160]. From 1954 to 1957, particles of uranium oxide (fuel), containing fission product activity (^{131}I, ^{137}Cs, ^{90}Sr), were discharged and deposited in the vicinity of the site [161]. Monitoring of milk and other foodstuffs, and autopsy samples of human bone, were analysed for ^{90}Sr at Harwell (Radiobiological Research Unit) or Woolwich (Atomic Energy Authority) from 1954 to 1957 [162, 163]. In October 1957, a fire at the nuclear reactor gave rise to the largest accidental release of radioactive material in the history of the nuclear industry in the UK [160-162, 164-170]. The amount of radioactivity released during the accident is not known precisely, but approximate estimates were made from the measurements of the radioactive iodine deposited on the ground in UK, and from measurements on air filters obtained both in the United Kingdom and continental Europe[165].

The catastrophe of the Chernobyl reactor on 26th April 1986 released a large quantity of many radionuclides during a period of 10 days. The generally northward flow air across western Europe brought detectable activity to eastern France, Belgium and the Netherlands on 1st May and to the United Kingdom on 2nd May. Contaminated air arrived in Greece on 2nd May in the north and on 3rd May in the south [171, 172]. Airborne activity was also reported in Israel, Kuwait, and Turkey in early May.

Long-range atmospheric transport spread the released activity throughout the northern hemisphere. Reported initial arrival times were 2nd May in Japan, 4th May in China, 5th May in India, and 5-6th May in Canada and the United States [173-175].The estimated release of radioactivity from the destroyed reactor reached a total of about 13 Exa Bq (1 Exa Bq = 10^{18} Bq) [176-178].

On the 11th March 2011, an earthquake and subsequent tsunami severely damaged the Fukushima–Daiichi Nuclear Power Plant (FNPP), Japan. The damage to the plant resulted in hydrogen explosions on 12th and 14th March in the Unit 1 and 3 reactors, respectively. The

atmospheric release of radioactive fission products started on 12th March 2011 with a maximum release phase from 14th to 17th March. The radioactivity released was dominated by volatile fission products including isotopes of the noble gases xenon (^{133}Xe) and krypton (^{85}Kr), iodine (^{131}I, ^{132}I), caesium (^{134}Cs, ^{136}Cs, ^{137}Cs) and tellurium (^{132}Te) [179-183]. All of them were transported across the Pacific toward the North American continent and reached Europe despite dispersion and deposition along the route of the contaminated air masses [184]. Airborne fission products (e.g. ^{131}I, ^{137}Cs) were detected in Seattle, USA [185]; Krasnoyarsk, Russia [186]; and more than 150 sampling locations over Europe [184].

The FNPP accident also caused an additional ^{90}Sr pollution. The total amount of ^{90}Sr released into the sea was estimated to be ranging between 0.09 and 9 PBq [187], 1 and 6.5 PBq [188]. The ^{90}Sr activity concentration in surface seawater near the harbour of FNPP was found to be ranging between 0.2 and 400 kBq/m^3 [188].

2.2 Determination of ^{90}Sr

The determination of ^{90}Sr in environmental samples requires radiochemical separation, i.e., to separate the nuclide of interest from other radioactive ions that are present using a precipitation technique, solvent extraction, ion exchange techniques, extraction chromatography or mix of them [189]. Also, it requires purification from some of the sample matrix as well as other interfering radionuclides, particularly of the elements close in the periodic table, prior to radiometric counting [190-192]. For example, the analysis of ^{90}Sr and ^{89}Sr requires separation from calcium-45 (^{45}Ca), Yttrium-91 (^{91}Y), Zirconium-95 (^{95}Zr), Ruthenium-106 (^{106}Ru), Barium-140 (^{140}Ba). These radionuclides are fission products [193-197] and decay with the emission of beta particles which can interfere during the instrument measurement with strontium [198, 199].

The traditional radioanalytical method is based on the precipitation of an acid leached sample in concentrated fuming nitric acid [192, 200, 201]. It is a robust method and has the great advantage of handling large amounts of sample [201, 202]. However, this approach is also a time-consuming and labour-intensive process, and uses fuming nitric acid, which is both hazardous and expensive. This traditional procedure was improved by replacing fuming nitric acid with other chemicals to separate strontium from the sample matrix, for example, sodium hydroxide [203], cation exchange resin associated with cryptand 222 (4,7,13,16,21,24-hexaoxa-1,10-diazabicyclo[8.8.8]-hexacosane [204] (see Figure 21), tributyl phosphate (TBP) [205] (see Figure 22), bis(2-ethylhexyl) phosphoric acid (HDEHP) [206] (see Figure 23), strontium resin – 4,4'(5')-bis(t-butylcyclohexano)-18-crown-6 (see Figure 24) and many others. A review of analytical methods on determination of ^{90}Sr has been published to give an overview about the development of both separative and analytical methods [190, 207]. Specific preparative procedures were also developed such as sample

decomposition, pre-concentration and selective separation of ^{90}Sr using precipitation, ion exchange extraction, solvent extraction and chromatographic extraction.

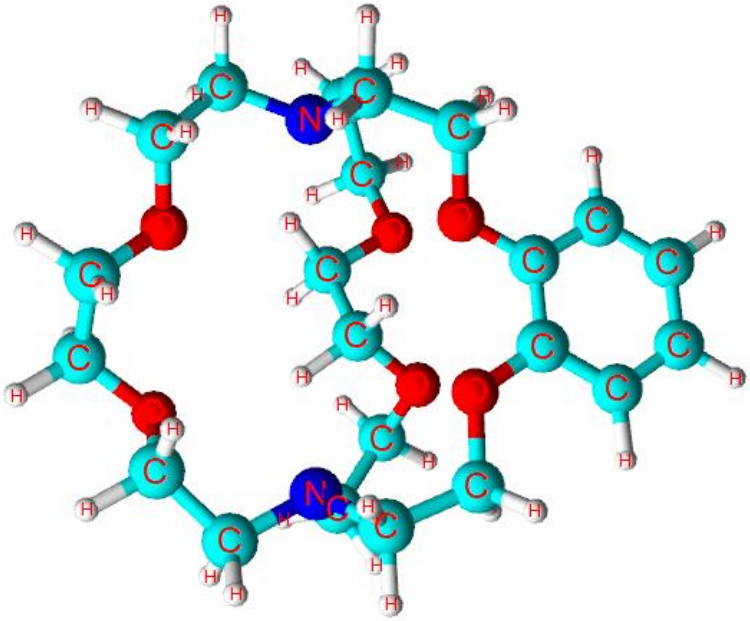

Figure 21. Structure of 4,7,13,16,21,24-hexaoxa-1,10-diazabicyclo[8.8.8]hexacosane (Crypland 222)

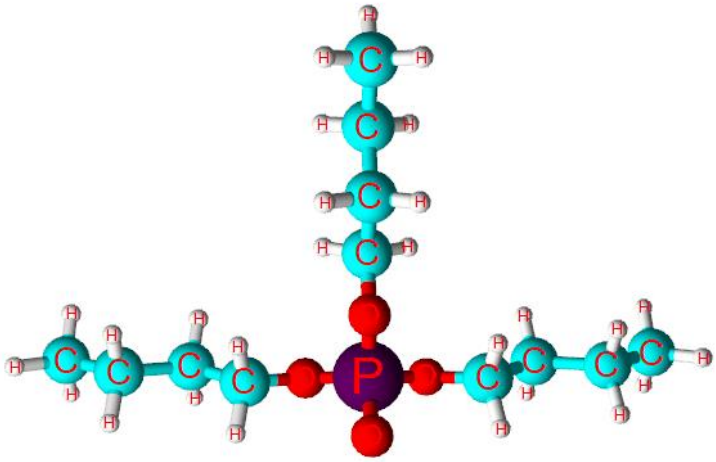

Figure 22. Structure of tributyl phosphate (TBP)

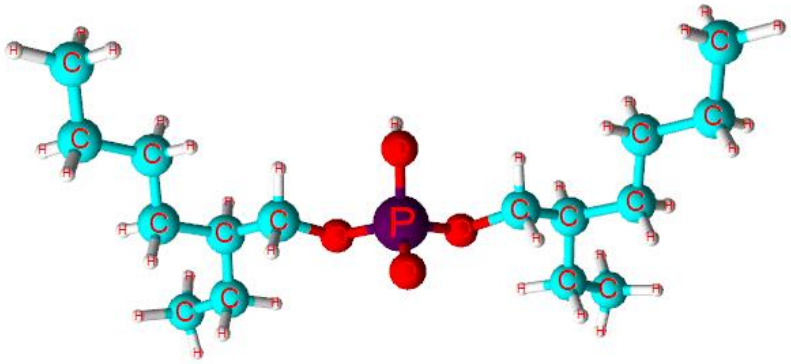

Figure 23. Structure of bis(2-ethylhexyl) phosphoric acid (HDEHP)

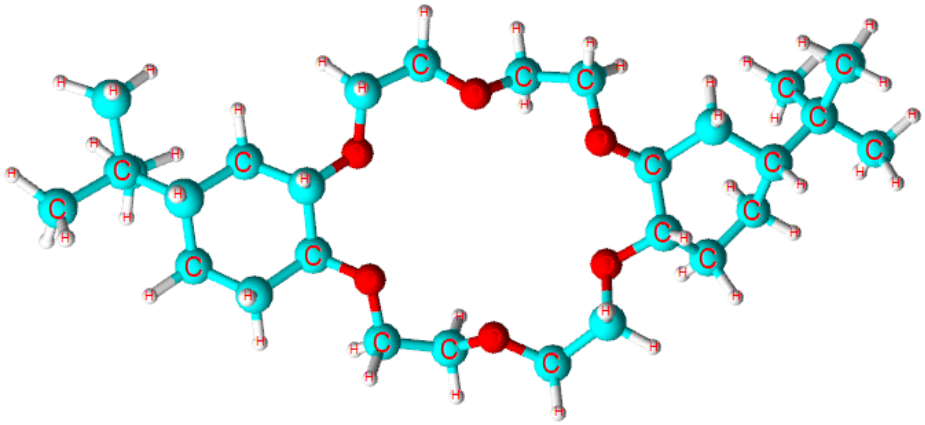

Figure 24. Structure of 4,4'(5')-bis(t-butylcyclohexano)-18-crown-6 (strontium resin)

The strontium resin (4,4'(5')-bis(t-butylcyclohexano)-18-crown-6) is a selective extraction chromatographic material that offered a new option in radiostrontium analysis in 1992 [208]. As an alternative separative method, the solution of 4,4'(5')-bis(tert-butylcyclohexano)-18-crown-6 in 1-octanol is adsorbed on an inert polymeric substrate (Sr-resin, TrisKem International), providing a simple and effective method for the separation of strontium from nitric acid media. This resin showed an excellent selectivity for strontium over a number of alkalis, alkaline earth, and other metal cations e.g., calcium (see Equation 6). Many authors have reported methods using Sr-resin for strontium separation in various environmental samples prior to radiometric measurement [209-219].

$$Sr^{2+}_{(aq)} + Crown_{org} + 2NO^{-}_{3,aq} \leftrightarrow Sr(NO_3)_2 Crown_{org} \quad (6)$$

Scientists have used Sr-resin for ^{90}Sr separation in soil, brown rice, tea and milk powder [210], radioactive waste [211, 215, 219], reference materials (milk powder, whey powder, clover, soil) [212], seawater [213, 219], deer bones [214], meat and fish [216], milk and dairy products (yoghurt, curd cheese, butter) [209, 217, 218]. The use of this particular Sr preparative resin is much simpler, safer, and faster than the traditional fuming nitric acid method.

Usually, ^{90}Sr concentration is determined indirectly by measuring its daughter product, Yttrium-90 (^{90}Y), after ingrowth until secular equilibrium is reached (~15 days). This measuring technique is called Cerenkov counting and is performed by liquid scintillation counting (LSC). Cerenkov counting is a technique used for the determination of medium to high-energy beta emitters (>263 keV E_{max} - in water) in solution using a liquid scintillation counting instrument. Cerenkov radiation is produced by a charged particle (e.g., beta particle) passing through a medium at a velocity greater than the speed of light in that medium [220-223]. This particle can exchange its energy with the molecules of the medium and produces polarisation of solvent molecules along the path of the particle. After the particle has moved on, the energy of polarised molecules de-excites with the emission of electromagnetic radiation. Cerenkov radiation is analogous to the sonic boom produced by aircraft traveling faster than the speed of sound (see Figure 25).

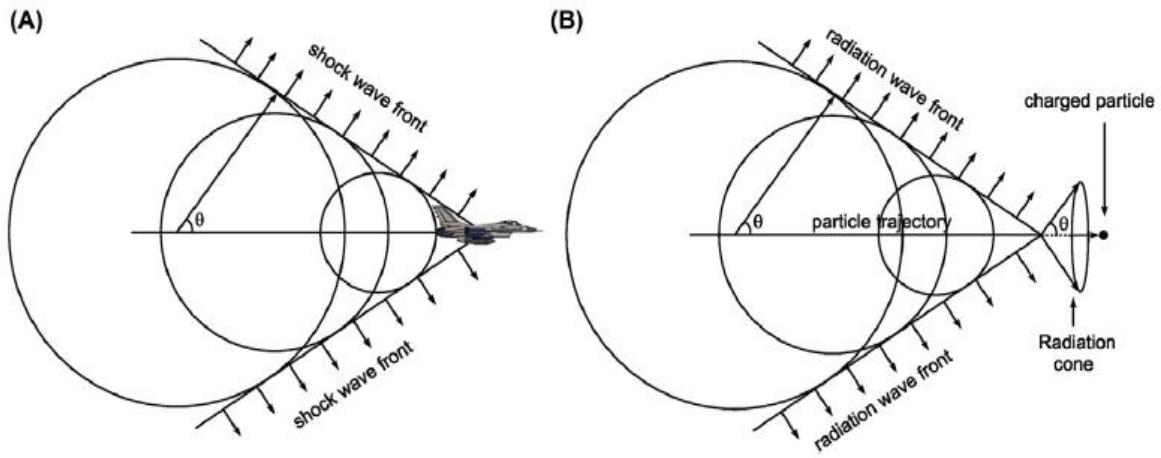

Figure 25. Conical wave fronts produced by (A) a jet traveling at supersonic speed and (B) a charged particle traveling at super-light speed in a transparent medium, i.e., a speed exceeding the speed of light in the medium. The supersonic jet produces a conical shock wave front while the charged particle produces a conical wave front of Cherenkov radiation. The Cherenkov photons are emitted at an angle θ to the particle trajectory [224]

As with sonic boom, the Cerenkov radiation is emitted in a cone with a half-angle, θ. The half-angle is dependent on the velocity of the charge particle including the radiation and refractive index of the medium and is given by the form of Equations (7) or (8):

$$\cos\theta = \frac{c}{vn} \tag{7}$$

where:

c – speed of light; n – refractive index of medium; v – velocity of charge particle.

n – refractive index of is the ratio of the velocity of light of a specified wavelength in the air to its velocity in the examined substance [225].

$$\cos\theta = \frac{1}{\beta n} \tag{8}$$

where:

β- particle relative phase velocity (velocity of particle (v)/speed of light (n);

n - refractive index of medium.

The threshold can be calculated following Equation 9 [226]:

$$E_{min} = 0.511\left[\left(1-\frac{1}{n^2}\right)^{-0.5} - 1\right]\text{MeV} \tag{9}$$

where:

0.511 MeV – rest energy of an electron [227];

n - refractive index of medium.

Cerenkov radiation consists of a continuous spectrum of wavelengths extending from the ultraviolet region into the visible part of the spectrum (negligible in the infra-red region) peaking at about 420 nm [228, 229], so it can be detected by the photomultipliers of the liquid scintillation counter. As both ^{90}Sr (E_{max} = 545.9 keV, half-life = 28.80 years and ^{89}Sr (E_{max} = 1495.1 keV, half-life = 50.57 days) are fission products, they could be both released to the environment from discharges from nuclear facilities or nuclear accident. The efficiency of detecting Cerenkov radiation from ^{90}Sr is around 1% [230]. In comparison, the typical detection efficiency for its daughter product ^{90}Y (E_{max} = 2278.7 keV, half-life = 64.04 hours – as shown in Figure 4 previously) is usually ranging from 40% to 70% [231-237]. The detection efficiency for ^{89}Sr is generally between 20% - 40% in various matrices: water, milk, soil [209, 231, 233]. Thus, the Cerenkov counting method is very often used to determination of ^{90}Sr(^{90}Y) and ^{89}Sr in environmental matrices. However, this approach is limited by the requirement for secular equilibrium (~ 15 days), as described in Figure 26. Secular equilibrium is steady-state condition of equal activities between a long-lived parent radionuclide and short-lived daughter – that is, negligible decay of the parent occurs during numerous half-lives of the daughter. In other words, the daughter must have a relatively short half-live in comparison to the parent radionuclide [238].

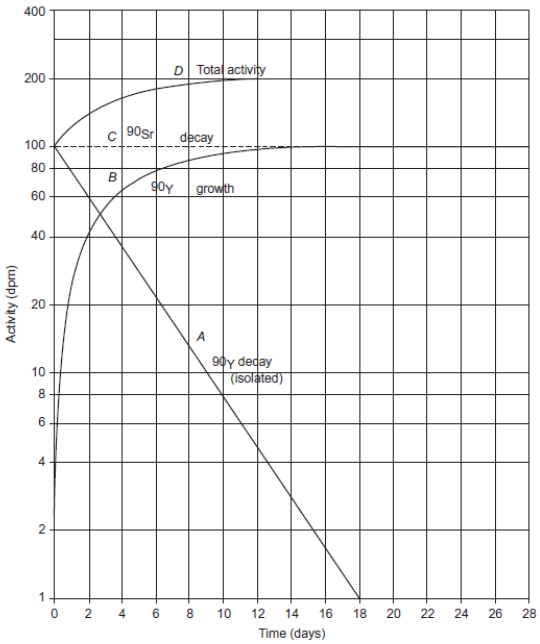

Figure 26. Growth and decay curves following the separation of ^{90}Sr(^{90}Y) in secular equilibrium. (A) Decay of isolated ^{90}Y; (B) Ingrowth of ^{90}Y with ^{90}Sr; (C) Decay of isolated ^{90}Sr; (D) Total activity from isolated ^{90}Sr, representing both ^{90}Sr decay and ^{90}Y growth until secular equilibrium is attained [239]

The relative differences in half-lives of the parent and daughter nuclides may be expressed as (Eq.10):

$$\frac{\lambda_P}{\lambda_D} < \sim 10^{-3} \quad (10)$$

where:

λ_P, λ_D – decay constant of parent and daughter, respectively.

Note: the decay constant is defined as (Eq. 11):

$$\lambda = \frac{0.693}{t_{1/2}} \quad (11)$$

where:

$t_{1/2}$ – half-life of nuclide.

For ^{90}Sr/^{90}Y the ratio of relative difference in half-lives is $2.54\ x\ 10^{-4}$.

The measurements of ^{90}Sr and ^{89}Sr can be performed using a proportional counter and liquid scintillation counter.

A proportional counter work on the principle that as radiation passes through a gas. Radiation ionises the gas as it enters into the chamber, creating free electrons and positively charged ions both called ion pairs. The number of electrons and positively charged ions created is related to the properties of radiation type [240] - β particles for ^{90}Sr, ^{89}Sr [241-243].

The technique of liquid scintillation counting is different and requires placing the sample containing the radioactivity into a glass or plastic container, called a scintillation vial, and adding a special scintillation cocktail containing organic compounds (fluors) dissolved into suitable solvents [244]. The beta particles dissipate its energy by collision in the medium (solvent). The excited solvent molecules can transfer energy to another and also to organic compounds (fluors) which raising it to a state of excitation. This molecule returns to the ground state with emission of photon light which is detected by a photomultiplier tube (see Figure 27). Several examples of liquid scintillation counting (LSC) applications for the determination of ^{89}Sr and ^{90}Sr can be found in the literature [206, 230, 245-247].

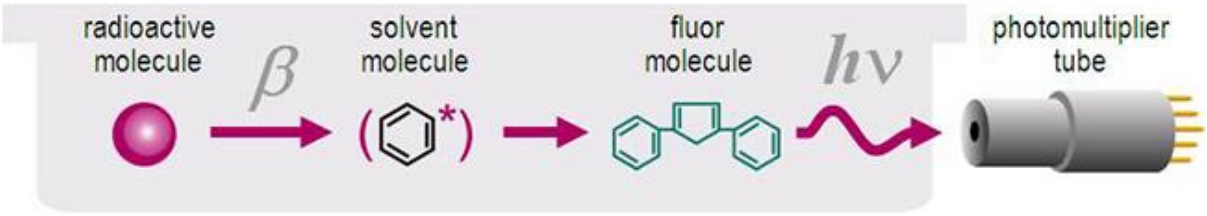

Figure 27. Schematic overview of the scintillation process [226]

The measurement of the number of events (in Cerenkov, gas proportional and liquid scintillation counting) requires the acquisition of data over time. For environmental samples, where level of contaminants (e.g., ^{90}Sr, ^{89}Sr) are generally low or expected to be low, extended counting times – ranging from hours to a full day - are required to accumulate sufficient decay events for statistical measurements and reliable uncertainty estimates. Longer counting times increase the total number of detected events, improving the signal to noise ratio and thereby the relative statistical uncertainty., which ensures more reliable and reproducible quantification of low-level radionuclides. Therefore, long counting times are required to obtain acceptable precision at the environmental levels. However, it may not be totally appropriate in an emergency situation, where a fast response is required, and time is priority in decision making (for consequence management). Therefore, there is a need to develop faster separation method with good and faster data acquisition.

The recent accident at the Fukushima Nuclear Power Plant in March 2011 highlighted the need to develop more efficient analyses for radionuclides in environmental samples in the event of a nuclear accident [243]. Development is essential for emergency response and further for potential routine monitoring to provide quick delivery of analysis. This requirement can be addressed by replacing the traditional separation methods and counting procedures with separation on Sr-resin followed by Inductively Coupled Plasma Mass Spectrometry (ICP-MS) analysis.

2.3 Determination ^{90}Sr by ICP-MS

ICP-MS with collision/reaction cell is an alternative analytical solution to traditional radiometric counting systems for the fast and sensitive determination of some radionuclides [248]. A few papers and reviews have been published describing the detection of ^{90}Sr in various matrices such as natural waters, sediments, plants etc. Detection limits ranging from 0.02 to 0.2 Bq g^{-1} were achieved [72, 249-255]. These concentrations exceed typical levels in target matrices (natural waters, sediments, plants, and aquatic organism) by three orders of magnitude, rendering this approach less suitable for low level analyses compared with conventional radiometric techniques, which offer greater sensitivity and precision for trace radionuclide determination. The use of mass spectrometry techniques for measuring ^{90}Sr suffers mainly from isobaric interferences due to the presence of ^{90}Y (decay product of ^{90}Sr) and ^{90}Zr (decay product of ^{90}Y) in all types of samples. In

addition, high concentrations of natural strontium (stable ^{88}Sr) also present a challenge as it creates a hydride in the ^{90}Sr signal [54, 256] (see Figure 28).

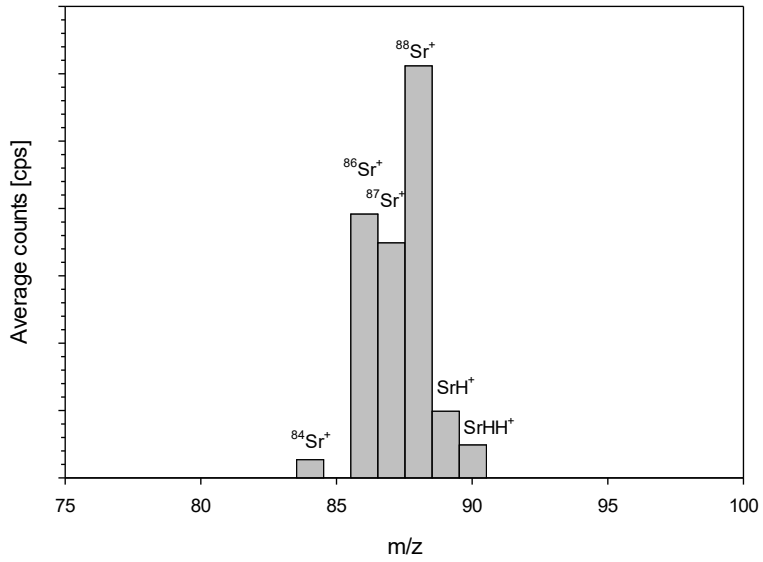

Figure 28. Mass spectra of strontium and strontium hydrides (SrH^+ and $SrHH^+$) (iCAP TQ ICP-MS, 500 ppb solution)

The observed tailing in the ^{88}Sr peak results from the formation of a double hydride species (hydrogen adduct – $SrHH^+$, mass to charge ratio - $m/z = 90$) in plasma environment. Also, single hydride is present (SrH^+, $m/z = 89$). Therefore, these specific isobaric interferences should be investigated as a part of research in optimisation of ICP-MS instrument. In Table 3 are summarized isobaric interferences in determination of ^{90}Sr and the required mass resolution. The primary interference originates from ^{90}Zr, which is present both as a natural isotope in the environment and as a radiogenic product on nuclear decay. Additional interference can arise from molecular ions as a mentioned above as a decay product as well as natural occurrence in environment. Resolving these interferences requires instrumentation with very high mass resolving power ($m/\Delta m$). Separation of ^{90}Sr from ^{90}Zr demands a resolution exceeding ≈30,000, while molecular interferences (e.g., $^{50}V^{40}Ar^+$, $^{50}Ti^{40}Ar^+$) needed higher resolving capability. However, the need for high resolution introduces practical limitations to number of mass spectrometers can achieve this level of performance and their operation is associated with high cost (e.g., SF-ICPMS, TIMS, AMS). Consequently, accurate quantification of ^{90}Sr in environmental and biological samples matrices relies on combination radiochemical purification to remove zirconium and yttrium, with advanced high-resolution mass spectrometric techniques to achieve the discrimination necessary for detection. As an alternative, triple quadrupole ICP-MS (ICP-TQMS) has become increasingly attractive for ^{90}Sr determination, as its use of reaction/collision

gases in tandem quadrupole mode allows effective suppression of isobaric and polyatomic interferences without relying on extreme mass resolution. This approach significantly improves accessibility to these instruments (e.g., lower costs compared to high resolution instruments) and enable accurate quantification of ^{90}Sr in environmental and biological matrices when combined with rigorous radiochemical separation techniques.

Table 3. Potential polyatomic interferences impacting ^{90}Sr quantification by ICP-MS.

Radionuclide	Interference	Required mass resolution $(m/\Delta m)$
^{90}Sr	$^{180}W^{2+}$	1,370
	$^{180}Hf^{2+}$	1,372
	$^{58}Ni^{16}O_2^{+}$	2,315
	$^{74}Ge^{16}O^{+}$	10,765
	$^{52}Cr^{38}Ar^{+}$	19,987
	$^{50}V^{40}Ar^{+}$	49,894
	$^{54}Fe^{36}Ar^{+}$	155,548
	$^{50}Ti^{40}Ar^{+}$	158,287
	$^{90}Zr^{+}$	29,877
	$^{89}Y^{1}H^{+}$	15,148
	$^{78}Se^{12}C^{+}$	9392
	$^{78}Kr12C+$	7106
	$^{76}Ge^{14}N^{+}$	5165
	$^{76}Se^{14}N^{+}$	6179
	$^{76}Se^{16}O^{+}$	9313
	$^{55}Mn^{35}Cl^{+}$	107,416
	$^{53}Cr^{37}Cl^{+}$	76,000
	$^{50}Cr^{40}Ar^{+}$	78,522

Several quadrupole ICPMS instruments used for the determination of ^{90}Sr in environmental and biological matrices and reported in the literature are summarised in Table 4.

Table 4. Comparison of some reported procedures for determination of ^{90}Sr by ICPMS.

Sample	Separation/resin	Instrumentation/ Measurement	Limit of detection pg L^{-1} or pg kg^{-1} (Bq L^{-1} or Bq kg^{-1})	Sample size	Ref.
Urine	Sr phosphate precipitation, TRU-resin, Sr-resin	ICP TQ MS (Agilent 8800)	N/A	1.2-1.6 L	[252]
Soils (Chernobyl samples)	Sr-resin	Quadrupole ICP-MS (Perkin Elmer)	200 (2000)	0.001 kg	[256]
Soils (Fukushima samples)	Sr-resin	Quadrupole ICP-MS (Perkin Elmer)	0.8 (3.9)	N/A	[257]
Sediments Plants Water	Sr-resin	Quadrupole ICP-MS (Perkin Elmer)	100 (500) 40 (200) 3 (15)	0.002 kg 0.002 kg 1 L	[258]
Soils (Fukushima samples)	Sr-resin	ICP TQ MS (Agilent 8800)	0.12 (0.6)	0.001 kg	[68]

For example, the validation of ICP-TAMS in synthetic urine resulted in detection limit 1 Bq per sample[252], with a processing time of 10 hours, indicating satisfactory sensitivity and efficiency for biomonitoring purposes. However, this level of performance is still inadequate for assessing low-level exposures, where enhanced precision and lower detection limits are crucial. In similar vein, for contaminated soils in proximity to Chernobyl[256], ICP-MS has been proposed as a time- and cost-efficient alternative to radiometric methods, achieving detection limits of 20 Bq kg^{-1} following a two-step purification process to reduce ^{90}Zr interference. Nonetheless, this method is inherently less sensitive than radiometric techniques and is limited to samples with relatively high contamination, thereby restricting its effectiveness for the long-term monitoring of environmental contamination. Comparable challenges are observed in the research conducted by Takagai et al. and Taylor et al. [258], where detection limits exhibited significant variability across different matrices, ranging from 513.2 Bq kg^{-1} in sediments to 15.4 Bq L^{-1} in water. This variability highlights the deficiencies in robustness, reproducibility, and cross-matrix reliability of ICP-MS-based methodologies. More recently, Ohno et al.[68] documented a detection limit of 0.6 Bq kg^{-1} in soils from Fukushima, marking one of the most sensitive ICP-MS findings reported to date. However, even this progress does not address the ongoing issue of spectral interference, particularly the peak tailing from ^{90}Zr and isobaric overlap, both of which continue to undermine precision and accuracy.

When comparing ICP-MS to radiometric methods, the distinctions in strengths and weaknesses become more apparent. Radiometric techniques, including liquid scintillation counting and proportional counting, set the standard due to their unmatched sensitivity and precision, frequently achieving detection limits significantly lower than those attainable by ICP-MS. Nevertheless, these methods are characteristically slow, labor-intensive, and expensive, often necessitating weeks for chemical separation and counting.

In contrast, ICP-MS techniques provide swift analysis and lower operational costs, rendering them appealing for high-throughput screening or urgent monitoring. However, these benefits are compromised by their inadequate performance in low-activity samples and their vulnerability to spectral interferences, challenges that radiometric methods do not encounter.

Collectively, these observations underscore critical research deficiencies. Firstly, there is an urgent requirement to devise more effective methods for mitigating or correcting Zr-related interferences, which continue to be the main obstacle to accurate ^{90}Sr quantification via ICP-MS. Secondly, enhanced standardization and validation across various sample types are necessary to tackle the inconsistencies noted in different environmental matrices. Thirdly, methodological advancements must focus on bridging the sensitivity gap with radiometric techniques, especially for applications related to low-level contamination or long-term monitoring. Addressing these issues will be crucial for ICP-MS-based methods to progress beyond mere rapid screening and develop into dependable alternatives that can facilitate regulatory monitoring and public health risk evaluations.

Spectral interference is a serious intrinsic limitation of ICP-MS because it leads to inaccurate determination of the analyte concentration. Spectral interference refers to the signals generated by isobaric and polyatomic species which overlap with the mass to charge (m/z) ratio of the analyte being monitored. These overlapping signals result in an overestimated value compared to the genuine analyte concentration. Isobaric overlap is due to the monoatomic species that share the same m/z ratio as the target analyte (e.g. $^{58}Fe^{+}$ and $^{58}Ni^{+}$). Polyatomic interfering species may come from plasma gas, plasma-entrained atmospheric gas (forming the C (carbon adduct), H (hydride adduct), N (nitrogen adduct), O (oxygen – oxides) and Ar (argon)-containing adduct), acids or solvents (generating the oxide, hydroxide, C, Cl (chloride) or S (sulphur) based polyatomic adduct), or buffers and salts (yielding the S (sulphur) and P (phosphorous) containing adduct) in the sample matrix. Furthermore, formation of these interfering complex species can also originate from a combination of some elements present in the plasma gas, acids, or solvents

with that from the sample matrix, which makes the situation more complicated and difficult to predict [63]. Careful considerations must be given to every analysis in order to determine the most appropriate method for accurate measurement.

The primary limitation affecting ICP-MS measurement of ^{90}Sr is an isobaric interference from the presence of stable ^{90}Zr as mentioned above – a naturally occurring radioisotope, and its decay product, ^{90}Y (see Figure 19). This interference can be selectively removed or shifted in m/z ratio prior to mass spectral analysis by the addition of specific reagent gases to collision/reaction cell - use of the oxygen (O_2) in the reaction cell of ICP-MS for the resolution of the $^{90}Y/^{90}Sr$ and $^{90}Zr/^{90}Sr$ interferences [259] – expressed in equations 37 to 39. Many experimental studies using oxygen reaction with standard analytes have been published to show the efficiency of reaction with yttrium and zirconium [259-261]. Therefore, optimisation of collision/reaction cell for reaction of ^{90}Y, ^{90}Zr with O_2, leaving ^{90}Sr free of interference, is essential for the determination of this radionuclide.

$$^{90}Sr + O_2 = SrO + O \qquad \text{slow} \qquad (37)$$

$$^{90}Y + O_2 = YO + O \qquad \text{fast} \qquad (38)$$

$$^{90}Zr + O_2 = ZrO + O \qquad \text{fast} \qquad (39)$$

In the study conducted by Eiden *et al.* [259], it was shown that Y and Zr reacted with O_2 over two orders of magnitude faster than Sr. It was also reported that ^{90}Sr could easily be detected in the presence of a 100-fold excess of either ^{90}Y or ^{90}Zr (although ^{90}Y arises from decay of ^{90}Sr, so that ^{90}Y cannot exceed the concentration of ^{90}Sr). Further details on these reactions can be found in the studies undertaken by Tanner *et al.* [262], Favre *et al.* [263], Narukawa and Chiba [264]. The mechanism of oxygenation of ions was explained by using the theoretical calculation for reactions between elemental ions and O_2. However, the O_2 flow in collision/reaction cell is not completely optimised in scientific literature for ^{90}Sr analysis. Thus, this particular gap still needs be explored and investigated.

Also, the lower ionisation potential of Sr in comparison to Zr (5.7eV and 6.8eV, respectively) suggests the plasma condition could be further investigated and optimised.

2.4 ^{90}Sr in milk and seawater samples by ICP-MS

Milk is a widely consumed food product for adults and children. Furthermore, milk is used widely in the food industry for the production of other foods e.g., cheese, powder milk, yogurt. Quantities

of household purchase of milk in the UK per week was 1.635 litres in 2022 year (www.gov.uk). Because of its nutritional importance and widespread consumption, analysis of milk plays an important role in monitoring of radioactivity in food. In the UK, the Radioactivity in Food and Environment (RIFE) programme monitors radioactivity in the environment and in the diet of people. The report brings all the results of monitoring of radioactivity in food and the environment (Radioactivity in food and the environment (RIFE) reports; www.gov.uk).

However, before any development of sample preparation and analysis of radiostrontium by ICPMS, the determination of natural strontium in sample matrices is required. This analysis provides an information for potential interferences coming from natural strontium content (Figure 28) and helps to design the extraction methodology using a strontium resin (4,4'(5')-bis(t-butylcyclohexano)-18-crown-6), with a reference uptake of 8 mg of strontium per 1 g of resin. In this study, a batch of milk and sea water samples were analysed to determine the concentration of natural strontium.

2.5 Aim

The assessment of ^{90}Sr in both environmental and biological samples is an essential endeavour within the realms of nuclear safety, environmental surveillance, and the evaluation of public health risks. As a long-lived fission product characterized by high radiotoxicity, ^{90}Sr presents considerable dangers due to its bioaccumulation in bone tissue and its potential transfer into the food chain through contaminated soil, water, and agricultural products. Despite its significance, the precise quantification of ^{90}Sr continues to pose challenges. Traditional radiometric methods, while exhibiting high sensitivity, are often labour-intensive, time-consuming, and expensive, rendering them impractical for swift or extensive monitoring. Conversely, ICP-MS techniques provide advantages in terms of speed and cost; however, they are hindered by notable analytical drawbacks, particularly spectral interferences caused by isobaric overlap and peak tailing of ^{90}Zr, which significantly undermine accuracy at low activity levels.

The main goal of this research was to optimize essential instrumental parameters, such as plasma conditions, extraction lens settings, and voltages for the first quadrupole entry lens, along with the gas flow in the collision/reaction cell, to improve the precision of ^{90}Sr measurement. Special attention was given to tackling the interference issues that have previously obstructed accurate quantification in ICP-MS studies. An additional objective was to assess and identify the ideal gas flow for the desolvation system (He and N_2), which significantly affects sensitivity, background suppression, and the ability to handle complex sample matrices. These optimized parameters were then utilized for the quantification of extremely low concentrations of

radiostrontium in milk and seawater - two matrices of environmental and biological importance that pose significant analytical challenges due to their elevated salt content and the presence of interfering elements. By addressing these issues, this study aims to reconcile the rapid yet interference-sensitive characteristics of ICP-MS with the sensitivity offered by radiometric methods, thus enhancing ICP-MS as a more dependable and effective instrument for monitoring ^{90}Sr in both environmental and biological settings.

It is expected that the enhanced ICP-MS parameters will greatly enhance the accuracy, precision, and sensitivity of ^{90}Sr measurements in complex matrices. This research seeks to illustrate that ICP-MS can act as a swift, economical, and dependable substitute for radiometric techniques in the determination of low-level ^{90}Sr, representing a significant methodological progress for the environmental and biological assessment of radiostrontium contamination.

2.6 Reagents

All standard solutions were prepared from elemental stock solutions in 1% HNO_3 (Aristar® VWR Chemicals). Hight purity de-ionised water (resistivity higher than 18.2 MΩ) produced from Q-Pod Millipore System (Merck, York, UK). The standard solution (1000 mg L^{-1}) of Sr, Y, Zr and Tb were sourced from VWR Chemicals.

Other reagents such as oxalic acid ($C_2H_2O_4$), ammonia (NH_3) and hydrogen peroxide (H_2O_2) were sourced from VWR Chemicals. The strontium resin (4,4'(5')-bis(t-butylcyclohexano)-18-crown-6) was provided by TrisKem International (France).

The study utilized materials that comprised a standard of stable ^{84}Sr in carbonate form, exhibiting an isotopic enrichment of 82.81%, which was sourced from Isoflex (USA). Additionally, a certified ^{90}Sr standard solution was obtained from Amersham PLC (UK). To ensure validation and facilitate method development, a certified reference material (CRM) of milk powder (CRM 7512-a) was utilized, imported from the National Metrology Institute of Japan and supplied by LGC Standards (UK). These standards and reference materials were instrumental in providing a foundation for precise calibration and quality assurance throughout the duration of the study.

2.7 Instrumentation

All measurements were performed using the Thermo Fisher iCAP ICP – Triple Quadrupole Mass Spectrometer (iCAP ICP-TQMS) controlled by computer with the Qtegra software installed. The instrument was equipped with a standard sample introduction system consisting of a MicroMist nebulizer and baffled cyclonic spray chamber. However, some modifications were made to the standard setup. Instead of a nickel sample cone and skimmer cone with high matrix skimmer

cone insert, a platinum tip sample cone and skimmer cone with high sensitivity skimmer cone insert were used. Samples were introduced directly into the ICP-MS using an ASX-520 autosampler with the standard peristaltic pump and tubing (internal diameter of 1.02 mm).

The Aridus 3 Desolvating Nebulizer System, equipped with a self-aspirating C-Flow PFA nebulizer operating at a flow rate of 100 µL min^{-1} (Teledyne Cetac Technologies), was integrated upstream of the iCAP ICP-TQMS system and controlled via The Aridus Link software. This setup was employed to enhance sample introduction efficiency, reduce solvent load, and improve signal stability during ^{90}Sr analysis. A key objective of this study was to evaluate and determine the optimal gas flow for the desolvation system, using helium (He) and nitrogen (N_2), as these parameters critically influence instrument sensitivity, background suppression, and the capability to accurately analyse complex sample matrices. Optimising these conditions was essential to maximise detection performance while minimising matrix-related interferences, particularly in challenging biological and environmental samples such as milk and seawater.

A multiwave 3000 microwave sample preparation system (Anton Paar, Graz, Austria) equipped with a HF100 rotor was used to digest all milk and seawater samples. The system was equipped with 16 high-pressure PTFE-TFM vessels, each with an internal volume of 100 ml and manufactured to resist a maximum pressure and temperature of 40 bars and 240°C, respectively.

A Hidex 300 SL Super Low Level liquid scintillation counter controlled by MicroWin software was also used to compare results obtained from the described ICP-TQMS method. This latter instrument was equipped with three low level photomultipliers, an active guard for lower background, an external source, a cooling system and a 40-position for 20 mL scintillation vials.

Hotplate with stirring, water bath, Millipore filtration apparatus with coarse porosity frit to accommodate 47 mm filter, 10 mL plastic columns were also used for extracting ^{90}Sr from milk and seawater samples via oxalate precipitation.

2.8 Methodology

In this study, a thorough examination of essential instrumental parameters was performed to enhance the efficacy of the ICP-TQMS system for ^{90}Sr analysis. The parameters investigated encompassed plasma conditions, which affect ionisation efficiency and overall sensitivity; optics voltages, which influence ion focusing and transmission through the instrument; collision and reaction cell gas flow rates, which are vital for reducing spectral interferences such as isobaric overlap from ^{90}Zr; and desolvation system gas flow, which is crucial for improving signal stability, decreasing background noise, and increasing tolerance to complex sample matrices. By meticulously assessing and refining these parameters, the research sought to optimise detection

sensitivity, accuracy, and reproducibility in the quantification of low-level ^{90}Sr in difficult biological and environmental samples.

Radio frequency power generator, induction coil and gas are used to form Inductively Coupled Plasma (ICP). Therefore, RF Power (W) of generator and nebulizer gas flow (L min^{-1}) are the main parameters for optimising the plasma condition.

The extraction lens and first quadrupole extraction lens voltage are also very important parameters for optimising a response from the instrument, as this is where separation of positive ions from neutral species, photons, and electrons occurs and where these same ions are transferred to the mass analyzer.

The collision/reaction cell gas are used to remove or react with interference(s). Oxygen was used to react with yttrium, zirconium, and hydrogen for removing hydrogen adduct. Therefore, optimised flow rates of these two collision/reaction gases were also important to establish.

Argon (Ar) and nitrogen (N_2) gases were used in the Aridus 3 Desolvation Nebulizer System to remove solvent from the sample analyte and improve analyte sensitivity. These additional gases flow rates were also considered in this study.

First sets of experiments focused on the plasma optimisation conditions, by gradually increasing the RF power between 1,000 and 1,600 W and assessing the m/z response at different nebulizer, as described in Table 5.

Table 5. Set of experiments for optimisation

No.	Nebulizer Gas Flow (L min^{-1})	RF Power (W)
1	0.90	1000 - 1600
2	0.95	1000 - 1600
3	1.00	1000 - 1600
4	1.05	1000 - 1600
5	1.10	1000 - 1600
6	1.15	1000 - 1600
7	1.20	1000 - 1600
8	1.25	1000 - 1600

The second set of experiments emphasised on the extraction lens and first quadrupole extraction lens voltage and was performed using the voltage of both extraction lens and the first quadrupole extraction lens as variables, to establish the highest m/z response of element.

The extraction lens and first quadrupole extraction voltages were both increased in 10 volts step and from the different m/z responses from ^{88}Sr were recorded.

The third set of experiments was concentrated on the collision/reaction cell gas flow rates, looking at different oxygen and helium gas flow rates and efficiency for removing isobaric interferences. The oxygen flow rate was increased from 0.01 to 0.50 ml min^{-1} in 0.01 ml min^{-1} steps and thereafter in 0.05 ml min^{-1} steps until a maximum of 1.00 ml min^{-1}. The helium flow rate was increased from 0.1 to 3.0 ml min^{-1} in 0.1 ml min^{-1} steps.

In the fourth set of experiments, different flow rates of argon (Ar) and next nitrogen (N_2) in the desolvation system (Aridus 3) were also tested to establish the highest m/z response of the ICPMS for ^{88}Sr. The argon and nitrogen flow rates in the Aridus 3 desolvation system were increased from 1.0 to 5.0 L min^{-1} and from 0.2 to 5.0 L min^{-1}, respectively.

A 0.5 mg L^{-1} (50ppb) solution of Sr nuclide in 1% nitric acid was used in the first and second sets of experiments. A 0.5 mg L^{-1} (50ppb) solution of Sr, Y, Zr nuclides in 1% nitric acid and a 0.05 mg L^{-1} (5ppb) solution of Sr nuclide in 1% nitric acid were used in the third and fourth sets of experiments, respectively. In each experiment, an additional 0.001 mg L^{-1} (1ppb) solution of terbium (Tb) nuclide in 1% nitric acid was used as instrumental internal standard. Solutions were introduced into the plasma using an ASX-520 autosampler and data were collected for 60 seconds with 1,000 sweeps for each individual m/z value.

To establish the natural strontium level in milk and seawater, samples were digested using a multiwave 3000 the microwave system prior to ICPMS using 5 g of material and 10 mL of HNO_3. The digestion program is described in Table 6.

Table 6. Microwave digestion program

Temperature [°C]	Ramp [minutes]	Hold [minutes]
120	10	10
200	10	20

In order to demonstrate the accuracy of the methodology, 0.5 g of milk powder (CRM 7512-a) from the National Metrology Institute of Japan was also used. This material is certified for 13 elements as shown in Table 7:

Table 7. Certified values of CRM 7512-a

Element	Certified value [g/kg]	Uncertainty [g/kg]
Ca	8.65	0.38
Fe	0.104	0.007
K	8.41	0.33
Mg	0.819	0.024
Na	1.87	0.09
P	5.62	0.23
Element	Certified value [mg/kg]	Uncertainty [mg/kg]
Ba	0.449	0.013
Cu	4.66	0.23
Mn	0.931	0.032
Mo	0.223	0.012
Rb	8.93	0.31
Sr	5.88	0.20
Zn	41.3	1.4

After digestion, solutions were transferred from vessel to 50mL centrifuge tubes and added high purity water up to 20mL of total volume. The solution were then diluted in 1% nitric acid prior to analysis.

To assess the accuracy and reliability of the developed method, various sample matrices were spiked with known quantities of ^{90}Sr. This strategy facilitated a direct evaluation of the method's ability to recover and accurately measure radiostrontium under controlled conditions. By contrasting the measured ^{90}Sr concentrations with the known spiked quantities, the research successfully validated both the sample preparation techniques and the optimized ICP-TQMS instrumental parameters, which included plasma conditions, optics voltages, collision/reaction gas flow, and desolvation gas flow. This spiking approach established a solid framework for method validation, ensuring that the analytical protocol could consistently detect and quantify very low concentrations of ^{90}Sr in complex matrices such as milk and seawater.

The standard solution at 1 ppb concentration of ^{159}Tb was employed as an instrumental internal standard in the ICP-MS analysis to account for potential signal fluctuations and matrix-induced

variations during measurement. By introducing a known concentration of ^{159}Tb into all samples and standards, variations in sample introduction efficiency, plasma stability, and instrumental sensitivity could be corrected, thereby improving the accuracy, precision, and reproducibility of ^{90}Sr quantification. The choice of ^{159}Tb as the internal standard was based on its mass proximity to strontium, its minimal natural abundance in the samples, and its chemical and ionisation behaviour in the plasma, which ensures it effectively monitors and compensates for instrumental drift without interfering with the analyte signal.

A standard solution of ^{84}Sr, prepared at a concentration of 10 ppm, was employed as a recovery standard throughout the analytical procedure in order to monitor method performance. The recovery standard served to quantitatively evaluate the accuracy and precision of the measurements.

Three hundred mL of raw milk from local farm (310 g, 1.033 g mL^{-1}) and 300 mL of seawater from North Sea (308 g, 1.026 g mL^{-1}) were spiked with 10 ppm of ^{84}Sr recovery standard. Two hundred mL of concentrated HNO_3 and a known amount of ^{90}Sr were then added to the samples. The different spiked quantities are detailed in Table 8. Each solution was then heated on a hot plate for 2h, stirred continuously using a magnetic stirrer and then filtered through paper filter (0.45 µm Whatman). One hundred mL of saturated $C_2H_2O_4$ was then added to the mixtures and the pH was adjusted to 4, using concentrated NH_3 for oxalate precipitation (SrC_2O_4). Each solution was then filtered again through a 0.45 µm Whatman filter paper and transferred to a 50 mL beaker. Ten mL of concentrated HNO_3 was added along with drop-wise addition of concentrated H_2O_2, until the oxalate precipitate redissolved in the solution. Each solution was then heated at 70 °C using a water bath to remove any excess of H_2O_2. Each solution was then loaded onto a Sr column (4 mL of resin ~ 1 g in 10 mL column), preconditioned with 8 M HNO_3, washed with 100 mL of 8 M HNO_3 and strontium was eluted from the column using 30 mL of 0.05 M HNO_3[208]. The concentration factor was therefore considered to be equal to 10 (i.e., from an initial volume of 300 mL to 30mL). Twenty mL of solution was finally transferred to a vial with 1 ppb ^{159}Tb for ICPMS analysis. For comparison purposes, the remaining 10 mL was transferred to a 20 mL plastic scintillation vial and stored for 21 days to rich secular equilibrium prior to liquid scintillation counting using the Cerenkov counting method. Each sample was counted for 3600 seconds using a Hidex 300SL liquid scintillation counter.

Table 8. ^{90}Sr spiked levels tested

Spiked level	Activity concentration [Bq L^{-1}]	Concentration [pg g^{-1}]
0	0	0
1	50	0.0098
2	100	0.0196
3	250	0.0491
4	500	0.0981
5	1000	0.1962
6	2000	0.3925
7	3000	0.5887

The set of ^{90}Sr standard concentrations used for the instrument calibration is detailed in Table 9.

Table 9. Set of ^{90}Sr calibration standard concentrations

Standard Level	^{90}Sr standard concentrations [Bq L^{-1}]	Concentration [pg g^{-1}]
1	25.11	0.0049
2	50.23	0.0099
3	125.56	0.0246
4	251.13	0.0493
5	502.26	0.0986
6	2511.29	0.4928
7	5022.57	0.9856
8	10045.14	1.9711
9	20090.28	3.9423

2.9 ICP-TQMS optimisation parameters for the detection of ^{90}Sr

2.9.1 Plasma condition optimisation

The solution of strontium standard at concentration of 50 ppm introduce to instrument plasma. The m/z signals from four natural isotopes of strontium: ^{84}Sr, ^{86}Sr, ^{87}Sr, ^{88}Sr as well as the $m/z = 89$ & 90 signals from hydrogen (^{89}SrH) and dihydrogen (^{90}SrHH) formations of ^{88}Sr were collected. Average counts for the four natural strontium isotopes, using varying carrier gas flow rates and RF

power, are presented in Table 10. The highest responses were observed when selecting 1.10 L min^{-1} carrier gas and a RF Power of 1600 W (shown in bold). A correlation between average counts at $m/z = 88$ (^{88}Sr) and nebuliser flow rates is also presented in Figure 29.

Table 10. Average counts obtained for the four natural isotopes of strontium using different carrier gas flow rates and applying different RF power

No.	Carrier Gas [L min^{-1}]	RF Power [W]	m/z=88 [Avg. Count]	m/z=84 [Avg. Count]	m/z=86 [Avg. Count]	m/z=87 [Avg. Count]
1	0.90	1000	4313731	31059	541950	387534
2	0.95	1050	5899183	41670	735324	531692
3	1.00	1200	6726313	47033	827528	598898
4	1.05	1350	7750227	53418	947780	683224
5	**1.10**	**1600**	**8584904**	**58744**	**1038625**	**752079**
6	1.15	1600	5941965	39872	710018	517002
7	1.20	1600	2714848	17834	327548	238406
8	1.25	1600	1374114	8394	156168	113860

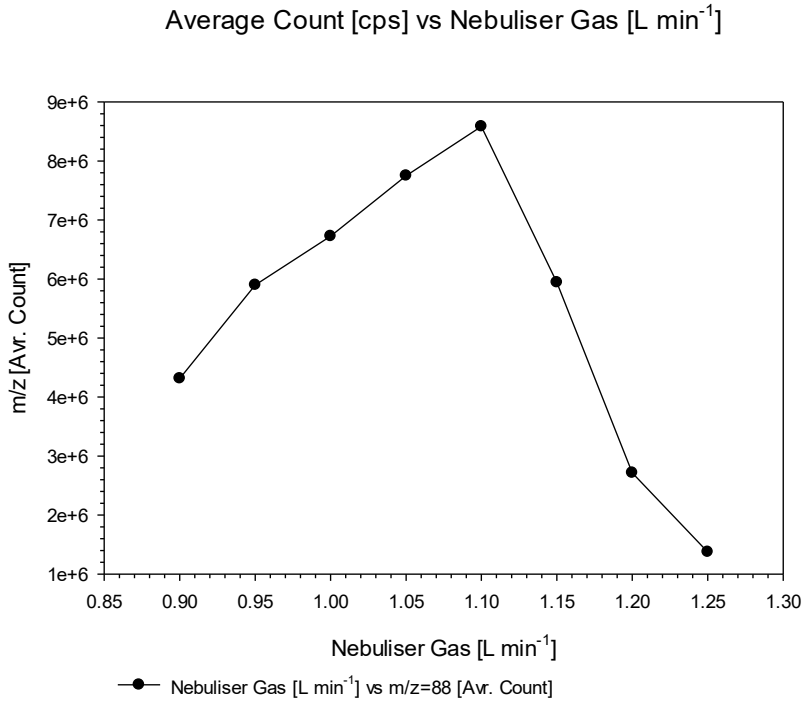

Figure 29. Correlation between average count for $m/z = 88$ (^{88}Sr) and nebuliser gas flow rate at optimised RF Power of 1600W

The individual abundance of the four natural strontium isotopes were calculated and compared with reference values from the literature[97] as a quality assurance. All results are shown in Table 11.

Table 11. Calculated abundance of strontium isotopes at optimum plasma condition

No.	^{84}Sr [%]	^{86}Sr [%]	^{87}Sr [%]	^{88}Sr [%]
1	0.59%	10.28%	7.35%	81.79%
2	0.58%	10.20%	7.38%	81.84%
3	0.57%	10.09%	7.30%	82.03%
4	0.57%	10.05%	7.24%	82.15%
5	0.56%	9.95%	7.21%	82.28%
6	0.55%	9.85%	7.17%	82.43%
7	0.54%	9.93%	7.23%	82.30%
8	0.51%	9.45%	6.89%	83.15%
Reference Values (ref)	0.56	9.87	7.04	82.53

Ratios of both hydro and dihydro formations of ^{88}Sr to ^{88}Sr were also assessed and results are presented in Table 12.

Table 12. Average counts of hydrogen and dihydrogen formations of ^{88}Sr and ratios against m/z =88 average counts

No.	Carrier Gas [L min^{-1}]	RF Power [W]	m/z = 88 [Avg. Count]	m/z = 89 [Avg. Count]	m/z = 90 [Avg. count]	m/z 89/88 ratio	m/z 90/88 ratio
1	0.90	1000	4313731	260	268	6.05E-05	6.21E-05
2	0.95	1050	5899183	234	330	3.97E-05	5.60E-05
3	1.00	1200	6726313	280	399	4.17E-05	5.94E-05
4	1.05	1350	7750227	320	469	4.13E-05	6.06E-05
5	**1.10**	**1600**	**8584904**	**424**	**673**	**4.94E-05**	**7.85E-05**
6	1.15	1600	5941965	255	343	4.30E-05	5.78E-05
7	1.20	1600	2714848	142	81	5.26E-05	3.01E-05
8	1.25	1600	1374114	98	11	7.13E-05	8.52E-06

As shown in Table 12, all ratios m/z 89/88 and 90/88 were found to be very low, ranging from 3.97E-05 to 7.13E-05 and 3.01E-05 to 8.52E-06, respectively.

2.9.2 Extraction lens voltage optimisation

In this second experiments, the optimised parameters obtained from experiment 1 were fixed (i.e., 1.10 L min^{-1} carrier gas and a RF Power of 1600W) and different voltages were applied to the extraction lens to test the instrumental response at $m/z = 88$. The results are presented in Table 13 and showed an optimal response when setting the extraction lens voltage at -210V. A correlation between average counts $m/z = 88$ (^{88}Sr) and the extraction lens voltage is also displayed in Figure 30.

Table 13. Summary of average counts and extraction lens voltage for optimised values

No.	Carrier Gas [L min^{-1}]	RF Power [W]	Extraction Lens [V]	m/z = 88 [Avg. Count]	m/z = 89 [Avg. Count]	m/z = 90 [Avg. Count]	m/z 89/88 ratio	m/z 90/88 ratio
1	1.10	1600	-260	5331109	228	1074	4.28E-05	2.01E-04
2	1.10	1600	-250	5727111	240	1149	4.19E-05	2.01E-04
3	1.10	1600	-240	5600603	213	1163	3.80E-05	2.08E-04
4	1.10	1600	-230	5743455	205	1253	3.57E-05	2.18E-04
5	1.10	1600	-220	5813233	209	1312	3.60E-05	2.26E-04
6	**1.10**	**1600**	**-210**	**5823415**	**199**	**1317**	**3.42E-05**	**2.26E-04**
7	1.10	1600	-200	5686426	176	1250	3.10E-05	2.20E-04

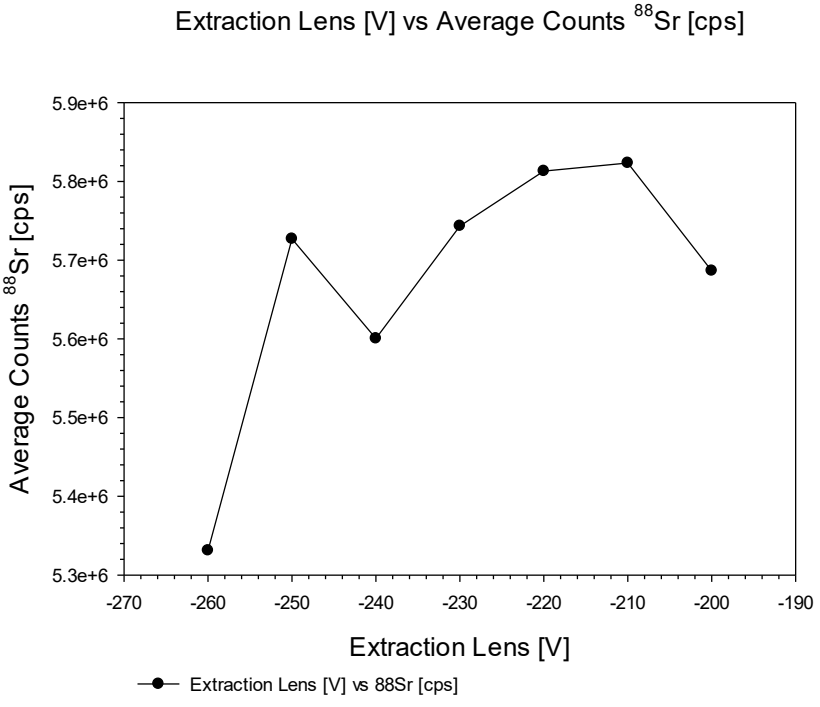

Figure 30. Correlation between average count at $m/z = 88$ (^{88}Sr) and extraction lens voltage

Different voltages were also applied to the first quadrupole extraction lens, and the optimal response was obtained when using -150V, as shown in bold in Table 14. A correlation between average counts $m/z = 88$ (^{88}Sr) and first quadrupole extraction lens voltage is also displayed in Figure 31.

Table 14. Summary of average counts and extraction lens voltage for optimised values

No.	Carrier Gas [L min^{-1}]	RF Power [W]	First Quadrupole Extraction Lens [V]	m/z = 88 [Avg. Count]	m/z = 89 [Avg. Count]	m/z = 90 [Avg. Count]	m/z 89/88 ratio	m/z 90/88 ratio
1	1.10	1600	-210	5255623	166	821	3.16E-05	1.56E-04
2	1.10	1600	-200	5492360	181	962	3.30E-05	1.75E-04
3	1.10	1600	-190	5568546	185	867	3.32E-05	1.56E-04
4	1.10	1600	-180	5598428	181	887	3.23E-05	1.58E-04
5	1.10	1600	-170	5650020	189	911	3.35E-05	1.61E-04
6	1.10	1600	-160	5649473	191	923	3.38E-05	1.63E-04
7	**1.10**	**1600**	**-150**	**5786485**	**203**	**1152**	**3.51E-05**	**1.99E-04**
8	1.10	1600	-140	5439730	192	894	3.53E-05	1.64E-04
9	1.10	1600	-130	5237370	184	881	3.51E-05	1.68E-04
10	1.10	1600	-120	5157603	183	878	3.55E-05	1.70E-04
11	1.10	1600	-110	4840437	182	858	3.76E-05	1.77E-04
12	1.10	1600	-100	4432636	173	875	3.90E-05	1.97E-04

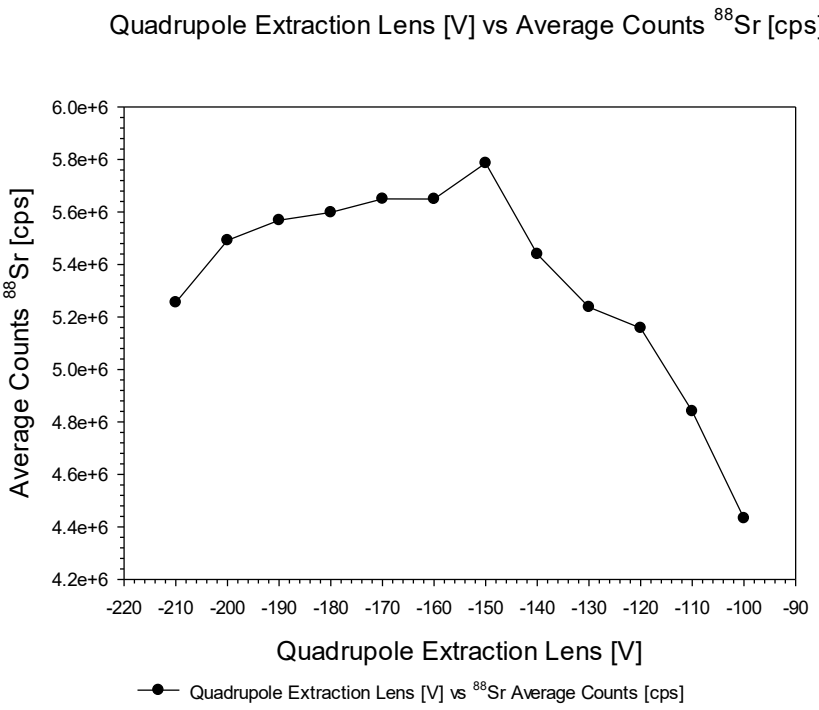

Figure 31. Correlation between average count for $m/z = 88$ (^{88}Sr) and first quadrupole extraction lens voltage

Table 13 and 14 show that the ratios m/z 89/88 decreased to 3.42E-05 and 3.51E-05, respectively, after plasma optimisation (Table 12), indicating enhanced suppression of hydride formation through further parameter refinement. Conversely, ratios m/z 90/88 increased by an order of magnitude from 10E-05 (Table 12) to 10E-4 (Table 13 and 14), indicating a differential effect of the optimisation on isotopic interference. This observation can be interpreted in two ways: either the further parameter optimisation favoured dihydride formation under the optimal conditions, or the optimisation enhanced the sensitivity of the measurements at m/z 90.

2.9.3 Oxygen gas flow rate optimisation for the removal of isobaric yttrium and zirconium interferences

Signals from oxygen products (oxides) at $m/z = 105$ ($^{89}Y^{16}O$), $m/z = 106$ ($^{90}Zr^{16}O$) and double oxides at $m/z = 121$ ($^{89}Y^{16}O^{16}O$), and $m/z = 122$ ($^{90}Zr^{16}O^{16}O$) were also measured (Figure 32). The highest efficiency of oxidation of yttrium and zirconium was obtained when supplying an oxygen flow of 0.36 ml min^{-1}.

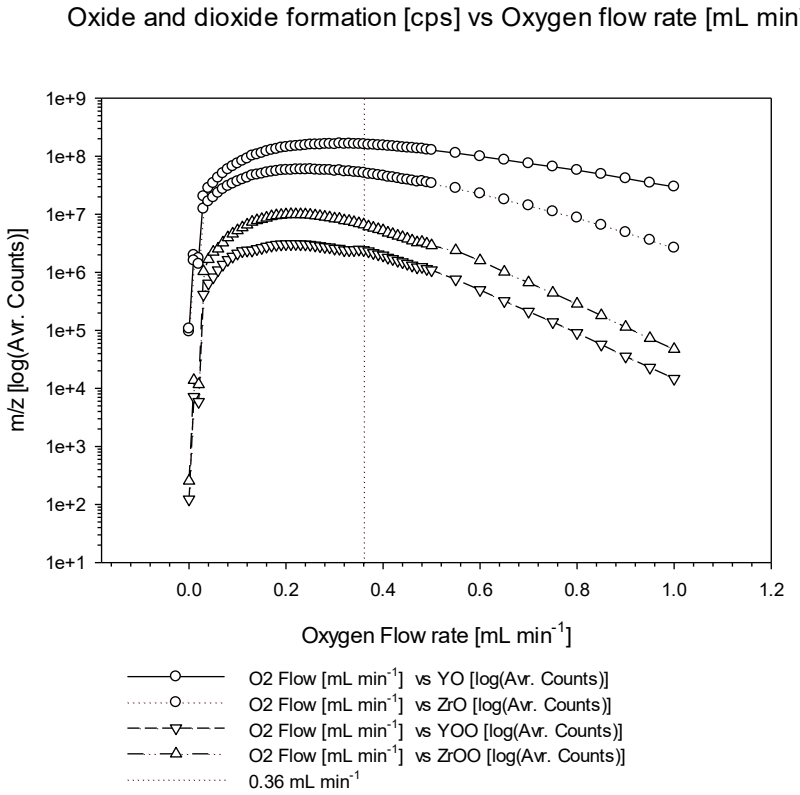

Figure 32. Oxide formation of yttrium and zirconium

Signal from strontium at $m/z = 88$ was not affected. Increasing trend was observed until an oxygen flow reached value at 0.36 ml min^{-1}. Beyond this point, further increases in the oxygen flow rate up to 0.50 ml min^{-1} resulted in a suppression of the signal at $m/z = 88$.

2.9.4 Collision/reaction gas flow rate optimisation for the removal of hydride formations

The experiment evaluated the influence of helium gas flow rate on the removal of hydrogen adduct (see Figure 33). A progressive improvement in the removal efficiency was observed with increasing helium flow until 1.9 ml min^{-1} and average counts at 500 cps.

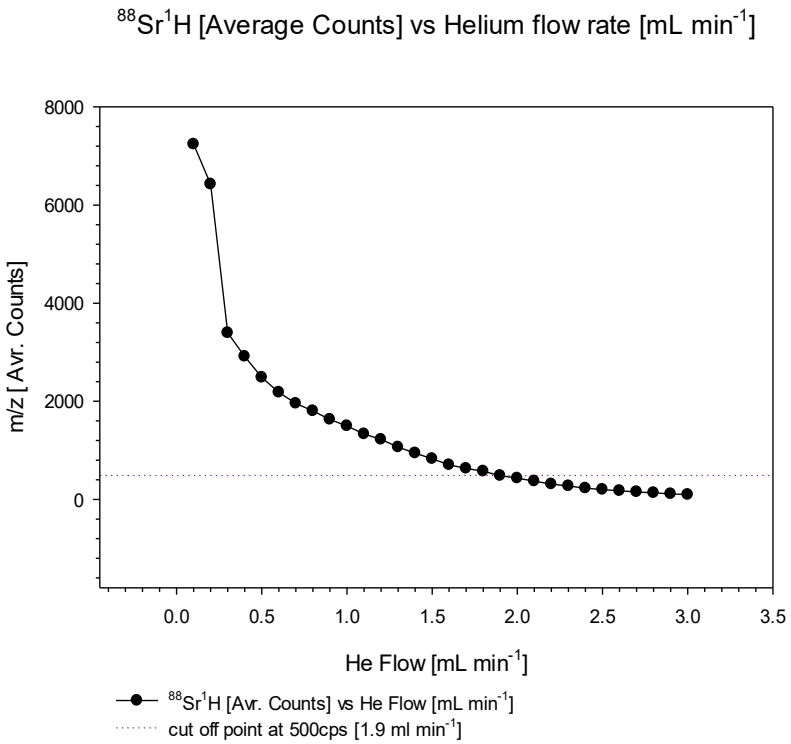

Figure 33. Hydrogen adduct removal with helium gas

NOTE: The determination of the cut-off point was influenced by the instrument's background at $m/z = 89$, which consistently varied around 500 counts per second (cps). Decision about cut off point was supported by this knowledge. This level was regarded as representative of the instrument intrinsic noise and therefore acceptable within the context of the measurements.

2.9.5 Argon and nitrogen flow rate optimisation for the Aridus 3 desolvation system

As shown in Figures 34 and 35, the optimal average counts at $m/z = 88$ (^{88}Sr) were obtained when using 3.5 L min^{-1} of argon and 0.7 L min^{-1} nitrogen gas.

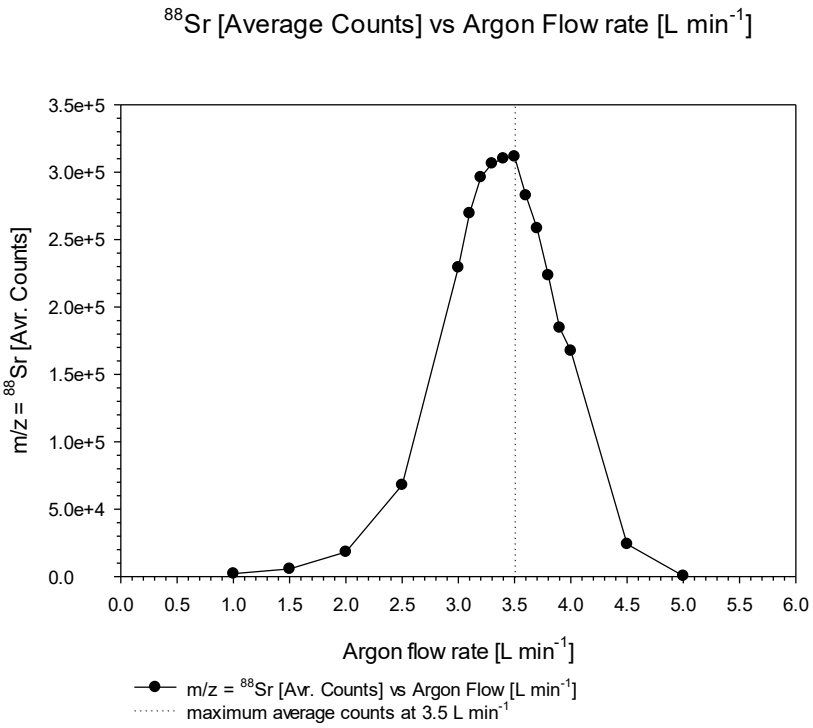

Figure 34. Aridus 3 desolvation system – argon flow rate optimisation

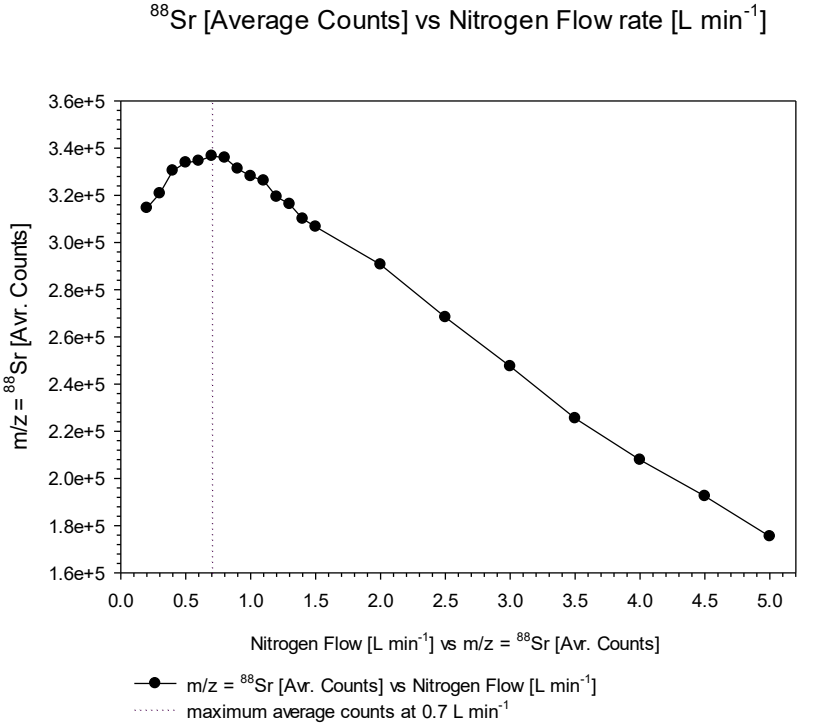

Figure 35. Aridus 3 desolvation system – nitrogen flow rate optimisation

2.9.6 Summary of optimisation parameters

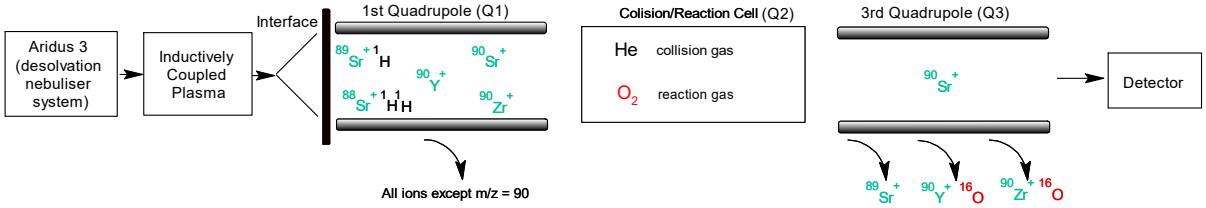

The optimised parameters for strontium analysis are summarised in Table 15. These parameters were then retained for measuring ^{90}Sr in selected milk and seawater samples. The data acquisition parameters are summarized in Table 16.

Table 15. Collated data of optimised parameters for strontium analysis

Plasma Power [W]	Plasma Flow [L min^{-1}]	Extraction Lens [V]	Q1 Entry Lens [V]	Collision/Reaction Cell		Aridus 3 Desolvation Nebulizer System	
				Oxygen Flow [mL min^{-1}]	Helium Flow [mL min^{-1}]	Argon Flow [L min^{-1}]	Nitrogen Flow [L min^{-1}]
1600	1.10	-210	-150	0.36	1.9	3.5	0.7

Table 16. Collated data of optimised parameters for strontium analysis

m/z	Analyte	Dwell time (s)	Number of sweeps	Analyses mode
84	^{84}Sr	0.1	1000	TQ
88	^{88}Sr	0.1	1000	TQ
89	^{89}Sr	0.1	1000	TQ
90	^{90}Sr	1.0	1000	TQ
175	^{159}Tb^{16}O	0.1	1000	TQ
7 - 245	Survey Scan	0.001	10	SQ

NOTE: The oxide product of Terbium at m/z = 175 was used to monitor a performance of instrument (signal stability) – an instrument internal standard. The survey scan is performed in single quadrupole mode.

Dwell time is the time that the instrument spends acquiring the data which make up a peak on the mass spectrum. The number of sweeps is the number of times the signal pulse passing through the quadrupole passes across the mass spectrum of the selected m/z values. During the same data acquisition time for the quantitative analysis of ^{90}Sr performed the survey scan (semi-quantitative concentration values for m/z = 7 to m/z = 245 in single quadrupole mode). The survey scan result can be used for method validation and to establish limit of detection.

2.10 Results and discussion

2.10.1 Blank background and sensitivity assessment

To enhance the analytical performance of the method, the Aridus3 Desolvating Nebulizer System was employed. This system enhanced analyte sensitivity by 3- to 5-fold and simultaneously reduced blank background signals a factor of four at m/z = 88. A comparative evaluation using stable of blank background for solution of 1 % nitric acid and sensitivity for ^{88}Sr solution standard solution in 1% nitric acid, with and without the Aridus3 system, are presented Table 17 and Table 18, respectively.

Table 17. Blank background counts for 1 % solution of nitric acid with and without Aridus3 system at m/z = 88.

Solution	Without the Aridus3 m/z = 88 [Avg. Count]	With the Aridus3 m/z = 88 [Avg. Count]	Reduced factor
1 % HNO_3	4837	1238	4

Table 18. Sensitivity for at m/z = 88 for ^{88}Sr standard solution with and without Aridus3 system

Concentration [pg g^{-1}]	Without the Aridus3 m/z = 88 [Avg. Count]	With the Aridus3 m/z = 88 [Avg. Count]	Increased sensitivity
1	197	1069	5
5	627	1675	3

The sensitivity of the ICPMS system for the analyte of interest at m/z = 90 was assessed using a blank solution of 1 % nitric acid, both with and without the Aridus3 desolvating nebulizer. The results are presented in Table 19.

Table 19. Blank background counts for 1 % solution of nitric acid with and without Aridus3 system at m/z = 90

Solution	Without the Aridus3 m/z = 90 [Avg. Count]	With the Aridus3 m/z = 90 [Avg. Count]	Reduced factor
1 % HNO_3	50	2	25

The implementation of the Aridus3 led to a substantial decrease in the background signal, diminishing it by roughly 25 times at m/z = 90. This decrease illustrates the efficacy of the Aridus3 in reducing solvent related interferences and boosting ion transmission efficiency, which in turn enhances the detection limits of the system.

The capabilities of Aridus3 illustrate a notable progression in the detection of analytes. This decrease directly enhances the reliability and reproducibility of the results, facilitating the confident detection of low-abundance analytes. These performance improvements establish Aridus3 as a formidable instrument for applications necessitating high sensitivity such as trace detection.

In summary, the data indicate that Aridus3 signifies a considerable enhancement over standard sample introduction system (see paragraph 1.1.1), providing both improved analytical sensitivity and diminished background interference, which collectively facilitate more reliable and sensitive measurements.

2.10.2 Method accuracy and performance

The accuracy and performance of the developed method was tested using the CRM 7512-a – (milk powder), milk and seawater samples. The concentration of strontium in milk can vary widely and depends mainly on the grazing animal diet [265-267]. Generally, the concentration ranges between 0.2 and 0.6 mg of strontium per litre of milk (i.e., 200 ppb to 600 ppb respectively). The concentration of strontium in seawater typically fluctuates between 8 and 9.5 mg of strontium per litre (i.e., 8 ppm to 9.5 ppm respectively).

The results obtained from the analysis of the selected milk, seawater and CRM samples are collated in Table 20. Results from milk and seawater were found to be in agreement with reference values available from the literature [268, 269] [270, 271].

Table 20. Strontium concentration in milk and sea water

		'Oxygen' mode	
Sample	Weight [g]	Concentration [mg kg^{-1}]	Uncertainty [mg kg^{-1}]
CRM 7512-a (1)	0.498	5.8041	0.1161
CRM 7512-a (2)	0.498	5.7765	0.1155
Milk 1	5.198	0.2279	0.0038
Milk 2	5.035	0.3163	0.0029
Milk 3	5.004	0.4137	0.0014
Milk 4	5.027	0.4810	0.0104
Milk 5	5.014	0.6531	0.0059
Milk 6	5.048	0.2856	0.0066
Milk 7	5.025	0.5637	0.0012
Milk 8	5.021	0.6748	0.0099
Sea water 1	8.316	5.5442	0.0023
Sea water 2	8.451	5.6342	0.0016
Sea water 3	9.350	6.2334	0.0017

The subsequent strontium recoveries are presented in Table 21 and results were found to be in a very good agreement with the certified value of 5.88 mg kg^{-1}.

Table 21. Comparison between the certified strontium concentration in CRM 7512a with experimental results

	'Oxygen' mode	
Certified value [mg kg^{-1}]	Observed Value [mg kg^{-1}]	Recovery [%]
5.88	5.80	98.7
5.88	5.78	98.2

The determination of natural strontium levels in milk and seawater samples, provided critical information for tailoring the sample preparation protocols, enabling more efficient and selective isolation of ^{90}Sr. This knowledge allowed for optimisation of chromatographic resin use,

minimizing matrix interference and improving both the recovery and accuracy of ^{90}Sr quantification in these complex matrices.

2.10.3 Sr-resin

Using Sr-selective resin, an amount of 3g per sample was found to provide near-quantitative retention of Sr^{2+}, effectively concentrating the analyte while minimizing interference competing cation such as Zn^{2+} - m/z = 90. Zinc was found not to be effectively retained on Sr-resin and was eluted in the column effluent during the loading step. In milk and seawater samples analysed without Sr-resin chromatography, the measured counts for m/z = 90 were on the order 10^6, whereas after the application of Sr-resin separation this value decreased to approximately 10^2. This represents a decontamination factor of the ^{90}Zr isobar of about 10^4 under the experimental conditions employed. The strong reduction in zinc-related interferences demonstrated the effectiveness of Sr-resin in improving the analytical specificity for strontium isotopes.

Strontium was successfully eluted from the column with a total volume of 30mL, facilitating effective recovery while preserving a concentrated analyte fraction that is appropriate for analysis. Elution profile of strontium solution from Sr-resin column showed on Figure 36. The elution volume present balance between a completely recovery of strontium and minimal dilution, thereby ensuring high sensitivity in later measurements.

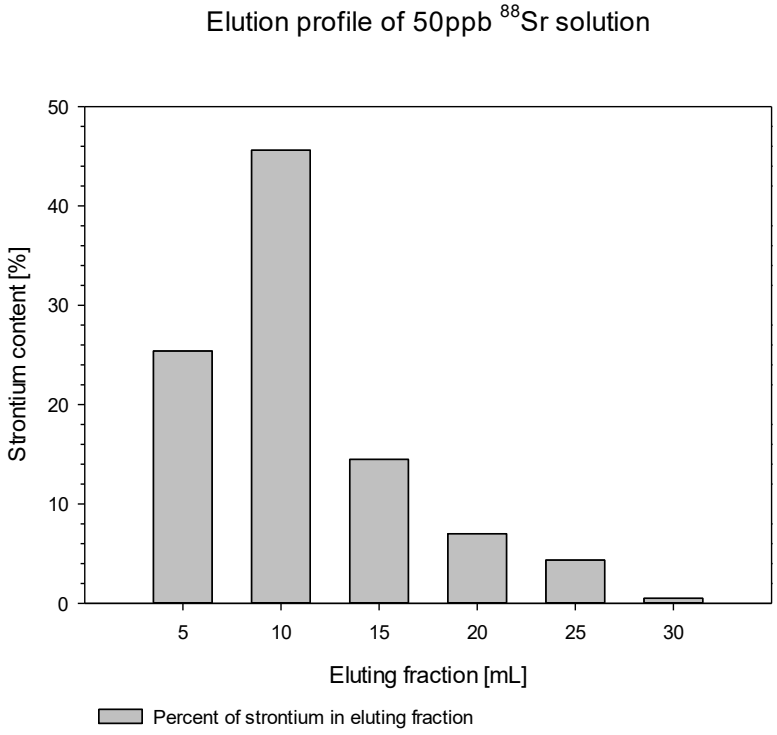

Figure 36. Elution profile 50ppb ^{88}Sr solution from 3g Sr-resin column

2.10.4 ^{90}Sr in milk and seawater

The ^{90}Sr results obtained in milk and seawater via both the presented ICPMS methodology and when using LSC as an analytical end point are collated in Table 22 and Table 23. The results are also displayed in Figure 37, Figure 38, to illustrate the comparison of the two approaches. All calculation of the results were based on the relationship between ion-counting versus radiation counting as described in Section 1.2.1.

Table 22. ^{90}Sr activity concentration in milk samples

Spiked Level	ICPMS measured	LSC measured
Bq L^{-1}	Bq L^{-1}	Bq L^{-1}
50 ± 0.75	62.96 ± 3.14	49.42 ± 0.71
100 ± 0.75	109.14 ± 1.50	98.21 ± 1.03
250 ± 0.45	260.09 ± 7.43	247.00 ± 1.58
500 ± 0.90	502.89 ± 10.15	495.14 ± 1.98
1000 ± 0.45	993.10 ± 26.31	993.48 ± 2.68
2000 ± 1.35	1966.44 ± 62.28	1996.79 ± 4.19
3000 ± 1.80	2941.70 ± 95.05	2971.74 ± 4.75

NOTE: Uncertainty figure for spiked level correspond to pipette uncertainty. For ICPMS and LSC measurements correspond to counting uncertainty.

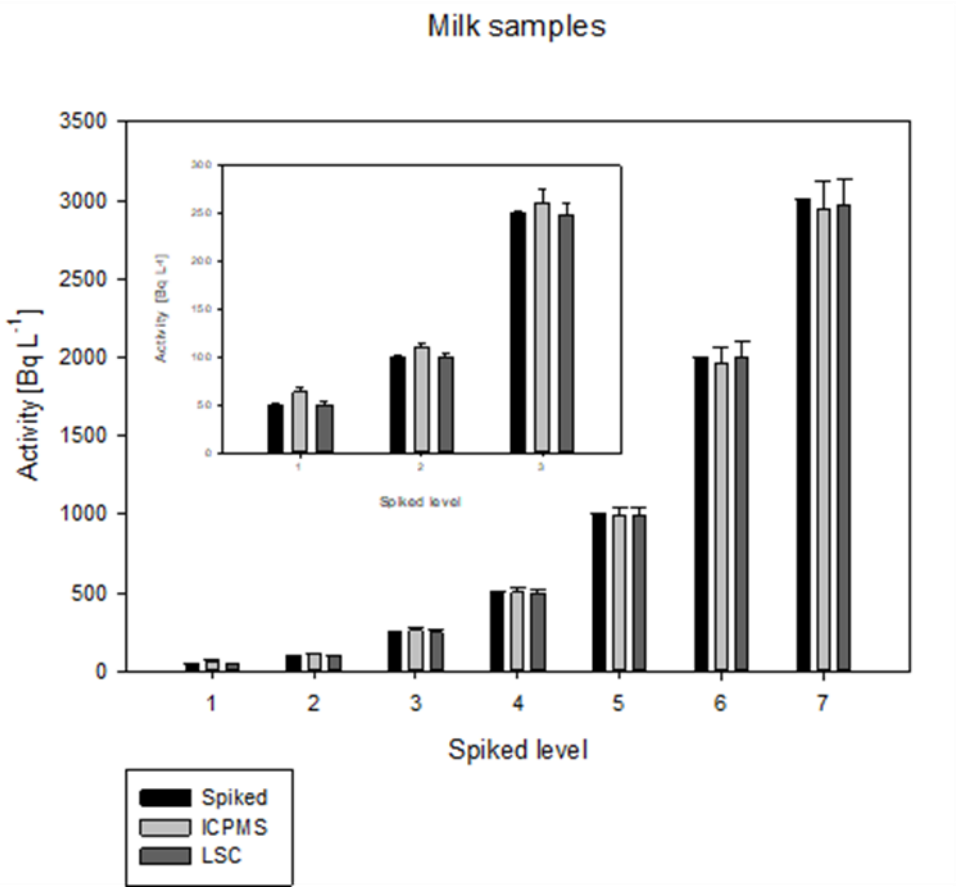

Figure 37. Comparison of ^{90}Sr activity concentration in milk samples

Table 23. ^{90}Sr activity concentration in seawater samples

Spiked Level	ICPMS measured	LSC measured
Bq L^{-1}	Bq L^{-1}	Bq L^{-1}
50 ± 0.75	58.14 ± 2.90	49.85 ± 0.64
100 ± 0.75	101.05 ± 3.68	98.64 ± 0.90
250 ± 0.45	232.29 ± 3.59	249.04 ± 1.49
500 ± 0.90	456.74 ± 1.40	497.10 ± 1.99
1000 ± 0.45	946.38 ± 12.19	993.48 ± 2.89
2000 ± 1.35	1938.60 ± 27.78	1996.86 ± 4.19
3000 ± 1.80	2981.33 ± 33.30	2979.86 ± 5.07

NOTE: Uncertainty figure for spiked level correspond to pipette uncertainty. For ICPMS and LSC measurements correspond to counting uncertainty.

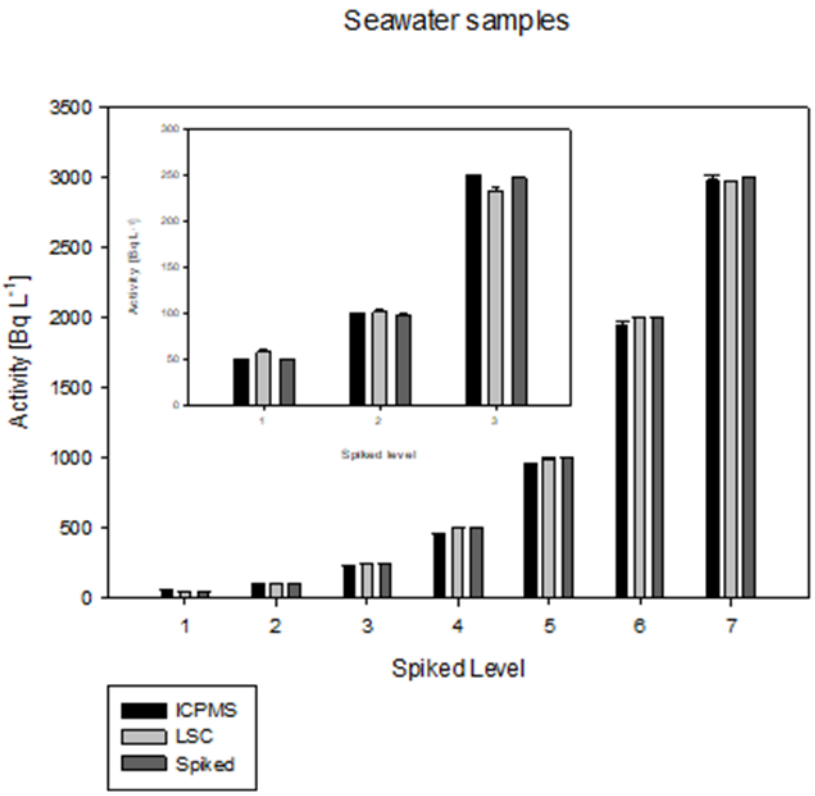

Figure 38. Comparison of ^{90}Sr activity concentration in seawater samples

As illustrated in Table 22 and 23, the ^{90}Sr results obtained from both ICPMS analysis and LSC counting were in a relatively good agreement across different spike levels. This indicates that ICPMS analytical method produced comparable measurements of ^{90}Sr activity, regardless of the concentration of the isotopic spike added to the sample.

The incorporation of chromatographic Sr-resin during the sample preparation was crucial in selective isolating strontium from complex matrices, including milk and seawater, which contain numerous other elements that could be potential interfere with the analysis. Furthermore, the use of collision/reaction gases during the ICPMS measurements significantly reduced isobaric interferences – ions with the same mass-to-charge ratio that could otherwise compromise the accuracy of the results. Table 24 shows the intensities of the analyte (strontium), key interferences (yttrium and zirconium) and their oxidation products. The stable strontium intensities (m/z = 84, 88) and their oxidation products (m/z = 102, 103, 120) are large compared to the analyte of interest (m/z = 90).

Table 24. The survey signal intensity of [counts per second - cps] of strontium, and their oxidation product

Spiked Level	m/z						
	84 (^{84}Sr)	88 (^{88}Sr)	90 (^{90}Sr) (^{90}Y) (^{90}Zr)	102 (^{86}Sr+^{16}O)	103 (^{87}Sr+^{16}O)	106 (^{90}Y+^{16}O) (^{90}Zr+^{16}O) (^{90}Sr+^{16}O)	120 (^{88}Sr+^{16}O+^{16}O)
	Intensity [cps]						
0	75,462,169	692,854,109	0	3,744,035	3,105,881	58,841	2,231,527
1	76,088,731	757,525,850	0	4,200,207	3,313,746	73,622	2,627,907
2	75,003,841	686,132,321	100	3,882,073	3,176,787	64,871	2,480,065
3	78,295,177	714,631,713	200	4,161,384	3,301,045	67,887	2,506,467
4	110,846,192	1,036,989,641	700	6,061,559	4,680,104	95,264	4,331,774
5	112,123,040	1,038,606,192	600	6,147,832	4,612,163	93,046	3,909,034
6	104,419,890	963,941,817	1400	5,506,173	4,284,324	88,415	3,630,801
7	94,938,425	924,144,901	2100	5,445,781	4,320,990	85,997	3,649,134

Matrix and chemical effects can significantly influence the overall ICPMS analysis (Chapter 1.2.5). The presence of strontium oxidation products (m/z = 102, 103, 120) indicates that the analyte of interest ^{90}Sr (m/z = 90), is also prone to oxidation (Chapter 2.3; equation 37). The signal observed at m/z = 106 is thought to be from the complex combination of yttrium, zirconium, and strontium oxides. Overall, the dynamic process occurring in the collision/reaction cell seems to have a non-negligible impact on the ability of ICPMS instrument to be accurate. The signal intensities observed at m/z = 90 are very low and therefore the matrix effect combined mainly with the oxidation processes reduce the scope of ICPQQQMS applications for very low levels of ^{90}Sr in complex environmental matrices. The signal intensities observed at m/z = 90 in selected milk and seawater samples are presented in Table 25.

Table 25. The signal intensity [counts per second - cps] of m/z = 90 (^{90}Sr)

Spiked level	Intensity [cps] in milk samples	Intensity [cps] in seawater samples
0	2.3	2.6
1	13.6	20.9
2	25.9	33.3
3	63.2	60.3
4	166.2	117.1
5	348.9	208.9
6	632.6	384.7
7	867.0	537.6
1 % nitric acid	1.9	1.8

These measurements demonstrated the response of the ICPMS system to increasing spiked level of ^{90}Sr, with the blank (1 % HNO_3) included as a reference. Signal intensities increase proportionally with the spiked concentration, indicating a clear analytical response, while the low count observed in the blank confirm minimal background contribution from the matrix.

2.10.5 The accuracy and reproducibility of the method

The evaluation of the performance of the ICPMS for the determination of ^{90}Sr was conducted with respect to accuracy and reproducibility across various spike levels (Table 22) in comparison to LSC measurement. In terms of accuracy, the measurements obtained via LSC were in close alignment with the spiked values, exhibiting recoveries that ranged from 99 % - 100 %, which suggest a minimal bias. Conversely, ICPMS also demonstrated a good correlation at elevated spike levels; however, a slight overestimation was noted at the lowest spike concentration (50 Bq L^{-1}), which is likely attributable to residual matrix effect or minor interferences. Regarding reproducibility, LSC exhibited exceptional precision, with standard deviations ranging from 0.64 to 5.07 Bq L^{-1}, while ICPMS displayed a higher variability at lower concentrations (SD 2.90 – 33.30 Bq L^{-1}), although it showed significant improvement at higher activity levels. In summary, these findings suggest that methodologies are dependable and robust for the quantification of ^{90}Sr in complex matrices, with LSC consistently delivering high accuracy and reproducibility across all tested concentrations, while ICPMS demonstrated strong performance, particularly at moderate to high levels.

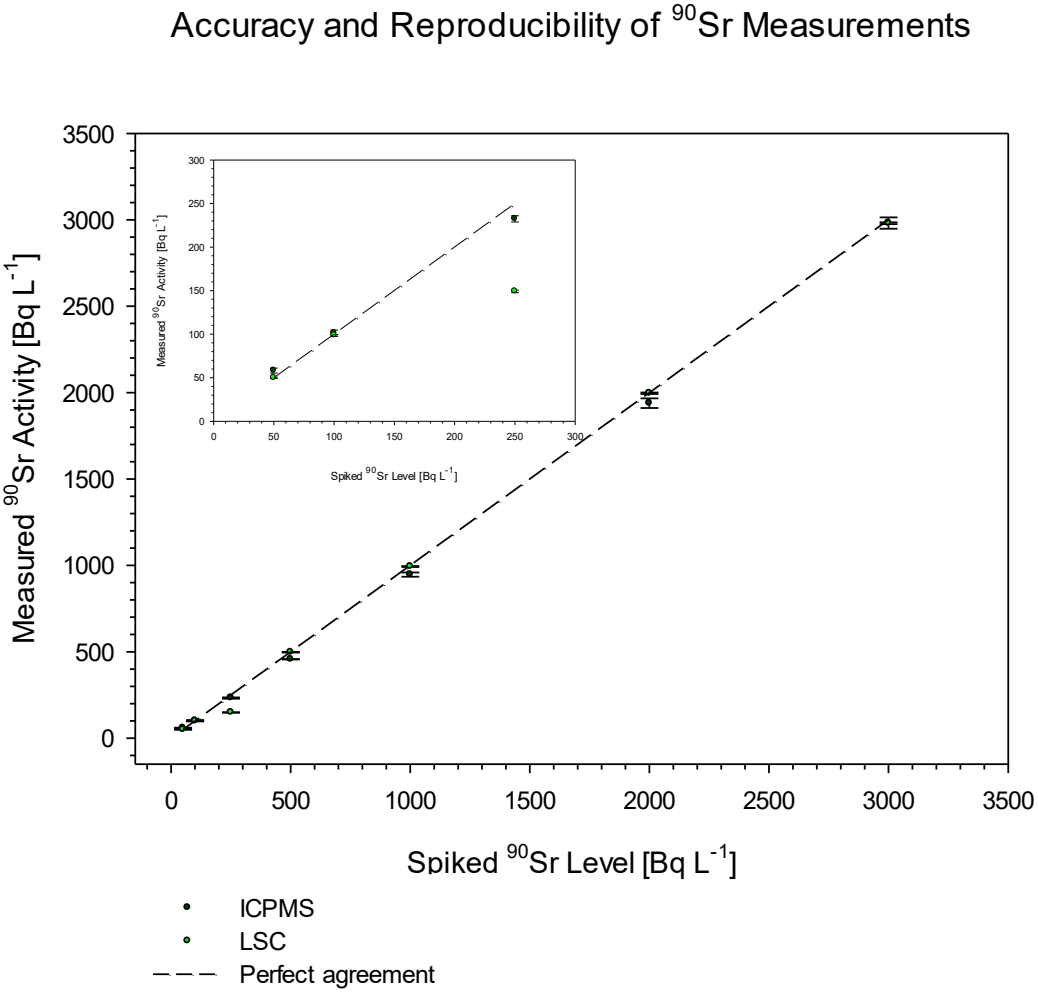

Figure 39. The accuracy and reproducibility of the method for spiked milk samples

2.10.6 Limit of Detection (LOD)

In general terms, the limit of detection (LOD) for a defined analyte present in a sample is its lowest measurable and statistically exploitable signal (m/z in the case of ICPMS analysis). In another words, the signal must be significantly different from that of a blank sample or the background signal. However, the significant difference can be replaced by the lowest signal or the lowest corresponding quantity that can be determined from the signal. The lowest quantity of the substance that can be distinguished from the absence of that substance (a blank value) with the stated confidence level.

The two lowest standards, level 1 corresponding to 25 Bq L^{-1} (0.0049 pg g^{-1}) and level 2 corresponding to 50 Bq L^{-1} (0.0099 pg g^{-1}) were tested here. The intensities from these standards and background are collated in Table 26. The results show very low counts, with values for the background and the lowest standards differing by only a small margin, highlighting the challenges in detecting ^{90}Sr at the trace levels. This demonstrates that at very low concentrations, the analytical response approaches the background noise, which must be carefully considered when

interpreting results. In our scenario, the LOD is effectively equal to the LOQ (Limit of Quantification), indicating that the ICPMS system can only reliably quantify ^{90}Sr at levels where it is also detectable above background noise, and very low-level measurements are inherently limited by signal overlap with the background.

Table 26. Signal intensities and background [counts per seconds - cps] of m/z = 90 (^{90}Sr) using the two lowest standards in selected milk and seawater samples

	Intensity [cps] in milk samples	Intensity [cps] in seawater samples
Standard level 1	2.0	1.3
Standard level 2	3.0	2.0
Background level	1.9	1.8

2.11 Conclusion

This work investigated the performance of an ICPTQMS system for measuring low levels of ^{90}Sr in milk and seawater samples. The operating parameters of the Thermo iCAP TQMS, including plasma condition, lens voltage, collision/reaction cell flow, were carefully optimised to enhance sensitivity and minimize interferences. Additionally, the Aridus3 desolvation system was employed and the flow rates of the nebulizer and carrier gases were adjusted to maximize ion transmission efficiency and reduced solvent-related background signals. Prior to analysis, sample were purified using a chromatographic Sr-resin, which selectively isolated strontium and removed potential isobaric and matrix interferences, thereby improving measurements accuracy. Through the combination of these optimized instrumental conditions and sample preparation techniques, the system was able to achieve extremely low limits of detection for 90Sr, on the order of 10^{-3} pg g^{-1} (parts per quadrillion – ppq). The analytical performance of the ICP-QQQ-MS system was found to approach that of traditional radiometric methods, such as liquid scintillation counting (LSC), demonstrating its suitability for trace-level demonstrations of ^{90}Sr in complex environmental and food matrices. This approach not only provides rapid and highly sensitive measurements but also minimizes the use of radioactive counting techniques, offering a safer and more efficient alternative for routine monitoring of ^{90}Sr contamination.

The sensitivity for measuring strontium was significantly enhanced, and the formation of hydrates and dihydrates was minimized, enabling the detection of ^{90}Sr in complex environmental matrices. Despite these improvements, certain limitations were observed, particularly when analysing samples with very low ^{90}Sr concentrations, where signal intensities were minimal and background levels exhibited instability. The sample preparation strategy, which included the precipitation of

calcium oxalate followed by purification with Sr-resin, effectively removed zirconium, a major isobaric interference that is critical for the accurate measurement of trace level of ^{90}Sr by ICPMS. The implementation of the Aridus3 desolvation system provided additional, no-negligible benefits for low-level detection. By optimizing gas flows and nebulization conditions, background signals were reduced, and ion transmission was enhanced, allowing the system to achieve detection limits in the parts-per-quadrillion (ppq) range. This combination of advanced sample preparation and optimised instrumental conditions demonstrates the capability if ICPMS, coupled with desolvation, as a powerful tool for the analysis of ultra-trace ^{90}Sr.

Nevertheless, it is important to note that this method has practical limitations. For routine food and environmental monitoring, it cannot reliable measure ^{90}Sr at activities below approximately 50 Bq L^{-1}, due to the combined effects of low signal intensity and background fluctuations.

However, this analytical approach could still be valuable in emergency response scenarios, decommissioning monitoring programs, providing a sensitive and relatively rapid alternative to traditional radiometric methods such as liquid scintillation counting. The method therefore offers a practical balance between sensitivity, speed, and applicability in specific low-level radiological assessments.

Chapter 3 Optimised removal of interferences for the measurement of ^{129}I in seaweed samples

3.1 Sources of Iodine in the environment

Iodine - symbol I, atomic no. 53; is a natural occurring non-metallic element of the halogen family (lying in group VIIa, period 5, between bromine and astatine in the periodic table). The mineral was discovered in 1811 by Bernard Courtois during the manufacture of saltpetre (potassium nitrate, KNO_3), using seaweed ash as a source of potassium. There are 37 isotopes of iodine, but only two are naturally occurring in the environment: ^{127}I and ^{129}I, which are stable and radioactive, respectively.

The total mass of stable iodine (^{127}I) on the Earth's surface is approximately 8.6×10^{15} kg. Marine sediments are the largest reservoir of iodine (68%), followed by sedimentary rocks (28%) and metamorphic and magmatic rocks (2.7%). However, sea waters contain the highest concentration of stable iodine[272]. From biological perspectives, iodine is an essential trace element for human life[273]. The iodine function lies in the formation and synthesis of thyroid hormones. Both iodine deficiency and excess may influence thyroid function. Iodine excess can cause hypothyroidism, which can result in muscle fatigue and myalgia. However, deficiency remains a major threat to health and can cause brain damage. The worldwide drive to eliminate iodine deficiency is universal salt iodization[274, 275].
Furthermore, radioiodine ^{131}I plays an important role in the diagnosis and treatment of various thyroid disorders. Treatment of thyroid carcinoma and hyperthyroidism with ^{131}I-labelled pharmaceuticals has been practiced for years, but other isotopes, i.e., ^{120}I, ^{123}I, ^{124}I and ^{125}I are also being produced and increasingly being used in various medical applications[276].

Radioactive ^{129}I (half-life at 1.57×10^7 years, decay scheme are shown Figure 44) is formed in nature from the interactions of cosmic rays with ^{129}Xe in the upper atmosphere and also by spontaneous fission of ^{238}U in the lithosphere[277]. These two sources are however negligible in comparison to nuclear-derived sources. More than 90 % of ^{129}I present in seawater is from anthropogenic sources, with the nuclear weapons tests, accidental releases and mainly nuclear fuel-reprocessing activities being the main sources[278].

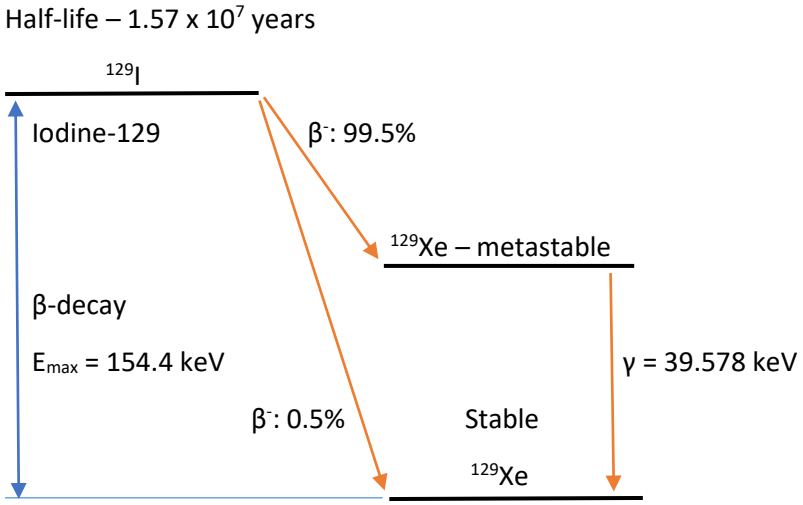

Figure 40. Iodine-129 decay diagram

Iodine-129 is an important tracer in geological and biological processes and is considered to be one of the most important radionuclides for assessing the global oceanic circulation[279]. It is commonly used as an oceanographic tracer for studying transport and exchange of water mass, and as a useful environmental tracer for investigating geochemical cycle of stable iodine.

Also, atmospheric chemistry studies have revealed that iodine also plays a significant role in the depletion of ozone and aerosol particles for cloud nucleation. Thus, considerable attention has been paid to understanding sources of inventory and distribution of iodine in many natural environmental compartments. The oceans represent the main source of iodine to the Earth's surface environments, and it is apparent that tracing the chemical species of iodine in ocean water provides further clue for incorporation in the atmosphere. As most of iodine atmospheric interaction is strongly linked to releases from ocean surface water, identifying iodine species in of the oceanic compartment is increasingly becoming important[280].

Nuclear reprocessing facilities at La Hague (France) and Sellafield (England) are responsible for 95 % of the anthropogenic production[281].

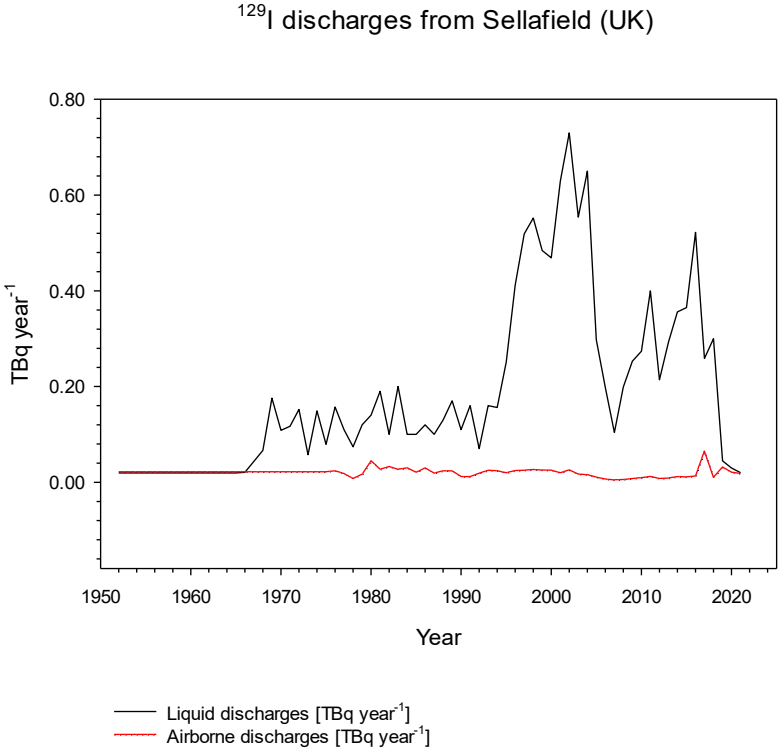

Figure 41. Airborne and liquid discharges from Sellafield (UK)[282, 283]

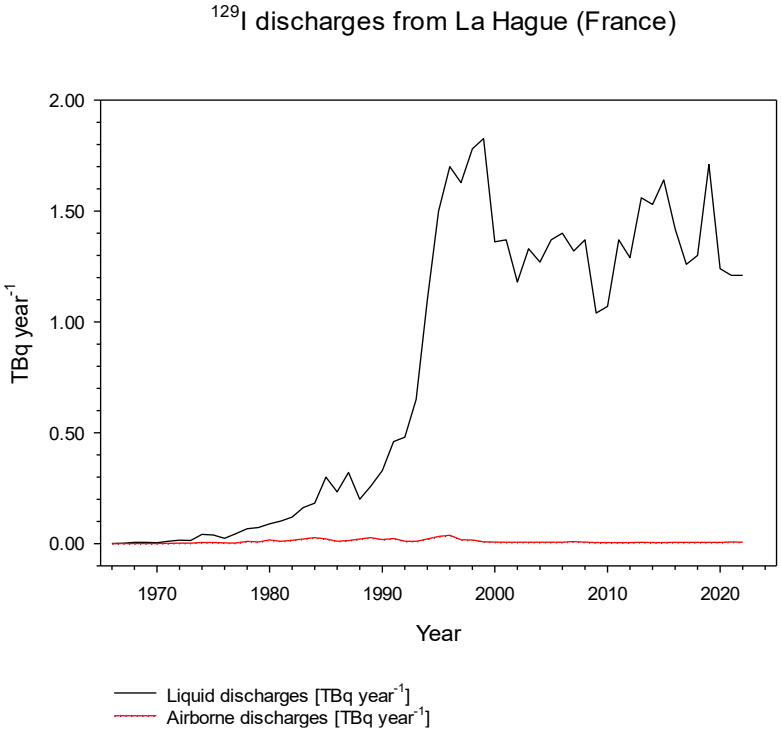

Figure 42. Airborne and liquid discharges from La Hague(France) [282, 283]

Releases of ^{129}I from Sellafield (UK) and La Hague (France) are shown in Figures 45 and 46, respectively. In both cases, the discharges of liquid effluent have exceeded atmospheric releases. Discharges from Sellafield have increased since the 1990s, with three peaks observed

in 2002, 2012 and 2016, and then reduced significantly and are now back to pre-commissioning levels observed in the 1960s. In comparison, discharges from La Hague (France),also increased significantly in the 1990s, but have been kept at a constant level since then.

The study conducted by Raisbeck et al.[278, 284] Frechou et al.[285] recommended that seaweed should be used for monitoring ^{129}I and in general ^{129}I should be used as an oceanographic tracer. Both the activity of ^{129}I and $^{129}I/^{127}I$ ratios are often used together to confirm the source of ^{129}I found in nature. Pre-nuclear ratios have been estimated at between 10^{-12} to 10^{-10} [285]. Following the commissioning of the two European nuclear reprocessing plants, enhanced ^{129}I concentrations were measured in seawater samples collected from different parts of the Irish Sea, English Channel, North Sea, and Nordic Seas, with $^{129}I/^{127}I$ ratios ranging between 10^{-8} to 10^{-5}. High ^{129}I concentrations, accompanied with $^{129}I/^{127}I$ ratios ranging between 10^{-6} to 10^{-4} were also measured in terrestrial samples collected near La Hague and Sellafield[286].

Iodine-129 has also been an important contributor to the radiation dose received by members of the public living near these sites, especially during peak discharges periods, with the most important exposure pathway known to be from initial deposition in soil, grass and ingested via milk consumption[287-292]. In the UK, iodine-129 has been amongst the biggest contributors to the public dose in the last 11 years near Sellafield (see Figure 47)[293].

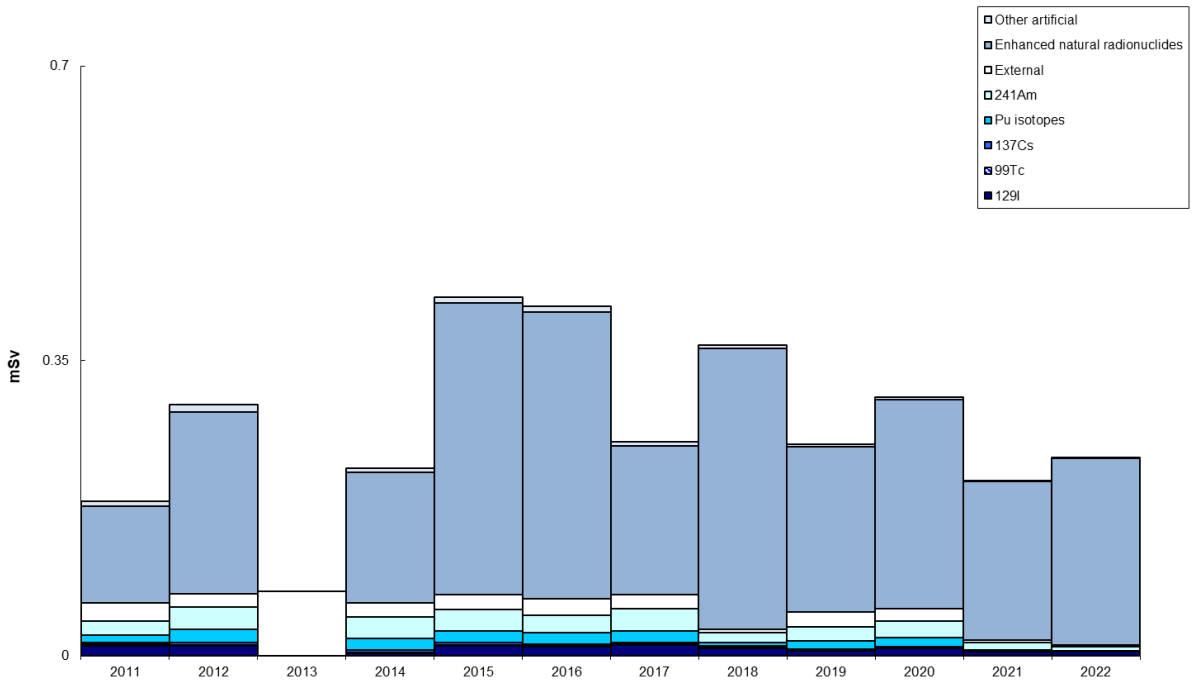

Figure 3.6 Contributions to 'total dose' from all sources at Sellafield, 2011 - 2022
(The highest 'total dose' in 2013 due to Sellafield discharges was to people living on houseboats near Barrow in Cumbria)

Figure 43. Total dose assessment to member of the public near Sellafield [www.gov.uk]

3.2 Analysis of ^{129}I

Iodine-129 is a beta, X-ray and gamma emitter. Therefore, it is often measured by gamma or X-ray spectrometry[294, 295]. Gamma and X-ray emission energies and intensities are low: 39.6 keV with 7.5 % intensity for gamma rays and 29.5 keV and 29.8 keV with 20.4 % and 37.7 % intensities for X-rays, respectively. Using these methods limit of detection (LOD) was reported as 0.1 – 0.2 Bq kg^{-1} or Bq L^{-1}. In addition, due to low counting efficiency of gamma detectors (< 2 %) and low energy of the X rays, large quantities of samples are generally required to achieve these LODs, typically 50g to 1kg of material must be used (50 – 1000 g). In order to obtain accurate result, a self-absorption correction also has to be carried out[295-297].

Neutron Activation Analysis (NAA) for the determination of ^{129}I is based on the nuclear reaction shown in Figure 44. The measurement is based on the production of ^{130}I via neutron irradiation of ^{129}I. The activation product, ^{130}I (half-life of 12.3 hours), then decays by emitting beta particles and gamma rays (418 keV – 34 % intensity; 536.1 keV – 99 % intensity; 668.5 keV – 96 % intensity and 739.5 keV – 82 % intensity).

$$^{129}I \xrightarrow{\text{irradiation}} {}^{130}I \xrightarrow{\text{beta, 12.3 hours}} {}^{130}Xe$$

Figure 44. Iodine-129 irradiation

Chemical separation and purification of pre- and post-irradiated samples are required. Many operating procedures have been published[288, 298-300]. A LOD of 1 μBq and $^{129}I/^{127}I$ ratio of 10^{-10} has been reported using this approach[300].

Accelerator Mass Spectrometry (AMS) is a very sensitive technique that can also be used for measuring ^{129}I and determining $^{129}I/^{127}I$ ratio. This other mass spectrometric tool has been used in many studies[301-305] and for a wide range of environmental materials: soil, plants, seaweed and milk. The iodine must be separated from the matrix prior to AMS analysis. Once the iodine is separated, generally in the form of silver iodide (AgI) precipitate, AMS can be performed and can reach very low detection limit of 10^{-9} Bq and $^{129}I/^{127}I$ ratio of 10^{-13} [306]. There are about 160 facilities worldwide equipped with AMS [307]. Despite these advantages, the technique is associated with substantial operational and analytical costs, and routine access is not straightforward. In particular, within the UK, opportunities to access AMS are constrained by limited infrastructure, meaning the samples often need to be sent abroad for measurement. Consequently, while AMS represents a gold standard for ultra-trace iodine isotope analysis, practical and financial considerations remain significant barriers to its widespread application.

Finally, as ^{129}I also decays by emitting beta particles of maximum energy of 154.4 keV (Figure 44), it can be measured by liquid scintillation counting (LSC). This traditional radiometric technique requires the iodine to be separated from the matrix and other radionuclides due to the limited energy resolution that can be achieved via LSC. A detection limit of 0.010 Bq have been reported in previous studies[308].

3.3 Measurement of ^{129}I by ICP-TQMS

In the last decade, different benchtop ICP-TQMS systems have been used to measure ultra-trace of ^{129}I in many environmental matrices[91, 286, 288, 309-314]. Analysis of iodine-129 (^{129}I) by ICP-MS mainly suffers from an isobaric spectral interference from the presence of xenon-129 (^{129}Xe), which is introduced from the argon plasma gas as an impurity. Polyatomic interferences such as $^{127}I^{1}H^{1}H$, $^{89}Y^{40}Ar$, $^{115}In^{14}N$, $^{113}Cd^{16}O$ can also affect its measurement[311]. Therefore, there is a need to first separate iodine from any elements present in potential polyatomic interferences prior to ICP-MS analysis. In addition, collision/reaction cell technology has been developed to overcome all of these interferences. For instance, it is possible to suppress the background intensity at $m/z = 129$ from ^{129}Xe using O_2 (1) [37, 67, 259, 309]

$$Xe^+ + O_2 \rightarrow Xe + O_2^+ \quad (1)$$

Reaction of $^{129}Xe^+$ with O_2 was studied by Eiden et *al.*[259]. It was observed that $^{129}Xe^+$ reacts at least 10^4 times faster with O_2 that $^{129}I^+$ does. Although iodine oxidation would affect the sensitivity of iodine, this process seems to be the most efficient one for removing the main isobaric interference[315].

$$I^+ + O_2 \rightarrow IO^+ + O \quad (2)$$

Also, due to its higher ionisation potential (10.45 eV), ionisation efficiency of iodine is lower than many other metals, resulting in lower analytical sensitivity[71]. Therefore, the optimisation of the plasma condition and the O_2 gas flow rate used in the collision/reaction cell are the most important factors to control when measuring ^{129}I by ICPMS. These optimisation parameters were investigated in this chapter, and a novel analytical method was developed to determine quantitatively ^{129}I in seaweed samples.

3.4 Extraction of ^{129}I from seaweed samples

Seaweed is often used as a bioindicator for monitoring radioactive contamination of the marine environment[316]. It is well known that it can concentrate iodine to a high level, with concentration factors as high as 10^4 in some brown seaweed species[317]. The relatively high stability of iodine in seaweed and the possibility of using dry seaweed materials enable the use of archived seaweed collected at different times and locations and therefore enables trend analysis of anthropogenic ^{129}I over time.

As with LSC, radiochemical preparation is required prior to ICP-MS analysis. Microwave digestion routes followed by solvent extraction alkaline fusion methods used in previous studies have been published [318]. However, pyrolysis offers a more effective solution for releasing iodine from solid samples and has been widely used for the separation of iodine from soil, sediment, rocks and vegetation samples[309, 319, 320]. In this method, all species of iodine are converted to gaseous iodine and released from the sample matrix. In pyrolyser system, iodine is carried by constant flow of gases and is trapped into a sodium hydroxide (NaOH) solution, with recovery of more than 95 % being reported in a previous study[321].

3.5 Aim

The primary objective if this research was to optimise key instrumental parameters, including plasma condition, the extraction lens, the first quadrupole entry lens voltage, and the collision/reaction gas flow, for determination of ^{129}I by ICP-TQMS. These optimised conditions were subsequently employed to quantify ^{129}I in seaweed samples and to assess the analytical performance of the ThermoFisher iCAP ICP – Triple Quadrupole Mass Spectrometer (iCAP ICP-TQMS). In addition, the influence of naturally occurring stable ^{127}I on the measurement of ^{129}I in both seaweed and seawater samples was systematically evaluated.

To ensure accurate measurements, isobaric interference from ^{129}Xe which can overlap with the ^{129}I signal, was eliminated by introducing oxygen into the collision/reaction cell (CRC) of the ICP-TQMS. Within the CRC, oxygen reacts with ^{129}Xe to form oxide species, which are shifted to different mass-to-charge ratios. This approach effectively prevents interference, allowing precise quantification of ^{129}I in the analysed samples.

3.6 Reagents

All standard solutions were prepared from elemental stock solutions in 0.5% and 1% tetramethylammonium hydroxide (TMAH) solution 25 wt. % (Merck, York, UK) using high purity de-ionised water (resistivity higher than 18.2 MΩ) produced from a Q-Pod Millipore System (Merck,

York, UK). Standard solutions (1000 mg L^{-1}) of ^{127}I (stable), ^{159}Tb (stable) and sodium hydroxide pallets (NaOH) were sourced from VWR Chemicals.

The ^{129}I (sodium iodide form in 0.1 M NaOH) standard solution was sourced from Eckert & Ziegler (USA).

3.7 Instrumentations

The ThermoFisher iCAP ICP – Triple Quadrupole Mass Spectrometer (iCAP ICP-TQMS) controlled by the Qtegra software was used to perform all measurements. The instrument was equipped with a standard sample introduction system consisting of a MicroMist nebulizer and baffled cyclonic spray chamber. However, some modifications were made to the standard set up. Indeed, a platinum tip sample cone and skimmer cone with high sensitivity skimmer cone insert were used instead of a nickel sample cone and skimmer cone with high matrix skimmer cone insert. . Samples were introduced directly into the ICP-TQMS using an ASX-520 autosampler with the standard peristaltic pump and tubing (internal diameter of 1.02 mm).

A Hidex 300 SL Super Low Level liquid scintillation counter controlled by MicroWin software was also used to compare the results obtained from the described ICP-TQMS method. This instrument was equipped with three low level photomultipliers, an active guard for lowering background, an external source, a cooling system and a 40-position autosampler for 20 mL scintillation vials.

The Pyrolyser-6-Trio (GenIV) furnace system (Raddec International, UK) was also used to prepare the samples prior to ICP-TQMS analysis. It is equipped with six individual work tubes and three independent heating zones, therefore capable of extracting volatile radionuclides of interest from six samples simultaneously.

3.8 Methodology

Plasma condition, optics voltage, collision/reaction gas flow rate and desolvation gas flow were the instrumental parameters investigated in this study.

Radio frequency power generator, induction coil and gas are used to form Inductively Coupled Plasma (ICP). Therefore, the RF Power (W) produced from the generator and the nebulizer gas flow (L min^{-1}) are the main optimising parameters affecting the plasma condition.

The extraction lens and first quadrupole extraction lens voltage are also very important parameters for optimising a response from the instrument, as this is where separation of positive

ions from neutral species, photons, and electrons occurs and where these same ions are transferred to the mass analyser.

The collision/reaction cell gas are used to remove or react with interference(s). Oxygen was used to remove isobaric interferences at $m/z = 129$. Therefore, different flow rates of oxygen applied in collision/reaction cell were tested in this study.

The first set of experiments focused on the plasma condition, by gradually increasing the RF power between 1,000 and 1,600 W and assessing the m/z response using different nebulizer gas flows, as described in Table 27.

Table 27. Set of experiments for plasma condition optimisation

No.	Nebulizer Gas Flow (L min^{-1})	RF Power (W)
1	0.90	1000 - 1600
2	0.95	1000 - 1600
3	1.00	1000 - 1600
4	1.05	1000 - 1600
5	1.10	1000 - 1600
6	1.15	1000 - 1600
7	1.20	1000 - 1600
8	1.25	1000 - 1600

The second set of experiments focused on the extraction lens and the first quadrupole extraction lens voltage, using different voltages at both lenses. The extraction lens and first quadrupole extraction voltages were both increased in 10 volts step and the different m/z responses, using ^{127}I as a reference.

The third set of experiments consisted of applying different oxygen gas flow rates and therefore testing the efficiency for removing isobaric interference at m/z = 129. The oxygen flow rate was increased from 0.01 to 0.25 ml min^{-1} in 0.01 ml min^{-1} steps and thereafter in 0.05 ml min^{-1} steps up to a maximum flow rate of 0.50 ml min^{-1}.

A 0.5 mg L^{-1} (50ppb) solution of ^{127}I in a 0.5 % TMAH (tetramethylammonium hydroxide) solution was used in all sets of experiments. In each experiment, an additional 0.001 mg L^{-1} (1ppb) solution of terbium (Tb) in a 0.5 % TMAH solution was used as instrumental internal standard. Solutions

were introduced into the plasma using an ASX-520 autosampler and data were collected for 60 seconds with 1,000 sweeps for each individual m/z value.

Iodine was extracted from seaweed materials using the Pyrolyser-6-Trio (GenIV) furnace system (Raddec International, UK) (see Figure 45).

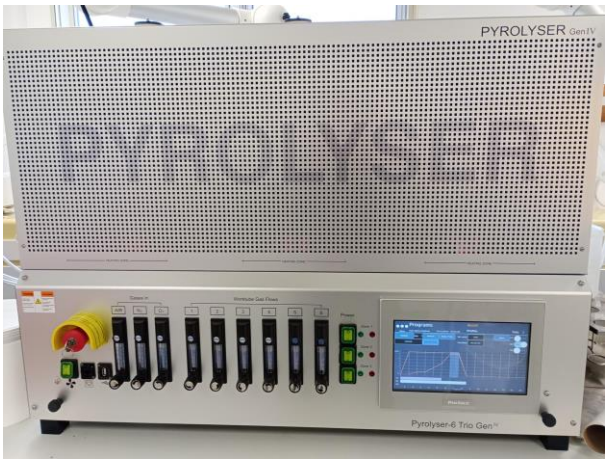

Figure 45. Pyrolyser-6-Tri (GenIV), Raddec International, UK

The first and the second heating zones was programmed, and details of the temperature programme is shown in Figure 46. The third zone (crushed silica) was kept constant at 950 °C during the whole extraction programme. The samples were introduced in separate tubes and were ashed in a silica tube using a mixture of air enriched in O_2 as combustion and carrier gas. The flow rate of combustion/carrier gases (air + O_2 before 500 °C and O_2 after 500 °C) was 100 mL min^{-1}. The combustion products were then transferred over crushed quartz.

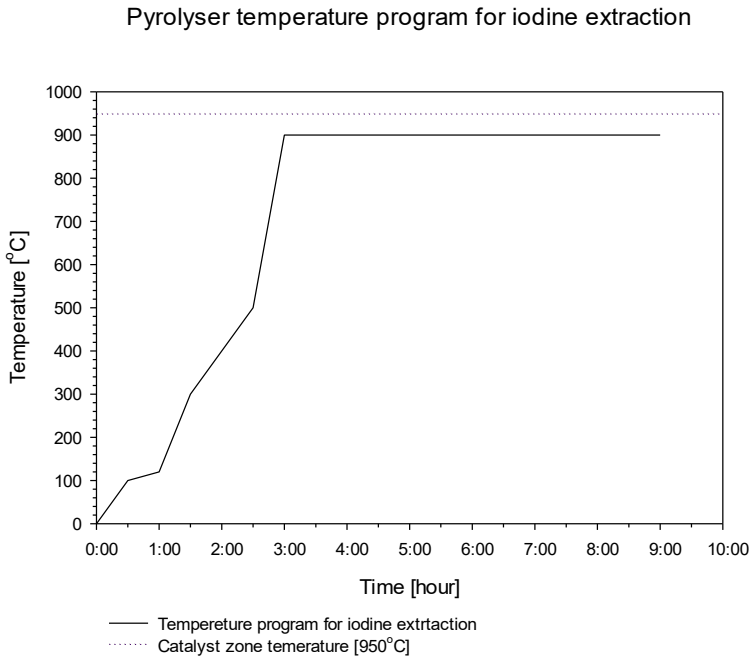

Figure 46. Pyrolyser temperature program

The ^{129}I was trapped in 15 g of 0.1 M NaOH solution. The solutions were weighed after the combustion process to compensate for any potential loss from evaporation. The solutions were then split ICP-TQMS measurement and LSC, using 10 grams of material, and the rest (around 5 gram), respectively.

Two kilograms of seaweed was collected in February 2023 from the Seascale Beach (54°24'19.0"N 3°30'07"W, see Figure 47). The sample was first air dried and then dried at 60 °C in an oven until constant weight for 7 days.

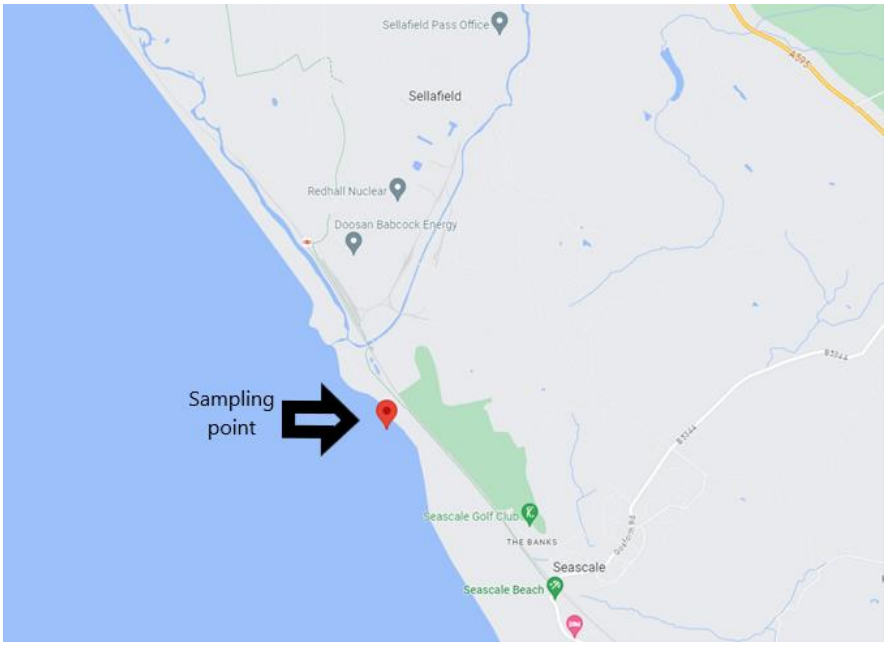

Figure 47. Seaweed sampling point

Seaweed samples weighing 1 – 2.5 g and seawater samples of 20 grams were introduced into a combustion tube furnace.

The different ^{129}I standard concentrations used for calibrating the ICP-TQMS instrument are detailed in Table 28.

Table 28. ^{129}I calibration standard concentrations

Standard Level	^{129}I standard concentrations [Bq kg^{-1}]	Concentration [pg g^{-1}]
1	0.38	57.54
2	0.56	86.30
3	0.75	115.07
4	0.94	143.84
5	1.88	287.68
6	3.76	575.36
7	9.40	1438.39

Polyatomic interferences at m/z = 129 (mainly coming from high concentration of stable iodine - ^{127}I and creating a peak tail at mass 129) were assessed by measuring the background levels at m/z = 129 (^{129}I) using different concentrations of ^{127}I. Two sets of standard concentrations were prepared, as detailed in Tables 29 and 30.

Table 29. ^{127}I standard concentrations (ppb – ng g^{-1})

Standard Level	Concentration [ng g^{-1}]
1	10
2	20
3	50
4	100
5	1000
6	2000
7	5000

Table 30. ^{127}I standard concentrations (ppm – µg g^{-1})

Standard Level	Concentration [µg g^{-1}]
1	10
2	20
3	40
4	80
5	200
6	300
7	400

To assess the impact of high stable iodine concentration (m/z = 127; ^{127}I) on the peak intensity at m/z = 129, two sets of calibration standards were prepared, as described in Tables 31 and 32. An internal standard of terbium (^{159}Tb), at concentration 1 ng g^{-1} in 0.5 % TMAH, was used to monitor plasma suppression. Terbium was selected because it is not typically present at measurable levels in environmental samples and its isotope ^{159}Tb is free from major spectral interferences in the mass range studied. By tracking the signal intensity of ^{159}Tb throughout the measurements, any reduction caused by matrix-inducted plasma suppression can be identified, thereby providing a reliable means to assess the sensitivity of the instrument for the accurate quantification of iodine isotopes.

Table 31. ^{129}I calibration standard concentrations with ^{127}I at 5 µg g^{-1}

Standard Level	^{129}I standard concentrations [Bq kg^{-1}]	^{129}I standard concentration [pg g^{-1}]	^{127}I standard concentrations [µg g^{-1}]
1	0.38	57.54	5.00
2	0.56	86.30	5.00
3	0.75	115.07	5.00
4	0.94	143.84	5.00
5	1.88	287.68	5.00
6	3.76	575.36	5.00
7	9.40	1438.39	5.00

Table 32. ^{129}I calibration standard concentrations with ^{127}I at 50 µg g^{-1}

Standard Level	^{129}I standard concentrations [Bq kg^{-1}]	^{129}I standard concentration [pg g^{-1}]	^{127}I standard concentrations [µg g^{-1}]
1	0.38	57.54	50.00
2	0.56	86.30	50.00
3	0.75	115.07	50.00
4	0.94	143.84	50.00
5	1.88	287.68	50.00
6	3.76	575.36	50.00
7	9.40	1438.39	50.00

3.9 Optimisation parameters for the detection of ^{129}I by ICP-TQMS

3.9.1 Plasma condition optimisation

The average counts for ^{127}I observed when applying varying carrier gas flow rates and RF power, are presented in Table 33. The highest response was observed when selecting 1.15 L min^{-1} carrier gas and a RF Power of 1550 W (as shown in bold). A correlation between average counts at $m/z = 127$ (^{127}I) and nebuliser flow rates is also presented in Figure 48.

Table 33. Average counts for natural ^{127}I using different carrier gas flow rates and applying different RF power

No.	Carrier Gas [L min^{-1}]	RF Power [W]	m/z=127 [Avg. Count]
1	0.90	1000	233080
2	0.95	1000	800938
3	1.00	1000	1312644
4	1.05	1150	1541362
5	1.10	1300	1789372
6	**1.15**	**1550**	**1973568**
7	1.20	1600	1599689
8	1.25	1600	778655

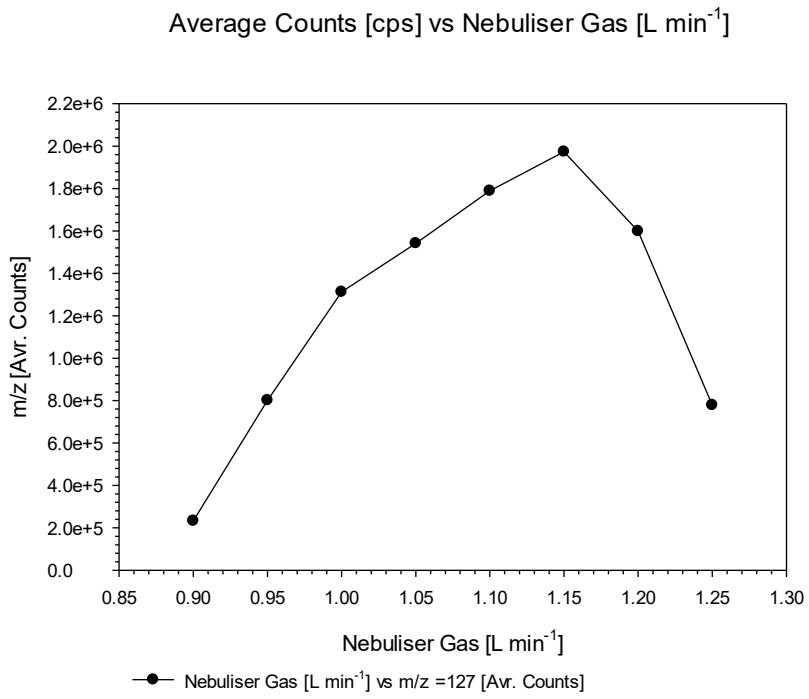

Figure 48. Correlation between average count at $m/z = 127$ (^{127}I) and nebuliser gas flow rate at optimised RF Power of 1550W

The optimised response at $m/z = 129$, present in trace amount in the argon plasma gas, was also assessed and results are presented in Table 34.

Table 34. Average counts at $m/z = 129$.

No.	Carrier Gas [L min^{-1}]	RF Power [W]	m/z = 127 [Avg. Count]	m/z = 129 [Avg. Count]
1	0.90	1000	233080	595
2	0.95	1000	800938	1942
3	1.00	1000	1312644	3040
4	1.05	1150	1541362	3476
5	1.10	1300	1789372	3842
6	**1.15**	**1550**	**1973568**	**4142**
7	1.20	1600	1599689	2779
8	1.25	1600	778655	964

3.9.2 Extraction lens voltage optimisation

In this second experiment, the optimised parameters obtained from experiment 1 were kept (i.e., 1.15 L min^{-1} carrier gas and a RF Power of 1550W) and different voltages were applied to the extraction lens to test the response of the iCAP ICP-TQMS instrument at $m/z = 127$. The results

are presented in Table 35 and showed an optimal response when setting the extraction lens voltage at -250V. A correlation between average counts $m/z = 127$ (^{127}I) and the extraction lens voltage is also displayed in Figure 49.

Table 35. Summary of average counts and extraction lens voltage for optimised values

No.	Carrier Gas [L min^{-1}]	RF Power [W]	Extraction Lens [V]	m/z = 127 [Avg. Count]
1	1.15	1550	-260	2115989
2	**1.15**	**1550**	**-250**	**2120676**
3	1.15	1550	-240	2108993
4	1.15	1550	-230	2116403
5	1.15	1550	-220	2114469
6	1.15	1550	-210	2110381
7	1.15	1550	-200	2110332
8	1.15	1550	-190	2109856

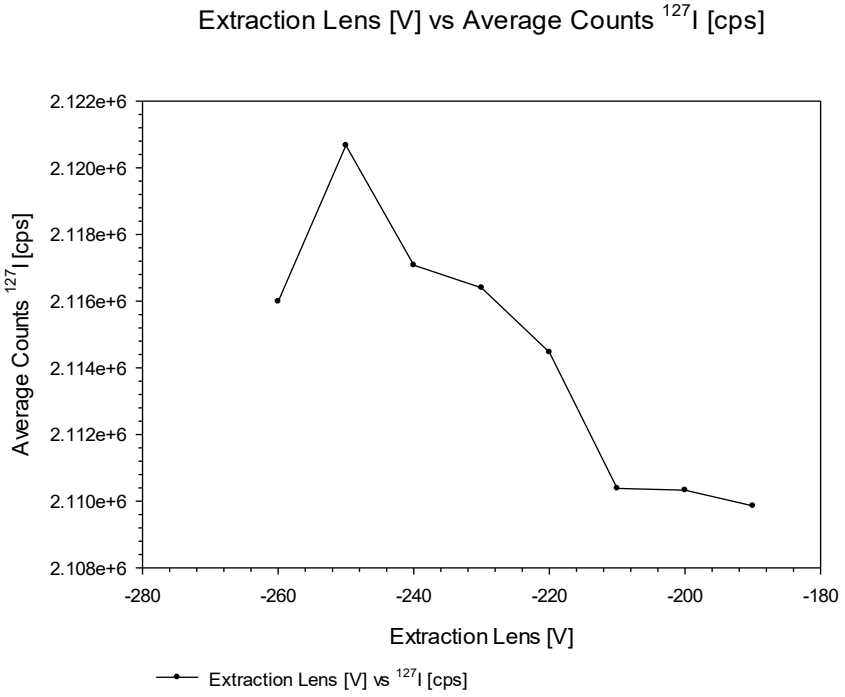

Figure 49. Correlation between average count at $m/z = 127$ (^{127}I) and extraction lens voltage

Different voltages were also applied to the first quadrupole extraction lens, and the optimal response was obtained when using -130V, as shown in bold in Table 36. A correlation between

average counts $m/z = 127$ (^{127}I) and the first quadrupole extraction lens voltage is also displayed in Figure 50.

Table 36. Summary of average counts and extraction lens voltage for optimised values

No.	Carrier Gas [L min^{-1}]	RF Power [W]	First Quadrupole Extraction Lens [V]	m/z = 127 [Avg. Count]
1	1.15	1550	-160	1928531
2	1.15	1550	-150	2031725
3	1.15	1550	-140	2062184
4	**1.15**	**1550**	**-130**	2086420
5	1.15	1550	-120	2082424
6	1.15	1550	-110	2067732
7	1.15	1550	-100	1990025
8	1.15	1550	-90	1825703

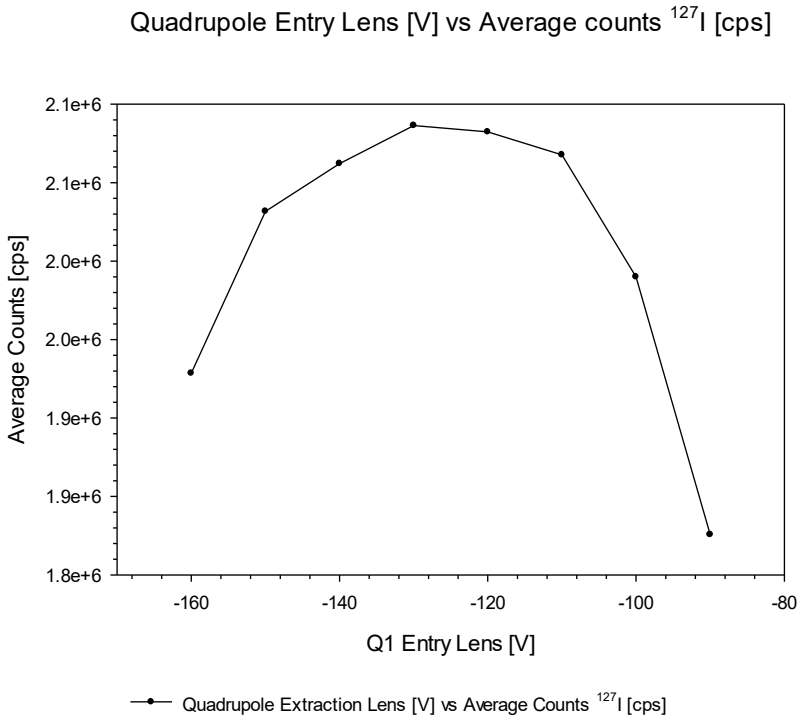

Figure 50. Correlation between average count for $m/z = 127$ (^{127}I) and first quadrupole extraction lens voltage

3.9.3 Isobaric ^{129}Xe interference removal

Signals at $m/z = 129$ arising from the presence of ^{129}Xe originating from the argon plasma gas, as well as from polyatomic interferences such as $^{127}I^{1}H^{1}H$, $^{97}Mo^{16}O^{16}O$, $^{89}Y^{40}Ar$, were systematically evaluated using varying O_2 gas flow rates, up to 0.5 ml min^{-1} (see Figure 51). The introduction of oxygen into the CRC facilitates the selective reaction of these interfering species, effectively removing their contribution to the signal at $m/z = 129$. By monitoring the resulting count rates, an oxygen flow of 0.21 ml min^{-1} was determined to provide optimal interference removal, corresponding to a stable signal of approximately 500 counts per second (cps). This balance between interference suppression and signal intensity was considered optimal, as higher oxygen flows led to unnecessary signal attenuation, while lower flows were insufficient to fully remove to interfering species. This flow rate was subsequently adopted for all further measurements, ensuring accurate and reproducible quantification of ^{129}I while minimising contributions from xenon and other polyatomic interferences.

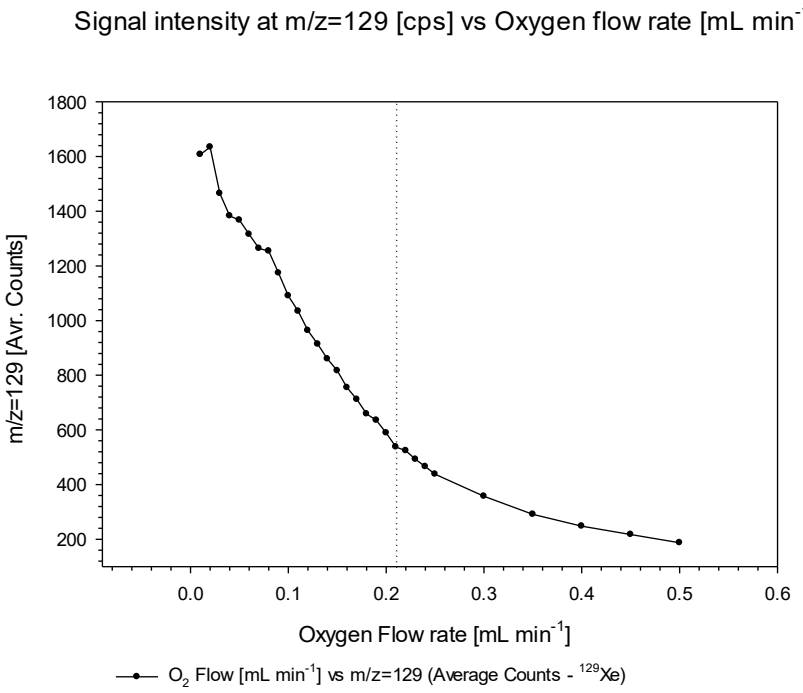

Figure 51. Signal intensity at $m/z = 129$ with increasing oxygen flow rate (cut off point at 0.21 mL min^{-1})

3.9.4 Summary of optimisation parameters

The optimised parameters for ^{129}I analysis are summarised in Table 37. These parameters were then retained for attempting to determine ^{129}I in seaweed and seawater samples. The data acquisition parameters are summarized in Table 38.

Table 37. Selected optimised parameters for ^{129}I analysis

Plasma Power [W]	Plasma Flow [L min^{-1}]	Extraction Lens [V]	Q1 Entry Lens [V]	CRC Oxygen Flow [mL min^{-1}]
1550	1.15	-200	-130	0.21

Table 38. Selected optimised parameters for ^{129}I analysis

m/z	Analyte	Dwell time (s)	Number of sweeps	Analyses mode
127	^{127}I	0.1	1000	TQ
129	^{129}I	0.5	1000	TQ
175	$^{159}Tb^{16}O$	0.1	1000	TQ
7 - 245	Survey Scan	0.001	100	SQ

NOTE: The survey scan is performed in single quadrupole mode.

Dwell time is the time that the instrument spends acquiring the data which make up a peak on the mass spectrum. The number of sweeps is the number of times the signal pulse passing through the quadrupole passes across the mass spectrum of the selected m/z values. During the same data acquisition time for the quantitative analysis of ^{129}I performed the survey scan (semi-quantitative concentration values for m/z = 7 to m/z = 245 in single quadrupole mode). The survey scan result can be used for method validation and to establish limit of detection.

3.10 Results and discussion

3.10.1 Dihydride formation

The results obtained from the study of peak tailing (i.e., from dihydride formation) are presented in Tables 39 and 40. As shown in Table 39, the concentration of ^{127}I in the final solution, ranging from 10 ng g^{-1} (10 ppb) to 5000 ng g^{-1} (5 ppm) did not show any dihydride formation ions ($^{127}I^1H^1H$) at m/z = 129 as the average count values were found to be constant. As displayed in Table 40, average counts at m/z = 127 ranged from 10^8 to 10^9, with the values at m/z = 129 being found constant up to 80 µg g^{-1} (80 ppm) for ^{127}I. However, average count values were observed higher by

up to 50% between 200 and 400 µg g^{-1}, suggesting the presence of dihydride ion formation ($^{127}I^{1}H^{1}H$) at m/z = 129.

Table 39. Average counts observed at mass 127 and 129 using different ng g^{-1} concentrations of a ^{127}I standard solution in 0.5% TMAH and associated 129/127 mass ratios

^{127}I concentration in 0.5 % TMAH solution [ng g^{-1}]	m/z = 127 [Avg. Count]	m/z = 129 [Avg. Count]	m/z = 129/127 ratio
0	12,039	188	1.56E-02
10	345,753	183	5.29E-04
20	716,497	179	2.50E-04
50	892,380	174	1.95E-04
100	1,755,940	172	9.80E-05
1,000	16,562,337	168	1.01E-05
2,000	30,977,010	164	5.29E-06
5,000	74,475,726	159	2.13E-06

Table 40. Average counts observed at mass 127 and 129 using different µg g^{-1} concentrations of a ^{127}I standard solution in 0.5% TMAH and associated 129/127 mass ratios

^{127}I concentration in 0.5 % TMAH solution [µg g^{-1}]	m/z = 127 [Avg. Count]	m/z = 129 [Avg. Count]	m/z = 129/127 ratio
0	14,612	89	6.09E-03
10	144,389,357	87	6.03E-07
20	269,257,507	85	3.16E-07
40	629,395,853	84	1.33E-07
80	1,247,391,520	88	7.05E-08
200	2,975,083,581	106	3.56E-08
300	4,827,706,699	119	2.46E-08
400	5,984,096,947	121	2.02E-08

3.10.2 Assessment of signal suppression

The results from the assessment of the impact of stable iodine at m/z = 127 on intensities at m/z = 129 are shown in Tables 41 and 42. A terbium (^{159}Tb) solution at concentration 1 ng g^{-1} was used

as internal standard and measured at m/z = 175 ($^{159}Tb^{16}O$) to monitor the signal suppression sensitivity following high matrix loading of stable ^{127}I. Two sets of calibration standards were used for ^{129}I with a constant concentration of ^{127}I at 5 and 50 µg g^{-1}, respectively.

Table 41. Average counts at masses 127, 129 and 175 using a 5 µg g^{-1} ^{127}I solution and associated 129/127 ratios

Standard Level	m/z = 127 [Avg. Count]	m/z = 129 [Avg. Count]	m/z = 129/127 ratio	m/z = 175 [Avg. Count]
1	615,058	246	4.00E-04	1,025,187
2	617,045	322	5.22E-04	1,061,595
3	617,775	383	6.20E-04	1,065,632
4	618,755	455	7.35E-04	1,073,624
5	618,145	798	1.29E-03	1,095,599
6	631,802	1,493	2.36E-03	1,108,656
7	620,904	3,504	5.64E-03	1,122,510

Table 42. Average counts at masses 127, 129 and 175 using a 50 µg g^{-1} ^{127}I solution and associated 129/127 ratios

Standard Level	m/z = 127 [Avg. Count]	m/z = 129 [Avg. Count]	m/z = 129/127 ratio	m/z = 175 [Avg. Count]
1	902,366,200	231	2.56E-07	908,899
2	893,509,660	285	3.19E-07	905,215
3	906,258,451	347	3.83E-07	906,004
4	865,521,610	393	4.54E-07	871,631
5	834,587,545	654	7.84E-07	838,722
6	763,519,306	1,113	1.29E-06	775,414
7	738,618,305	2,572	3.07E-06	748,559

In Table 41, the concentration of ^{127}I at 5 µg g^{-1} did not have any suppression effect on ^{129}I at m/z = 129. The internal standard signals at m/z = 175 were similar across the different standard levels tested. The ionization efficiency for terbium varied by 5%. As shown in Table 42, a higher concentration of ^{127}I, at 50 µg g^{-1}, was found to be affecting the signal at m/z = 129 – signal suppression by concomitant elements. This effect is also described in the literature [32, 322, 323] as the space charge effect and explains matrix effects. In this case, the efficiency of plasma ionisation dropped with increased concentrations of ^{129}I.

3.10.3 ^{129}I in seaweed

The results obtained from the analysis of seaweed via both the presented ICPMS and LSC methodologies are collated in Table 43. A range of sample masses were used for comparison purposes. Overall, the results were in a relatively good agreement. To evaluate the agreement between the two methods, the relative difference (% difference) was calculated for each sample using the formula:

$$\% \, Difference = \frac{ICPMS - LSC}{LSC} \times 100$$

Table 43. ^{129}I activity concentration in seaweed samples

Dry seaweed sample weight [g]	ICPMS measured Bq g^{-1}	LSC measured Bq g^{-1}	Difference %
1.0	0.0511 ± 0.0025	0.0559 ± 0.0016	8.6
1.0	0.0655 ± 0.0033	0.0666 ± 0.0019	1.7
1.0	0.0726 ± 0.0064	0.0760 ± 0.0022	4.5
2.0	0.0549 ± 0.0036	0.0532 ± 0.0015	3.2
2.0	0.0515 ± 0.0094	0.0589 ± 0.0017	12.5
2.5	0.0602 ± 0.0043	0.0674 ± 0.0019	10.7
2.5	0.0747 ± 0.0031	0.0708 ± 0.0020	5.5

The percentage of differences between ICPMS and LSC measurements ranged from 1.7 % to 12.5 %, with an average relative difference of approximately 6.8 %. This demonstrates that ICPMS provides results that are generally consistent with the established LSC method. Minor discrepancies are attributed to measurement uncertainties and the inherent differences between the two analytical techniques.

However, the ICPMS values in most cases were found to be lower in comparison to results from LSC measurements. This clearly indicated an impact of the matrix effect during ICPMS measurement. This was mainly related to the fact the extract used in both techniques was not fully purified and uncomplete extraction.

The full and partial mass survey scan spectra from using 1 g of seaweed extract are provided in Figures 52 and 53, respectively. The intensities are represented in log scale. Figure 56 showed

overall a complex spectrum with high intensities between m/z = 12 (^{12}C – combustion product from pyrolyser), m/z = 23 (^{23}Na – trapping solution) and m/z = 39 (^{39}K – trapping solution) up to 127 (^{127}I - seaweed) and m/z = 143.

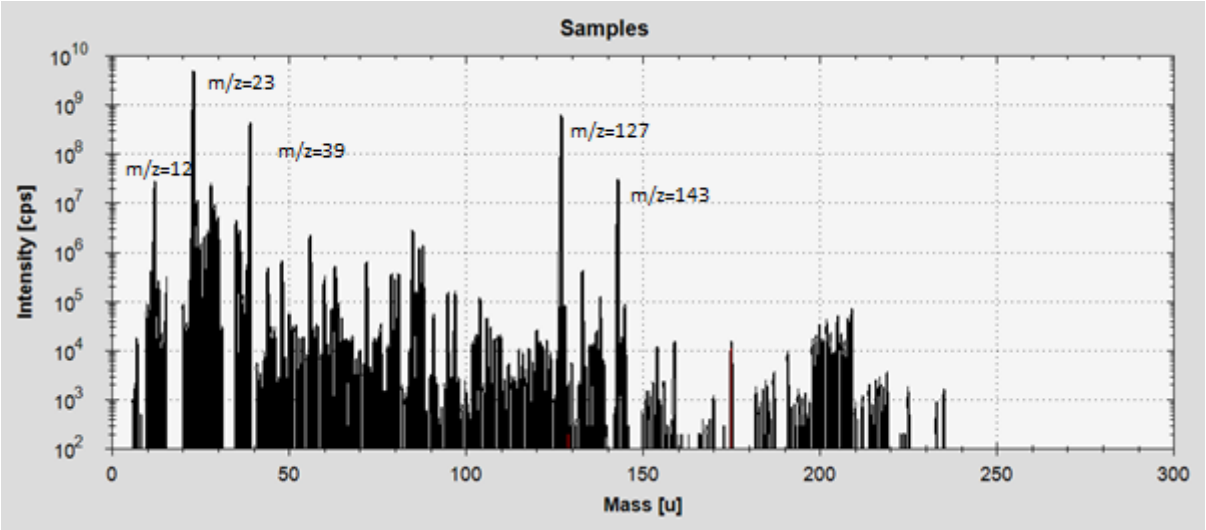

Figure 52. Full mass survey scan spectra using 1 g of a seaweed sample

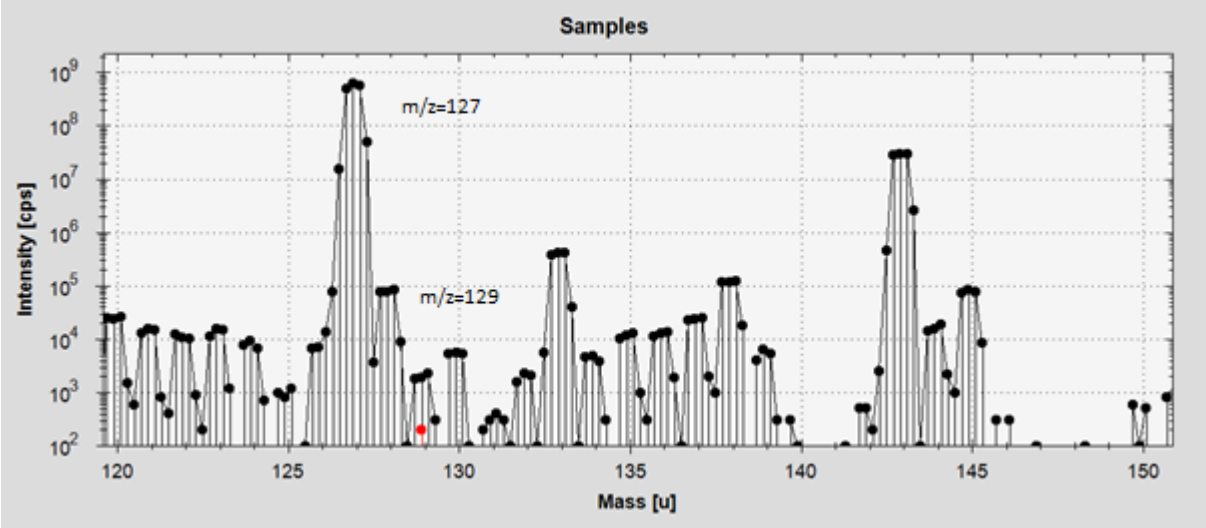

Figure 53. Survey scan from using a 1 g seaweed sample (fragment spectra from m/z = 120 to m/z = 150)

A narrowed spectrum between m/z = 120 and m/z = 150 is provided in Figure 56 and showed the large peak of ^{127}I at m/z = 127 in comparison with the analyte of interest ^{129}I at m/z = 129, with a subsequent ^{129}I/^{127}I ratio found to be approximately 10^{-6}. This value corresponds with other values found from the literature[286].

The main isobaric spectral interference from the presence of ^{129}Xe in argon plasma gas reacted with oxygen and contributed to the peak observed at m/z = 145 (^{129}Xe^{16}O). By reacting with oxygen, ^{127}I contributed to the peak displayed at m/z = 143 (^{127}I^{16}O). Other contributors at m/z = 143 and m/z = 145 could be ^{131}Xe^{14}N, ^{133}Cs^{12}C and ^{129}Xe^{14}N, ^{131}Xe^{12}C, ^{103}Rh^{40}Ar, respectively.

The ^{129}I result obtained from the analysis of a certified reference material – IAEA-418 (Mediterranean Sea Water) did not agree with the certified ^{129}I concentration activity of 3.2×10^{-7} Bq L^{-1} as it was too low for detection by ICPMS. The intensities from three replicates recorded at m/z = 129 were then compared with the results from analysing a blank solution. All results are collected in Table 44.

Table 44. ^{129}I intensities recorded from repeat analysis of the IAEA-418 CRM (seawater)

Sample	Intensities at m/z = 129 [Avg. counts]
Blank	154
20 g (1)	101
20 g (2)	110
20 g (3)	155

As can be seen in Table 44, the intensities observed from the analysis of the CRM IAEA-418 were found below or equal to the blank intensity. Unfortunately, 20 grams was the maximum quantity that could be introduced in the combustion boat, suggesting the need to pre-concentrate prior to the pyrolysis process.

3.10.4 Reproducibility of ^{129}I measurements

The reproducibility of the iCAP ICP-TQMS method for determining ^{129}I in seaweed was confirmed through consistent results across samples of varying masses – see Table 43. The measured activity concentrations ranged from 0.0511 to 0.0747 Bq g^{-1}, with overall mean value of 0.0616 Bq g^{-1}, and a weighted standard deviation of 0.0090Bq g^{-1}, corresponding to a weighted relative standard deviation (RSD) of approximately 14.6 %. Replicate analyses of equal sample weights (e.g. 1 g and 2 g) showed close agreement, demonstrating that variations in sample mass within the tested range (1 – 2.5 g) had negligible influence on the measured activity. These findings indicate a high level of analytical precision and method robustness, confirming that the iCAP ICP-TQMS provides reliable and reproducible measurements of ^{129}I in small biological samples. Furthermore, the strong reproducibility supports the overall method validation, verifying its accuracy, linearity, and compliance with the established detection limit. This demonstrates the suitability of the technique for routine environmental monitoring, inter-sample comparison, and long-term bioindicator studies using seaweed as a sensitive tracer matrix.

3.10.5 Limit of Detection for measurements of ^{129}I (LOD)

The background from using of 0.5 % TMAH solution and lowest standard counts of ^{129}I corresponded to a concentration of 57.54 pg g^{-1} (0.38 Bq kg^{-1}) at m/z = 129 from three runs summarised in Table 45. The limit of detection was calculated by converting three times the standard deviation of background counts into a concentration value using the calibration function equation provided by the operating Qtegra software.

Table 45. ^{129}I limit of detection

0.5 % TMAH solution background counts [cps]	^{129}I Level 1 standard counts [cps]	Limit of detection [pg g^{-1}]	Limit of detection [Bq g^{-1}]
146	292	3.60	2.35×10^{-5}
154	297	2.34	1.53×10^{-5}
188	315	2.72	1.77×10^{-5}

The limit of detection for ^{129}I was determined to be in the pg g^{-1}, corresponding to an activity concentration to 10^{-5} Bq g^{-1} from minimal sample sizes ranging from 1 to 2.5 g, demonstrating the significant potential of quadrupole ICP-MS for monitoring trace elements in biological matrices. Compared to other techniques and sample types, this approach offers a practical and sensitive solution for rapid, low sample analyses, as summarized in Table 46.

Table 46. Comparison of Limit of detection of ^{129}I

Sample	**Instrumentation/ Measurement**	**Limit of detection pg g^{-1} (Bq g^{-1})**	**Sample size**	**Ref.**
Water	Accelerator Mass Spectrometry (AMS)	(2.4×10^{-13})	0.6 L	[324]
Soils	ICP-MS with DRC	15.2 (9.9×10^{-6})	30 – 180 g	[325]
Decommissioning matrices	Quadrupole ICP-MS	16 (1.05×10^{-4})	0.5 – 1 g	[91]
Soils	Liquid Scintillation Counting (LSC)	(10^{-3})	100 g	[326]
Seaweed	iCAP ICP-TQMS	3.6 (2.35×10^{-5})	1 – 2.5 g	This work

In comparison, AMS achieves ultra-trace detection in water but requires large sample volume, while ICP-MS with DRC or LSC provides good sensitivity for solid but demands substantially larger

sample masses. Quadrupole ICP-MS for decommissioning matrices shows similar sensitivity with minimal sample input. These comparisons highlight that seaweed, represents a highly efficient, low-sample, and sensitive approach for routine environmental monitoring of trace elements, particularly in marine and coastal ecosystems.

3.11 Conclusion

A novel analytical method for the determination of ^{129}I in seaweed samples was developed using the iCAP ICP-TQMS instrument. During the method development, the plasma conditions and the voltage of the ion optics well systematically optimised to minimize the formation of dihydride species $^{127}I^{1}H^{1}H$, which originate from the abundant stable isotope ^{127}I and can interfere with accurate ^{129}I measurements. Additionally, the use of O_2 as a collision/reaction gas effectively eliminated the isobaric interference from ^{129}Xe at m/z = 129, enabling selective and sensitive quantification of ^{129}I.

To extract iodine from complex matrices such as seaweed, a combustion-based extraction procedure was successfully employed. This approach produced consistent and reproducible results across multiple samples, demonstrating both reliability and robustness of the method. The performance of the ICP-TQMS approach was found to be comparable to traditional radiometric techniques, such as liquid scintillation counting (LSC), with respect to sensitivity, precision and accuracy.

The method exhibits an instrumental limit of detection (LOD) of 1.53 10^{-5} Bq g^{-1} (equivalent to 2.34 pg g^{-1}) for ^{129}I, which is sufficiently low for environmental monitoring applications. Given its sensitivity, reproducibility, and adaptability, this method has potential applications beyond seaweed, including the analysis of other solid and liquid environmental matrices.

The determination of 129I in environmental samples is of significant scientific and ecological interest. 129I is a long-lived radionuclide produce both naturally and anthropogenically, for example, as a by-product of nuclear fuel reprocessing. Its low concentration in the environment and its mobility make it an importance tracer for studying the cycles and monitoring the impact of nuclear activities on ecosystems.

Compared to traditional radiometric techniques, such as LSC, the ICP-TQMS approach several advantages, including faster analysis, lower sample volume requirements, and the ability to handle complex matrices without extensive chemical separations. However, potential limitations include the need for careful optimisation of plasma conditions and interference management. Future improvements could focus on further reducing interferences form other isotopes or

molecular species, increasing sample throughput, and expanding the method to other challenging environmental matrices, such as soils, sediments, and industrial effluents.

Overall, the combination of optimised ICP-TQMS detection with a robust combustion extraction procedure provides a rapid, accurate, and reliable analytical approach and long-term ecological assessment, providing a valuable tool for understanding the fate and transport of radioactive iodine in diverse environmental systems.

Chapter 4 Improved sensitivity for measuring ^{226}Ra in reference materials and seawater samples by ICP-TQMS

4.1 Natural and human sources of ^{226}Ra in the environment

Radium has the symbol Ra and the atomic number 88. Radium is an alkaline earth metal lying in the bottom of group IIa in the periodic table. The element was discovered in 1898 by Marie and Pierre Curie. Their work was closely linked to the discovery of special rays continuously emitted by uranium salts by Henri Becquerel in 1896. This property of emission of rays was called radioactivity. The Curies discovered that several minerals had stronger radioactivity than the oxides of uranium and thorium. Their conclusions were that these minerals contained some new element with radioactivity which was much stronger than uranium and thorium and which might be present in the minerals in only a very small proportion. This particular hypothesis was verified with the discovery of Ra and polonium (Po) from pitchblende ore in 1898[327, 328].

There are 34 radium isotopes known up to date and all of them are radioactive. The mass numbers of the known isotopes range from 201 to 234[329]. There are four naturally occurring isotopes present in the environment: ^{223}Ra, ^{224}Ra, ^{226}Ra, ^{228}Ra as decay products within the three natural radioactive decay series (Thorium, Uranium, and Actinium series – Figure 54). The longest-lived isotope of radium, and most common present in environment, is ^{226}Ra that occurs from the decay chain of ^{238}U (often referred to as the radium series). The half-life of ^{226}Ra is 1,602 years. The next longest-lived isotope is ^{228}Ra, a product of ^{232}Th breakdown, with a half-life of 5.75 years. Both ^{223}Ra and ^{224}Ra are short-lived isotopes with a half-life of 11.7 and 3.64 days, respectively.

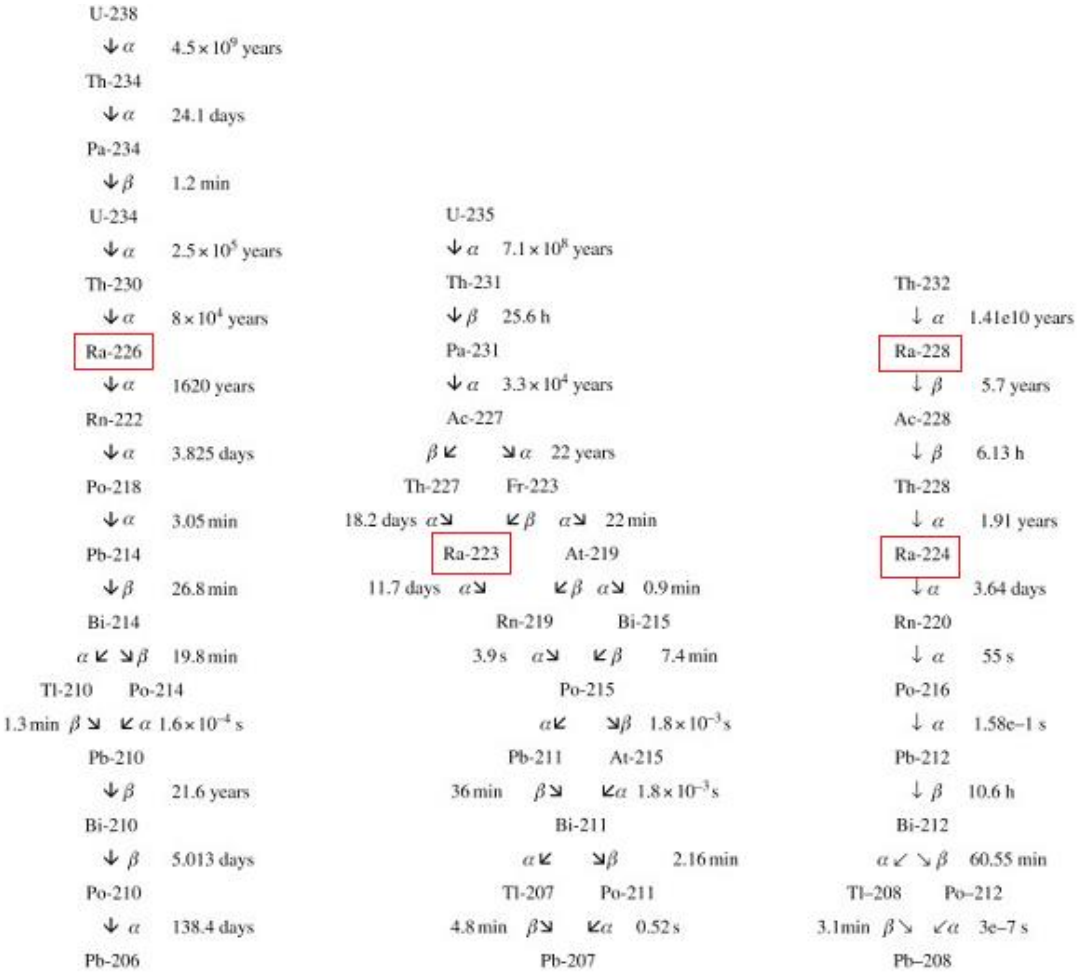

Figure 54. Uranium, Actinium and Thorium (from left) natural radioactive series[330]

Radioluminescent paint was invented in the early 1920s and originally contained ^{226}Ra. This paint was used in the production of watches, nuclear panels, aircraft switches, clocks, and instrument dials. Many former watch-dial painters who used their lips to shape the paintbrush died from the direct exposure to radioactivity from ^{226}Ra, which over time, accumulated in bones[328]. Radium was also used as an additive in the food industry to improve taste and preserve food longer. This industrial practice also led to death cases directly related to radiation exposure[331]. Radium was also used as an additive in many cosmetic products. Such products soon fell out of vogue and were prohibited by authorities in many countries, after discovering they could have serious adverse health effects[332].

As a group IIa element, radium has a similar property to calcium and can be easily incorporated into bones. Furthermore, the consumption of food and water containing radium led to accumulation in body and contribute to the radiological dose. In some geographical regions presenting naturally elevated concentrations of radium in surrounding soil and rocks, the risk of

ingestion may be higher as a result of consumption of plants, animals and animals products[333-335].

Radium isotopes are often present in industrial waste originating from various mineral ore mining and processing activities e.g.: uranium, phosphate, coal, metal, oil and gas[336-342] and sludge arising from water treatment plants[343]. These substances with enhanced concentration of radium and other naturally occurring radionuclides are referred to as NORM (Naturally Occurring Radioactive Material) or TENORM (Technically Enhanced Naturally Occurring Radioactive Material).

NORM activities may be associated with the following[344]:

- Materials including products, residues, and waste with enhanced concentration of natural radionuclides resulted from technological processes in non-nuclear industries,
- Raw materials or waste rock material with natural elevated concentrations of natural radionuclides,
- Waste (sludge) with enhanced concentrations of natural radionuclides resulted from processes of treatment of drinking water or wastewater,
- Mining or industrial processes related to release solid or dissolved natural radionuclides to surface water or ground water.

These may cause enhanced exposure to workers and members of public from discharging NORM waste in the environment.

Determination of radium in the environment is important from human and environmental health reasons. With similar chemical properties as Ca, strontium (Sr) and barium (Ba), Ra can easily accumulate in the body very easy incorporated into bones[345, 346]. Accumulation of radium in bones and in the muscle, tissue enhance the total annual radiation dose[347]. In the UK, the concentration of ^{226}Ra in water intended for human consumption is regulated under the Natural Mineral Water, Spring Water and Bottled Drinking Water (England) Regulation 2007. According to Schedule 12 of these regulations, the derived concentration for ^{226}Ra is set at 0.5 Bq L^{-1} (13.7 pg L^{-1}), and the associated analytical methods are generally required to achieve a limit of detection of 0.04 Bq L^{-1} (1.1 pg L^{-1}). [legislation.gov.uk]

Radium-226 is also a powerful tool for assessing the transfer mechanisms of other organic or inorganic chemicals present in NORM waste. It is also often measured in sediment cores to determine indirectly the amount of unsupported lead-210 (^{210}Pb), used as a geochronological tool and characterise sediment-water exchange or ocean mixing processes[348, 349].

4.2 Traditional methods and established ICP-MS methods for measuring ^{226}Ra in environmental matrices

^{226}Ra is an alpha-emitter, with emissions of 4.78 MeV (94.45%), 4.60 MeV (5.55%), and associated gamma-ray emission at 186.1 keV. A number of techniques has been reported in the literature for the determination of ^{226}Ra. These include α-spectrometry[350, 351], β-γ coincidence counting[352], ^{222}Rn-emanation counting in a Lucas cell[353, 354], γ-spectrometry[355], liquid scintillation counting (LSC)[356], inductively coupled plasma-mass spectrometry (ICP-MS)[357], thermal ionisation mass spectrometry (TIMS)[358, 359] and accelerator mass spectrometry (AMS)[360]. All these techniques differ in terms of performance, selectivity, analytical effort, reproducibility, and stability. The performance of these techniques, when applied to different matrices has been reported widely[344, 361-365]. Among these techniques, ICP-MS was found to be capable of dealing with liquid samples containing relatively high levels of ^{226}Ra, with minimum detectable activities (MDA) varying between 0.22 Bq L^{-1} (6.0 pg L^{-1}) and 11 Bq L^{-1} (300.5 pg L^{-1})[366]. Nevertheless, the recent development of chromatographic resins and novel sample introduction system (e.g., desolvation unit) is believed to enable to achieve lower detection limits. Several ICPMS procedures used for the determination of ^{226}Ra in environmental matrices and reported in the literature are summarised in Table 47, including their respective limits of detection and method detection limits.

The limit of detection represents the lowest analyte concentration distinguishable from background noise and reflects the sensitivity of the instrument itself. The method detection limit, in contrast, accounts for the entire analytical procedure, including sample preparation, and provides a practical measure of the lowest concentration reliably detectable in routine analysis.

Table 47. Comparison of some reported procedures for determination of ^{226}Ra by ICPMS.

Sample	Separation/resin	Instrumentation/ Measurement	Limit of detection [pg L^{-1}]	Method detection Limit [pg L^{-1}]	Nebuliser system	Preconcen. factor	Ref.
Water, river, and seawater	AG 50W-X8 and Sr-resin	Quadrupole ICP-MS		0.02	APEX-Q introduction system	30	[357]
Seawater	Self-prepared MnO_2 and AG 50W-8	SF-ICP-MS		0.084	Medium resolution	333	[367]
Seawater	Seawater MnO2 coprecipitation and ion exchange purification (AG 50W-X8 (duplicate), Sr-resin, AG 1 x 8	MC-ICP-MS	0.091		Cetac Aridus II desolvating system	220-500	[368]
River water	Diphonix, 50W-X8 and Sr-resin	HR-ICP-MS	0.270	0.0014	Double pass cyclonic spray chamber	200	[369]
Groundwater	AG 50W-X8 and Sr-resin	SF-ICP-MS		0.090	APEX-Q introduction system	50	[370]
Thermal water	Radium specific solid phase extraction disc	Quadrupole ICP-MS	2	0.020	Ultrasonic nebulizer, expansion chamber, desolvation unit	100	[371]
Lake sediment	AG 50W-X8 (duplicate) and Sr-resin	SF-ICP-MS	0.006	0.020	APEX-Q introduction system		[372]

Sample preparation prior to ICPMS analysis is vital to eliminate isobaric or polyatomic interferences present in the plasma. The main polyatomic interferences for ICPMS analysis of ^{226}Ra have been reported[372-375] and are summarised in Table 48.

Table 48. Potential polyatomic interferences impacting ^{226}Ra quantification by ICP-MS.

Radionuclide (atomic mass u)	Interference	Atomic mass u	Required mass resolution ($m/\Delta m$)
^{226}Ra (226.025403)	$^{92}Mo^{94}Mo^{40}Ar^{+}$	225.774281	900
	$^{88}Sr^{138}Ba^{+}$	225.810855	1,100
	$^{87}Sr^{139}La^{+}$	225.815227	1,100
	$^{86}Sr^{140}Ce^{+}$	225.814696	1,100
	$^{88}Sr^{138}La^{+}$	225.812721	1,100
	$^{44}Ca_2{}^{138}Ba^{+}$	225.816203	1,100
	$^{89}Y^{137}Ba^{+}$	225.811669	1,100
	$^{86}Kr^{140}Ce^{+}$	225.816044	1,100
	$^{146}Nd^{40}Ar^{2+}$	225.837878	1,200
	$^{186}W^{40}Ar^{+}$	225.916747	2,100
	$^{187}Re^{39}K^{+}$	225.919458	2,200
	$^{194}Pt^{16}O_2{}^{+}$	225.952494	3,100
	$^{203}Tl^{23}Na^{+}$	225.962099	3,600
	$^{207}Pb^{19}F^{+}$	225.974284	4,500
	$^{208}Pb^{18}O^{+}$	225.975796	4,600
	$^{209}Bi^{16}O^{1}H^{+}$	225.983123	5,400
	$^{208}Pb^{16}O^{1}H_2{}^{+}$	225.987201	6,000

Their respective contribution to the signal at $m\ /\ z = 226$ will mainly depend on the sample matrix of interest, the ICPMS instrument used, and the gas modes selected in the collision/reaction cell of the instrument.

4.3 Aim

The main aim of this work was to optimise the plasma condition, extraction lens and first quadrupole entry lens voltage for measuring ^{226}Ra using the iCAP ICPTQMS system manufactured by ThermoFisher Scientific. The second part of this work was to determine the optimum gas flow (He, N_2) used in the desolvation system. These optimised parameters were then used to attempt the quantification of ^{226}Ra in seawater samples and IAEA solid reference materials.

4.4 Reagents

All standard solutions were prepared from elemental stock solutions in 1% HNO_3 (Aristar® VWR Chemicals). Hight purity de-ionised water (resistivity higher than 18.2 MΩ) was also produced using a Q-Pod Millipore System (Merck, York, UK). The internal standard solution of Tb was sourced from VWR Chemicals.

Other reagents such as hydrochloric acid (HCl), nitric acid (HNO_3), ammonia (NH_3), potassium permanganate ($KMnO_4$), manganese chloride ($MnCl_2$) were sourced from VWR Chemicals. The anion exchange resin Dowex 50W X8 was provided by Sigma Aldrich (UK). The strontium resin (4,4'(5')-bis(t-butylcyclohexano)-18-crown-6) was provided by TrisKem International (France).

The certified ^{226}Ra standard solution was supplied by Amersham PLC (UK), the certified reference materials were purchased from the International Atomic Energy Agency (Austria).

4.5 Instrumentation

All measurements were performed using the ThermoFisher Scientific iCAP ICP – Triple Quadrupole Mass Spectrometer (iCAP ICP-TQMS) controlled by the Qtegra software. The instrument was equipped with a standard sample introduction system consisting of a MicroMist nebulizer and baffled cyclonic spray chamber. A platinum tip sample cone and skimmer cone with high sensitivity skimmer cone insert were used instead of the standard and original nickel sample and skimmer cones. Samples were introduced directly into the ICP-MS using an ASX-520 autosampler with the standard peristaltic pump and tubing (internal diameter of 1.02 mm).

The Aridus 3 Desolvating Nebulizer System equipped with self-aspirating C-Flow PFA nebulizer with a flow rate of 100 µL min^{-1} (Teledyne Cetac Technologies) and controlled by The Aridus Link software was also used at the front of the iCAP ICP-TQMS system.

Hotplate, stirring plate, centrifuge and filtration apparatus with coarse porosity frit to accommodate a 47 mm diameter paper filter, 10 mL plastic columns were also used for extracting ^{226}Ra from seawater samples and certified reference materials.

4.6 Methodology

Plasma, optics voltage, collision/reaction gas flow rate and desolvation gas flow were the instrumental parameters investigated in this study.

As a radio frequency power generator, induction coil and gas are used to form Inductively Coupled Plasma (ICP), the RF Power (W) from the generator and the nebulizer gas flow (L min^{-1})

were the two main parameters investigation as part of the for plasma condition optimisation process.

Different extraction lens and first quadrupole extraction lens voltages were also tested to optimise a response from the instrument, as this is where separation of positive ions from neutral species, photons, and electrons and ion transfer to the mass analyzer occur.

Argon (Ar) and nitrogen (N_2) gases were used in the Aridus 3 Desolvation Nebulizer System to remove solvent from the sample analyte and improve sensitivity. These additional gases flow rates were also considered in this study.

The first sets of experiments focused on the plasma optimisation conditions, by gradually increasing the RF power between 1,000 and 1,600 W and assessing the m/z response at different nebulizer gas flows, as described in Table 49.

Table 49. Optimisation tests 1

No.	Nebulizer Gas Flow (L min^{-1})	RF Power (W)
1	0.90	1000 - 1600
2	0.95	1000 - 1600
3	1.00	1000 - 1600
4	1.05	1000 - 1600
5	1.10	1000 - 1600
6	1.15	1000 - 1600
7	1.20	1000 - 1600
8	1.25	1000 - 1600

The second set of experiments emphasised on the extraction lens and first quadrupole extraction lens voltage and was performed applying different voltages to both extraction and first quadrupole extraction lenses to establish the highest m/z response at mass 226.

The extraction lens and first quadrupole extraction voltages were both increased in 10 volts step and responses at $m/z = 226$ were recorded.

In the third set of experiments, different flow rates of argon (Ar) and next nitrogen (N_2) in the desolvation system (Aridus 3) were also tested to establish the highest m/z response of the ICPMS for ^{226}Ra. The argon and nitrogen flow rates in the Aridus 3 desolvation system were increased from 1.0 to 5.0 L min^{-1} and from 0.2 to 5.0 L min^{-1}, respectively.

A 0.5 µg L^{-1} (500ppt) solution of ^{226}Ra nuclide in 1% nitric acid was used in all three experiments and in an additional 0.001 mg L^{-1} (1ppb) solution of terbium (Tb) nuclide in 1% nitric acid was used as instrumental internal standard. Solutions were introduced into the plasma using an ASX-520 autosampler and data were collected for 60 seconds with 1,000 sweeps for each individual m/z value.

Seawater samples were first filtered through a 0.45 µm Whatman paper to remove particulate matter. One litre of seawater (1,026 g, 1.026 g mL^{-1}) was spiked with a known amount of ^{226}Ra standard. The different spiked quantities are detailed in Table 50. The solution was continuously stirred using a magnetic stirrer, followed by the addition of 0.75 mL saturated solution of $KMnO_4$, 1.5 mL of $MnCl_2$, and pH adjusted to values 8-9 with ammonia solution. The solution was stirred for 60 minutes and then left overnight to settle MnO_2 precipitate. The supernatant was decanted, and the precipitate was transferred to 50 mL centrifuge tubes and centrifuged at 3000 rpm for ten minutes. After decanting the solution, the precipitate was dissolved in 10 mL of 3 M HCl and loaded onto an anion exchange column (10 mL of resin Dowex 50W X8), preconditioned sequentially with 100 mL hight purity de-ionised water (resistivity higher than 18.2 MΩ), washed and conditioned with 50 mL of 3 M HCl, respectively. Sample loaded onto column and washed with 100 mL of 3 M HCl, and radium was eluted using 100 mL of 3 M HNO_3. Eluted fraction was evaporated to dryness and dissolved in 2 mL of 3 M HNO_3, then loaded onto a Sr-specific resin column (Sr-resin, 8 mL of resin ~ 2 g in 10 mL column) preconditioned with 100 mL of 3 M HNO_3. Radium was eluted using 20 mL of 3 M HNO_3, and the eluent was evaporated to dryness and finally dissolved in 20 mL of 1 % HNO_3 for analysis.

Ten grams of each three reference materials: IAEA-410 (Bikini Atoll Sediment), IAEA-434 (Phosphogypsum) and IAEA-465 (Baltic Sea Sediment) was boiled with 100 mL of 6 M HCl on hotplate for 2 hours. Then solution was filtered through paper filter (0.45 µm Whatman) and solution were transferred to 50 mL centrifuge tubes and centrifuged at 3000 rpm for ten minutes. The solution decanted to 100 mL beaker and evaporated to dryness. Then added 50 mL of 3 M HCl and then solution loaded onto an anion exchange column, following Sr- resin column described above.

NOTE: Boiling the samples in hydrochloric acid (HCl) is not intended to achieve complete dissolution of the matrix e.g. rocks. Instead, this step serves to selectively leach easily soluble minerals, carbonates, and surface-bound species, including radium and other alkaline earth metal, into solution. Partial acid treatment also helps remove potential surface contaminants and improves contact between the sample and subsequent reagents, facilitating efficient separation and pre-concentration of the target analytes for analysis.

The set of ^{226}Ra standard concentrations used for calibration is detailed in Table 51.

Table 50. ^{226}Ra spiked levels tested in seawater samples

Spiked level	Activity concentration [Bq L^{-1}]	Concentration [pg g^{-1}]
1	1	0.0273
2	2	0.0546
3	4	0.1093
4	5	0.1366
5	7.5	0.2049
6	10	0.2732

Table 51. Set of ^{226}Ra calibration standard concentrations

Standard Level	^{226}Ra standard concentrations [Bq L^{-1}]	Concentration [pg g^{-1}]
1	0.7483	0.0204
2	1.4967	0.0409
3	2.9933	0.0818
4	9.3541	0.2556
5	18.7082	0.5112
6	37.4163	1.0223
7	74.8327	2.0446
8	149.6654	4.0893

4.7 ICP-TQMS optimisation parameters for the detection ^{226}Ra

4.7.1 Plasma condition optimisation

The m/z signals from ^{226}Ra were collected and average counts using varying carrier gas flow rates and RF power, are presented in Table 52. The highest responses were observed when selecting 1.15 L min^{-1} carrier gas and a RF Power of 1400 W (shown in bold). A correlation between average counts at $m/z = 226$ (^{226}Ra) and nebuliser flow rates is also presented in Figure 55.

Table 52. Average counts obtained for ^{226}Ra using different carrier gas flow rates and applying different RF power

No.	Carrier Gas [L min^{-1}]	RF Power [W]	m/z=226 [Avg. Count]
1	0.90	1000	229129
2	0.95	1000	920660
3	1.00	1000	2101521
4	1.05	1100	2358840
5	1.10	1250	2645029
6	**1.15**	**1400**	**2744433**
7	1.20	1550	2672559
8	1.25	1600	2189422

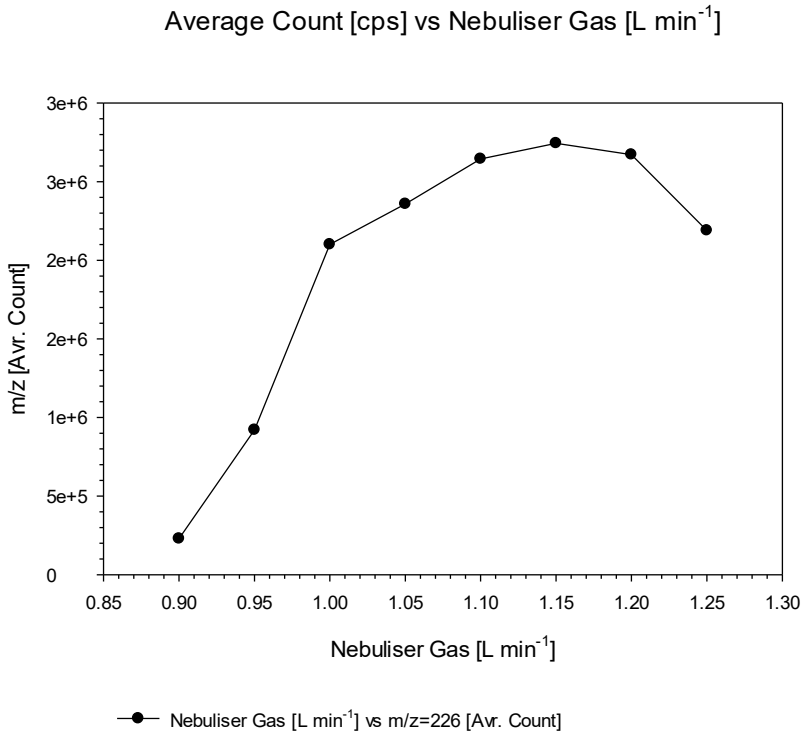

Figure 55. Correlation between average count for $m/z = 226$ (^{226}Ra) and nebuliser gas flow rate at optimised RF Power of 1400W

4.7.2 Extraction lens voltage optimisation

For this second experiment, the optimised parameters obtained from experiment 1 were retained (i.e., 1.15 L min^{-1} carrier gas and a RF Power of 1400W) and different voltages were applied to the extraction lens to test the instrumental response at $m\ /\ z = 226$. The results are presented in

Table 53 and showed an optimal response when setting the extraction lens voltage at -200V. A correlation between average counts $m/z = 226$ (^{226}Ra) and the extraction lens voltage is also displayed in Figure 56.

Table 53. Summary of average counts and extraction lens voltage for optimised values

No.	Carrier Gas [L min^{-1}]	RF Power [W]	Extraction Lens [V]	m/z = 226 [Avg. Count]
1	1.15	1400	-260	2755957
2	1.15	1400	-250	2819418
3	1.15	1400	-240	2827630
4	1.15	1400	-230	2850686
5	1.15	1400	-220	2850057
6	1.15	1400	-210	2852562
7	**1.15**	**1400**	**-200**	**2879181**
8	1.15	1400	-190	2809484

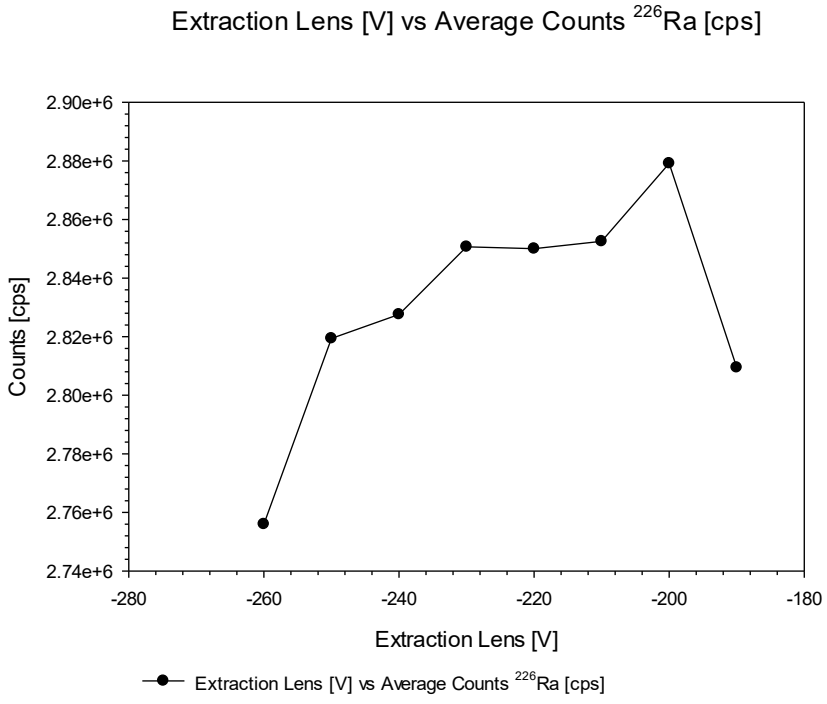

Figure 56. Correlation between average count at $m\ /\ z = 226$ (^{226}Ra) and extraction lens voltage

Different voltages were also applied to the first quadrupole extraction lens and the optimal response was obtained when using -120V, as shown in bold in Table 54. A correlation between

average counts $m/z = 226$ (^{226}Ra) and first quadrupole extraction lens voltage is also displayed in Figure 57.

Table 54. Summary of average counts and extraction lens voltage for optimised values

No.	Carrier Gas [L min^{-1}]	RF Power [W]	First Quadrupole Extraction Lens [V]	m/z = 226 [Avg. Count]
1	1.15	1400	-150	2291688
2	1.15	1400	-140	2508642
3	1.15	1400	-130	2576553
4	**1.15**	**1400**	**-120**	**2660295**
5	1.15	1400	-110	2583812
6	1.15	1400	-100	2538429

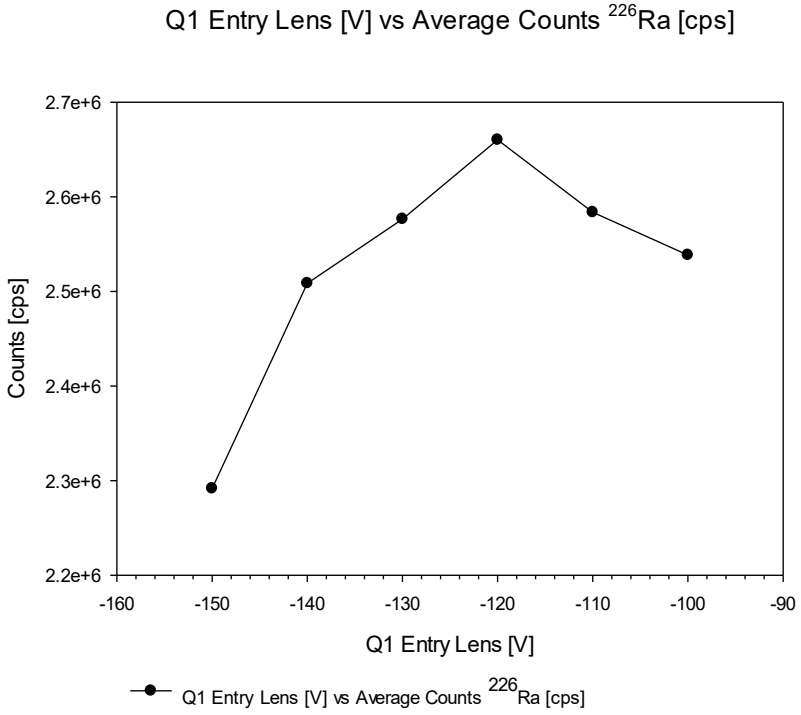

Figure 57. Correlation between average count for $m/z = 226$ (^{226}Ra) and first quadrupole extraction lens voltage

4.7.3 Aridus 3 desolvation system argon and nitrogen flow rate optimisation

As shown in Figures 58 and 59, the optimal average counts at $m/z = 226$ (^{226}Sr) were obtained when using 3.5 L min^{-1} and 1.0 L min^{-1} of argon and nitrogen gases, respectively.

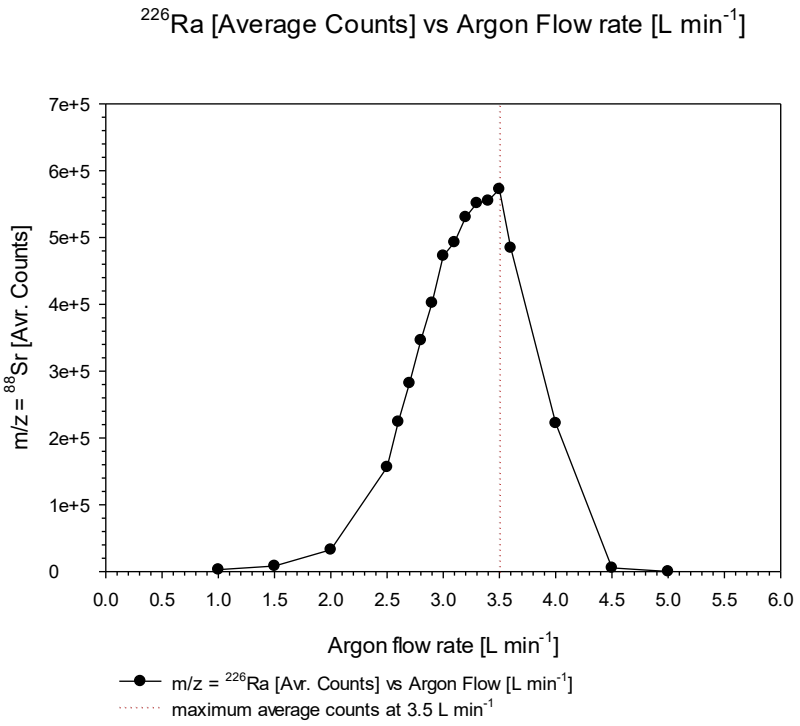

Figure 58. Aridus 3 desolvation system – argon flow rate optimisation

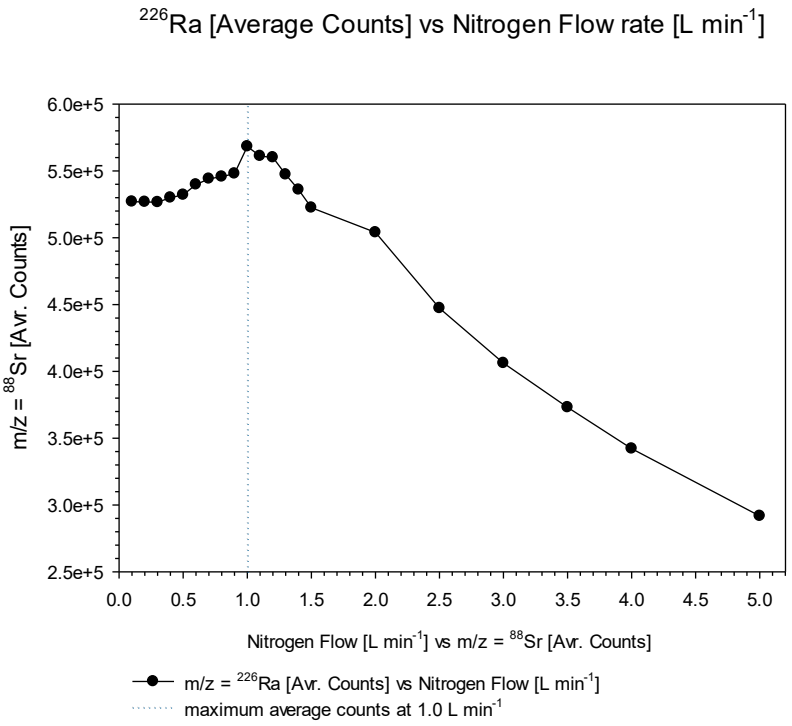

Figure 59. Aridus 3 desolvation system – nitrogen flow rate optimisation

4.7.4 Kinetic Energy Discrimination for ^{226}Ra measurement

Kinetic Energy Discrimination (KED) is a technique widely used in ICP-MS to enhance the accuracy of ^{226}Ra measurements by minimising polyatomic interferences. In KED mode, the collision/reaction cell is filled with an inert gas, typical helium, causing ions to undergo collisions. Polyatomic interfering ions undergo more collisions and lose more kinetic energy than the heavier target radium ions ($^{226}Ra^{+}$), and an energy barrier at the cell exit allows only ions with sufficient kinetic energy to reach detector. This significant improves the signal-to-noise ratio, detection limits, and measurement precision for a trace radium analysis in complex matrices such as soils, sediments, and water. When compared to alternative interference-reduction strategies, such as the Dynamic Reaction Cell (DRC), Kinetic Energy Discrimination (KED) offers a straightforward and highly efficient approach for mitigating polyatomic interferences in ICP-MS analyses.

In KED mode, helium was used as the collision gas at a flow rate of 4.75 mL min^{-1}, which correspond to the instrument's default setting. This flow rate is optimised by the manufacturer to provide an effective balance between interference removal and ion transmission.

4.7.5 Summary of optimisation parameters

The optimised parameters for radium analysis are summarised in Table 55. These parameters were then retained for measuring ^{226}Ra in selected seawater and sediment samples. The data acquisition parameters are summarised in Table 56.

Table 55. Collated data of optimised parameters for ^{226}Ra analysis

Plasma Power [W]	Plasma Flow [L min^{-1}]	Extraction Lens [V]	Q1 Entry Lens [V]	Collision/Reaction Cell	Aridus 3 Desolvation Nebulizer System	
				KED mode - Helium Flow [mL min^{-1}]	Argon Flow [L min^{-1}]	Nitrogen Flow [L min^{-1}]
1400	1.15	-200	-120	4.75	3.5	1.0

Table 56. Collated data of optimised parameters for ^{226}Ra analysis

m / z	Analyte	Dwell time (s)	Number of sweeps	Analyses mode
226	^{226}Ra	0.5	1000	TQ
159	^{159}Tb	0.1	1000	TQ
7 - 245	Survey Scan	0.001	10	SQ

NOTE: The survey scan is performed in single quadrupole mode.

Dwell time is the time that the instrument spends acquiring the data which make up a peak on the mass spectrum. The number of sweeps is the number of times the signal pulse passing through the quadrupole passes across the mass spectrum of the selected m / z values. During the same data acquisition time for the quantitative analysis of ^{226}Ra performed the survey scan (semi-quantitative concentration values for m / z = 7 to m / z = 245 in single quadrupole mode). The survey scan result can be used for presence and interpretation the potential polyatomic interferences which may impact on ^{226}Ra quantification by ICP-MS.

4.8 Results and discussion

4.8.1 ^{226}Ra in seawater samples

The results obtained from the three repeats of seawater measurements and associated recoveries based on the spiked concentration are presented in Table 57. For each nominal spike level, the measured concentrations were consistently lower than expected, with recoveries ranging from 61 % to 79 %. The discrepancy between measured and expected values increases at higher spike levels, indicating a concentration dependent bias. Relative range widths, defined as the spread of measured values expressed as a percentage of the mean, are generally smaller at intermediate concentrations but increase at the highest spikes, reflecting greater measurement variability.

Table 57. ^{226}Ra activity concentration in seawater samples

Spiked Level Bq L^{-1}	ICPMS measured Bq L^{-1}	Uncertainty Bq L^{-1}	Mean measured Bq L^{-1}	Range widths Bq L^{-1}	Relative range (% of mean)	Recoveries [%]
1.00 ± 0.01	0.62 – 0.79	0.04 – 0.12	0.71	0.17	24	61 – 79
2.00 ± 0.07	1.23 – 1.48	0.10 – 0.16	1.36	0.25	18	61 – 74
4.00 ± 0.14	2.44 – 2.56	0.16 – 0.32	2.50	0.12	5	61 – 64
5.00 ± 0.18	3.37 – 3.72	0.39 – 0.67	3.55	0.35	10	67 – 74
7.50 ± 0.27	4.55 – 4.96	0.37 – 0.77	4.76	0.41	9	61 – 66
10.00 ± 0.12	6.15 – 7.12	1.40 – 2.36	6.64	0.97	15	61 – 71

NOTE: The uncertainty figures for spiked level corresponded to the micropipette uncertainty. Regarding ICPMS measurements, associated uncertainties were entirely related to counting. Natural content of ^{226}Ra (low concentration) in seawater has been omitted at this stage.

The points on the plot (see Figure 60) represent the mean measured activities for each spiked concentration, with vertical error bars illustrating the observed measurement range (i.e., the variability between replicate determinations). The dashed line denotes the ideal 1:1 relationship, where measured and spiked values would be equal in the absence of analytical bias or loss. In this case, all measured values consistently fall below the 1:1 line, clearly indicating systematic under-recovery across the full concentration range this trend suggests that the analytical method, while generally linear, underestimates the true activity levels – likely due to incomplete analyte recovery during sample preparation, matrix effects, or instrumental inefficiencies such as signal suppression. The growing divergence between the measured data points and the ideal line at higher concentrations suggests that this bias is not constant but slightly increases with spike level, indicating that further method development is needed to achieve full quantitative accuracy.

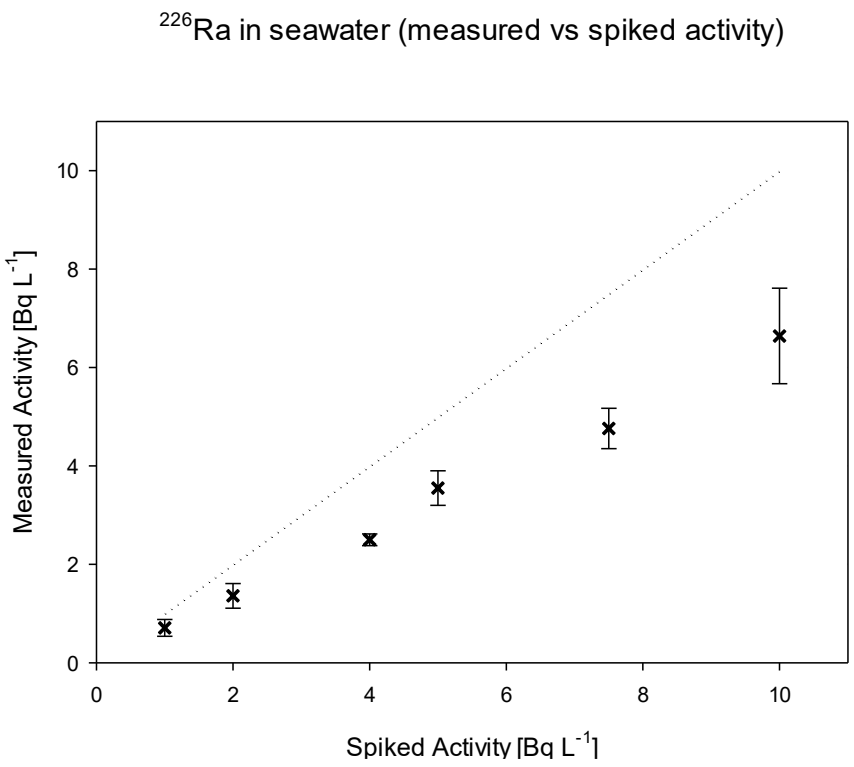

Figure 60. Measured vs spiked activity of ^{226}Ra in seawater samples

4.8.2 Reproducibility

The reproducibility of the ICP-MS measurements was evaluated across the spiked activity range of 1 – 10 Bq L^{-1}. The measured values (Table 57) showed relative variations between 5 % and 24 %

with the lowest reproducibility observed at the lowest spike level (1 Bq L^{-1}) and the highest reproducibility occurring around mid-range concentrations (4 – 7.5 Bq L^{-1}). This pattern indicates that the measurement precision improves as activity increases, likely due a=to a stronger signal relative to background and counting uncertainty. At higher spike levels (10 Bq L^{-1}), a slight increase in variability was observed, which may reflect to matrix effects at elevated concentrations. Overall, the data demonstrate acceptable reproducibility, with an average relative variability of 10 – 15 %, consistent with expected performance for low-level radionuclide quantification by ICP-MS.

However, despite the reasonable reproducibility, the associated recovery results (ranging from 61 % to 79 %) reveal a consistent underestimation of the true activity levels across all spike concentrations. This indicates a systematic bias in the analytical method, likely arising from incomplete analyte recovery during sample preparation or matrix inducted signal suppression during concentrations. Such low and variable recoveries reduce confidence in the quantitative accuracy of the method, particularly for trace-level determinations where precision and accuracy are equally critical. Therefore, further method development is required to improve analyte recovery to ensure the procedure achieves both reproducibility and accurate quantification.

4.8.3 Signal interferences

As shown in Table 57, the method recoveries varied overall between 61 and 79 %, using 1 to 10 Bq L^{-1} spike levels. These results suggested that the combination of the chromatographic an anion exchange column followed by the Sr-resin as well as the use of a Kinetic Energy Discrimination (KED) mode for the collision/reaction gases was suitable for measuring accurately ^{226}Ra in seawater samples. Nevertheless, some results were associated with relatively large uncertainties, suggesting some limitations. Survey scan spectra were then assessed further to understand better the main factors affecting the precision of this approach. Figures 61 and 62 showed the full and fragmental mass scan from using Qtegra software and using the highest spike level (i.e., 10 Bq L^{-1}; 0.2732 pg g^{-1}; $m/z = 226$), respectively. The black lines represented the intensity of detected m/z (mass (u) unit described in Qtegra software).

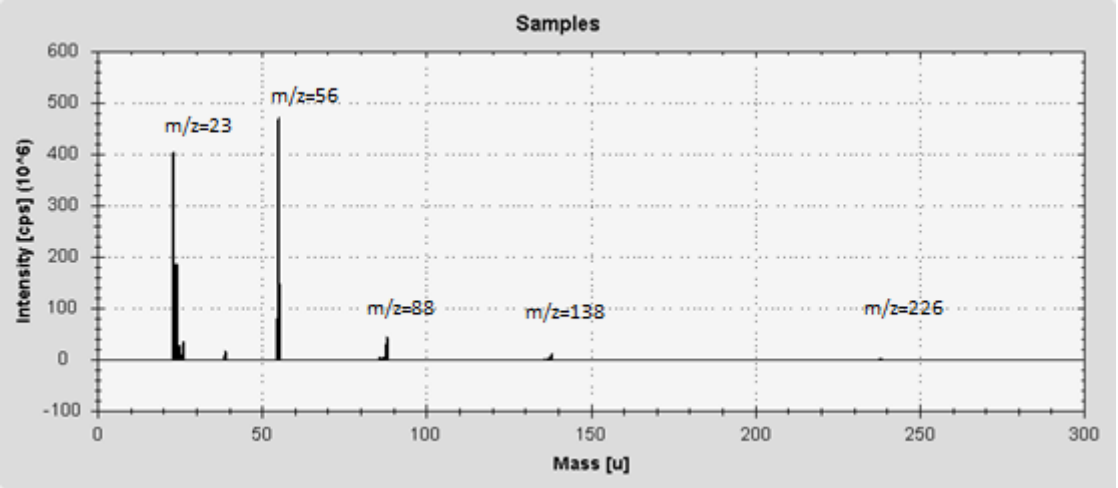

Figure 61. Full mass scan using spike level 7 (10 Bq L^{-1}; 0.2732 pg g^{-1}) in a seawater sample

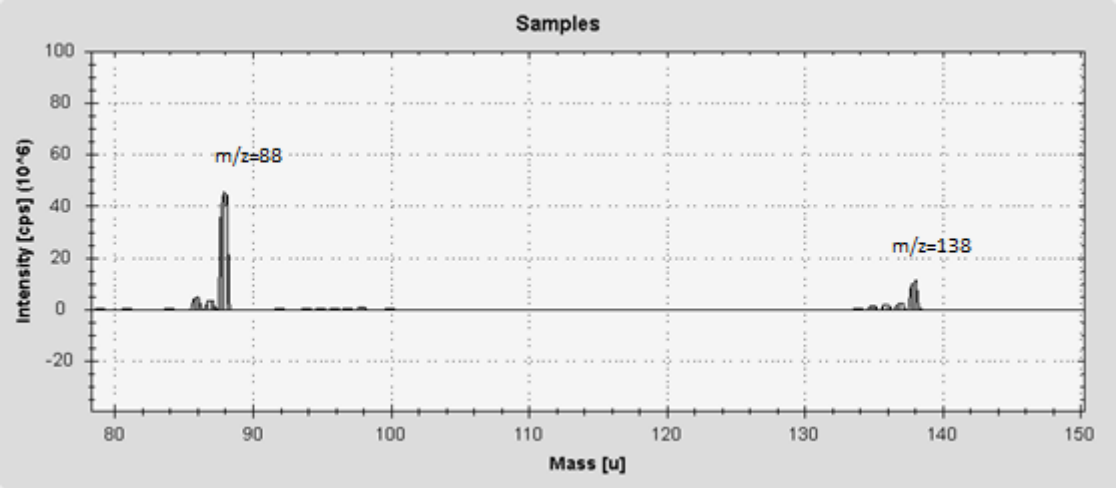

Figure 62. Fragmental mass scan from $m/z = 80$ to $m/z = 150$ using spike level 7 (10 Bq L^{-1}; 0.2732 pg g^{-1}) in a seawater sample

Figure 62 showed the presence of a signal at $m/z = 88$ (^{88}Sr) and $m/z = 138$ (^{138}Ba), where combination of these two ions (see Table 41) could interfere with the signal of interest at $m/z = 226$. Survey scans from all spiked levels consistently revealed the presence of these two signals at $m/z = 88$ (^{88}Sr) and $m/z = 138$ (^{138}Ba), indicating that these interfering ions were present across all tested concentrations. This co-occurrence could result in a false positive signal during the analysis, thereby compromising the accuracy and reliability of the measured signal at $m/z = 226$ (^{226}Ra).

The persistence of ^{88}Sr and ^{138}Ba signal suggest that the chemical extraction and separation procedures employed were not sufficiently, as these interfering ions were not fully removed from the sample matrix. To mitigate such interferences, the use of Kinetic Energy Discrimination (KED) mode in the ICP-MS analysis could be explored (e.g., optimisation helium flow rate, collision/reaction cell exit voltage – energy barrier), which can help reduce polyatomic

interferences by collisional energy filtering. Additionally, optimisation of the chemical separation protocol, such as improving the selectivity of the resin, adjusting elution conditions, or introducing an additional purification step, may enhance the removal of ^{88}Sr and ^{138}Ba and improve the accuracy of ^{226}Ra measurements. Implementing these strategies could minimize false positives and ensure more reliable quantification of ^{226}Ra in complex matrices.

4.8.4 Performance method evaluation using IAEA CRMs

The performance of the presented ICP-MS methodology was assessed using three IAEA certified reference materials (CRMs) with a sample mass of 10 g. The measured activities and the corresponding recoveries relative to the certified values are summarized in Table 58.

Table 58. Performance of the presented ICPMS method using different IAEA CRMs

IAEA CRM	Certified activity [Bq g^{-1}]	ICPMS result [Bq g^{-1}]	Recovery [%]
Phosphogypsum (IAEA-434)	0.780	0.593	76
Bikini Atoll Sediment (IAEA-410)	0.195	0.432	221
Baltic Sea Sediment (IAEA-465)	0.052	0.066	128

The results indicate that the ICP-MS measurements of the two marine sediments (IAEA-410 and IAEA-465) were significantly overestimated in comparison to their certified activities, with recoveries of 221 % and 128 %, respectively. In contrast, the phosphogypsum CRM (IAEA-434) exhibited a closer agreement with its certified value, yielding a recovery of 76 %.

To further investigate these discrepancies, full survey scans of the three CRMs were assessed and are shown in Figures 63, 64 and 65, respectively.

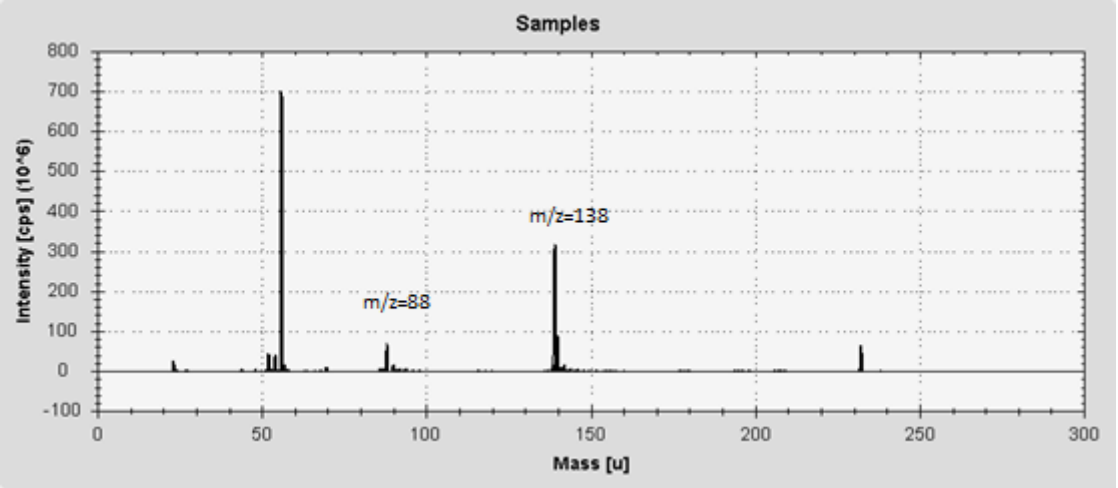

Figure 63. Full mass scan of IAEA-434 CRM (Phosphogypsum)

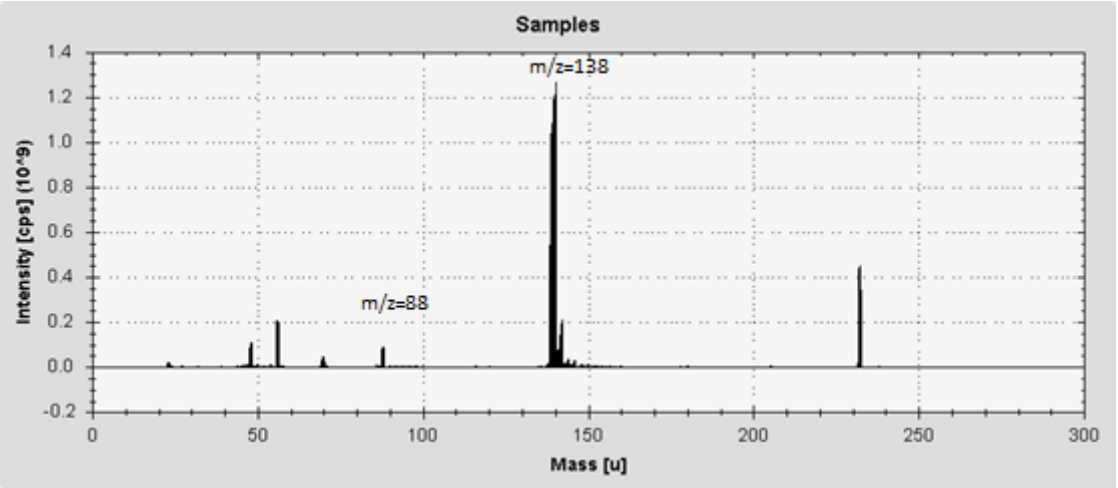

Figure 64. Full mass scan of IAEA-410 CRM (Bikini Atoll sediment)

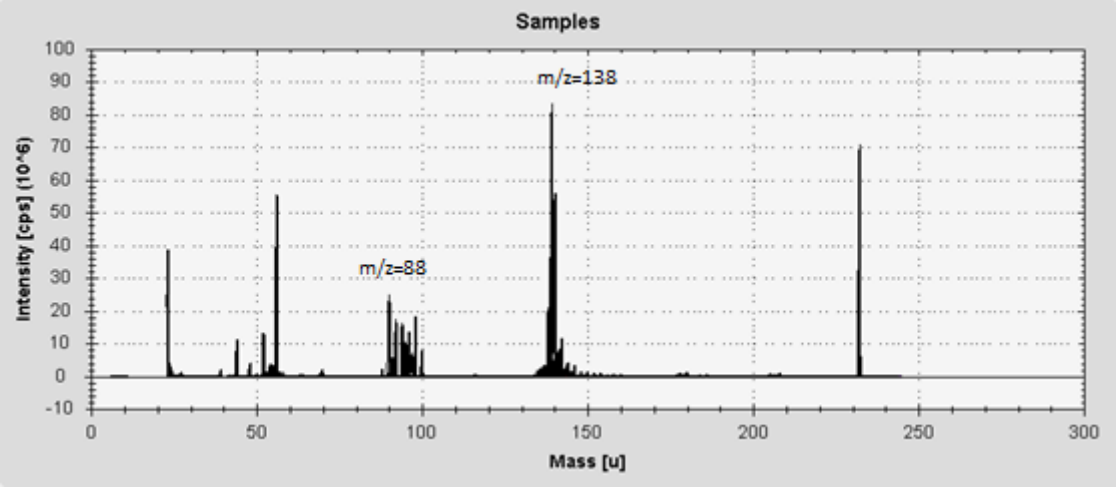

Figure 65. Full mass scan of IAEA-465 CRM (Baltic Sea sediment)

Analysis of the spectra revealed prominent signals at $m/z = 88$ (^{88}Sr) and $m/z = 138$ (^{138}Ba) in all three materials. These isotopes can combine to a form a major interference at polyatomic interference at $m/z = 226$, coinciding with the target analyte. The presence of this interference suggests that the elevated activities observed for the marine sediments may be enhanced due to unresolved polyatomic ions rather reflecting true radionuclide concentrations.

This observation highlights a critical limitation of the current method when applied to matrices with high Sr and Ba content, such as marine sediment. Conversely, the phosphogypsum sample, which contains lower levels of these interfering elements, yielding results in better agreement with the certified activity, indicating that matrix composition strongly influences the accuracy of the measurements.

These findings underscore the need for additional alternative analytical approaches to achieve reliable quantification of radionuclides in complex environmental matrices.

4.8.5 Limit of Detection (LOD)

The background signal, measured as the average count, when using a 1 % HNO_3 solution at m/z = 226, was found to be close to zero. This indicates that there is minimal interference from the acid matrix or other sources at this mass-to-charge ratio, providing a clean baseline for the analysis of 226Ra. Because the background was negligible, the limit of detection (LOD) could not be reliably estimated from blank measurements alone. Instead, the LOD was determined based on the analysis of a low-concentration calibration standard, as shown in Table 51, and calculated using the corresponding calibration function equation. This approach ensures that the LOD reflects the instrument's response under realistic measurement conditions rather than theoretical estimations.

The results from three independent runs are summarized in Table 59, showing both the LOD expressed in terms of mass concentration (pg g^{-1}) and the corresponding activity concentration (Bq L^{-1}).

Table 59. ^{226}Ra limit of detection

Limit of detection [pg g^{-1}]	Limit of detection [Bq L^{-1}]
4.88×10^{-5}	1.79×10^{-3}
5.64×10^{-5}	2.06×10^{-3}
6.26×10^{-5}	2.29×10^{-3}

These values correspond to activity levels in the millibecquerel per litre (mBq L^{-1}) range, demonstrating the high sensitivity of the method. Such a low LOD is particularly suitable for environmental monitoring, where radium concentrations are typically very low. Natural ^{226}Ra concentrations in drinking water and surface water usually range from 0.01 to 1 Bq L^{-1} depending on geology and source[376-379]. Achieving detection limits in the mBq L^{-1} range allows for the accurate quantification of ^{226}Ra in water samples and ensures that even trace levels can be reliably detected, which is crucial for assessing compliance with environmental safety standards and for studying natural radioactivity in aquatic systems.

4.9 Conclusion

This preliminary work investigated the performance of the iCAP ICPTQMS system equipped with the Aridus 3 desolvating system for measuring low levels of ^{226}Ra in seawater samples and selected solid CRMs from the IAEA. Operating parameters of the Thermo iCAP TQMS (plasma condition, lens voltage, collision/reaction cell flow) as well as the flow gas rates used in the Aridus 3 desolvation system were optimised for that purpose. A chromatographic separation, an anion exchange resin and Sr-resin, were used to remove potential interferences prior to analysis. However, the proposed separative approach could not remove entirely certain ions in the final extract, interfering at $m/z = 226$ (^{226}Ra) when combined. In particular, the combination of ^{88}Sr and ^{138}Ba was found to be the main polyatomic interference in the plasma ($^{88}Sr^{138}Ba$ ($m/z = 226$). Further chemical separative steps prior analysis would potentially be required to achieve accurate and precise analysis of low levels of ^{226}Ra by ICP-TQMS. One suggested option would be to preconcentrate radium with manganese dioxide prior to Sr-resin and eventually use a more concentrated HNO_3 solution during Sr-resin extraction. A modified version of Sr-resin, named TK-100 resin and also manufactured by Triskem International could also be envisaged. This recent resin contains the same extractant crown ether as Sr-resin used di(2-tethyl-hexyl) phosphoric acid (HDEHP) as the solvent as opposed to 1-octanol. In addition, further voltage optimisation tests in KED mode (helium gas) as well as He gas flow rate applied in the collision cell could be also investigated. Finally, the separate quantification of naturally occurring stable strontium and barium concentrations and their polyatomic impact on signal at $m/z = 226$ should also be investigated in detail before designing this complex chemical separative step.

The sensitivity for measuring ^{226}Ra was improved when using the desolvating system – Aridus 3. Also, the benefits of use Aridus 3 desolvation system showed non-negligible low-level detection limit. The detection limit to ppq levels made this combination of desolvating system with ICPMS a powerful tool for low-level detection. This can be used for very low-level measurement in food and environmental samples.

Chapter 5 Conclusion and future work

Over the last three decades, the inductively coupled plasma - mass spectrometry (ICP-MS) technique has progressively become an alternative analytical tool for measuring some nuclear-derived and naturally occurring radioelements in a wide range of environmental matrices. In comparison with traditional radiometric techniques, ICP-MS generally allows faster data acquisition, and sometimes does not require as labour-intensive sample preparative steps when using a collision reaction cell (CRC) to remove any potential isobaric and polyatomic interferences.

The development of ICP-MS equipped with an additional quadrupole after the CRC, also known as ICP - triple quadrupole detecting system (ICP-TQMS) or ICP-MS/MS have enabled further interference removal, therefore improved analytical performance and allowed the analysis of more complex matrices and more challenging analytes.

This research project focused on the optimised detection of three separate radioelements, ^{90}Sr, ^{129}I and ^{226}Ra and their quantification in diverse marine matrices using the iCAP ICP-TQMS instrument manufactured by Thermofisher Scientific. All three radioelements are of high interest for marine scientists at Cefas for different reasons and were selected for the different analytical challenges they presented.

Strontium-90 was the first radioisotope selected in this project and is traditionally measured using beta counting techniques. Although these radiometric techniques offer very low limits of detection, their applications require lengthy counting times, after a minimum of 3 weeks delay for allowing ^{90}Sr to be in secular equilibrium with ^{90}Y. The optimisation of certain instrumental parameters of the iCAP ICP-TQMS system (i.e., plasma, optics, collision/reaction gases) and use of a desolvating nebuliser system enabled the detection limit to be significantly improved and to reduce the production of hydrate ($^{88}Sr^{1}H$) and dihydrate ($^{88}Sr^{1}H^{1}H$) formation from the presence of naturally occurring strontium in the plasma.

The use of a Sr-resin was also selected to remove some interferences prior to analysis. One important consideration when designing this radiochemical preparative step was the total amount of natural strontium (^{88}Sr) content in the matrices of interest and therefore to understand beforehand the quantity of resin required for that purpose. The main instrumental consideration was related to the presence of natural zirconium (^{90}Zr) in all reagents used as well as decay products (^{90}Y, ^{90}Zr) from the decay of ^{90}Sr. The use of oxygen gas was found to be efficient for removing these isobaric interferences. Different chromatographic resins could be considered in future work. For example, TK100 resin, recently commercialised by Triskem International could

also be tested. This resin are based on the same crown-ether material as Sr-resin with the addition of a liquid cation exchange material – bis(2-ethylhexyl) phosphoric acid (HDEHP), allowing direct application of acidified seawater samples up to 0.5 L for example. Furthermore, this resin don't seem to retain both K and Ca (also present in the environmental samples of interest), in contrary to Sr-resin. Therefore, the use of this other chromatographic resin would not have an impact on strontium recoveries of strontium and would reduce the impact of polyatomic interferences composed of K and Ca.

A separate method was also developed for measuring ^{129}I in seawater and seaweed materials. The measurement was also based on optimised instrumental parameters, in particular the plasma condition, ion optics and the use of O_2 to remove the main isobaric ^{129}Xe interference. The potential tailing associated with the presence of high concentration of stable ^{127}I was also successfully removed in this process. The method was applied to selected seaweed samples collected in the direct vicinity of the Sellafield nuclear fuel reprocessing plant. A pyrolizer system was used to extract iodine from the selected environmental samples into a 0.5% tetramethylammonium hydroxide (TMAH) solution for ICPTQMS analysis. The ratios ^{129}I/^{127}I and ^{129}I measurements were found to be in good agreement with results reported in the scientific literature and from radiometric measurement, respectively. An instrumental limit of detection of 1.53×10^{-5} Bq g^{-1} (2.34 pg g^{-1}) for ^{129}I was obtained, confirming its suitability in specific marine monitoring applications. The development of new resins could potentially help improve signal quality and preconcentrate ^{129}I. For example, ion exchange resins such as Dowex 1 or AG-1) or CL resin, recently commercialised by Triskem International could be tested. Preliminary work have been published by Hou et al.[380] and Zulauf et al.[381].

In the last experimental study, the instrumental performance of the iCAP ICP-TQMS system was tested for the analysis of ^{226}Ra in seawater samples and selected solid reference materials. As in previous experiments, optimised operating parameters were investigated using the Aridus 3 desolvating nebuliser system to reduce the limit of detection as low as technically possible. A detection limit in the mBq L^{-1} order was obtained, but residual polyatomic interference from the presence of both ^{88}Sr and ^{138}Ba in the final extract affected the signal at $m/z = 226$ (^{88}Sr^{138}Ba). Future work should be focusing on the chemical separation with manganese dioxide extraction prior to Sr-resin or TK-100 (modified version of Sr-resin) resin in various concentration media (HNO_3, HCl) to separate more efficiently and remove Ba and Sr. Further assessment of strontium and barium concentration and their impact on the signal at $m/z = 226$ should also be considered. In addition, further voltage test (entrance and exit of CRC) in KED mode (helium gas) as well as He gas flow rate should be further investigated.

The work was focusing on the application of the iCAP ICP-TQMS instrument with combination of Aridus – 3 desolvation nebuliser system for radioanalysis in marine samples. This specific ICP-TQMS instrument presents a different configuration to equivalent systems in the market, with a 90° cylindrical lens, allowing ion transmission across the entire mass range. Furthermore, ICP introduction from a desolvation nebuliser system further enhanced the sensitivity of the instrument by reducing solvent loading to the plasma and the production of polyatomic interferences. Based on the limits of detection obtained in this study, the iCAP ICP-TQMS seems to be suitable for monitoring these three radioisotopes that can potentially be present at enhanced concentration in certain marine matrices. Nevertheless, the radiochemical preparation of these complex environmental matrices remains the critical part of the work, with the iCAP ICP-TQMS only being the analytical endpoint. Further radiochemical research is needed here to improve the removal and separation of some mass interferences. The continuous development of engineered chromatographic resins coupled with ongoing improvement of benchtop ICP-MS systems is expected to replace progressively the use of traditional radiometric techniques for monitoring these radioisotopes in the environment in the near future

Bibliography

1. Igarashi, Y., et al., *Application of Inductively Coupled Plasma Mass Spectrometry to the Measurement of Long-Lived Radionuclides in Environmental Samples A Review*. Analytical Sciences, 1990. **6**(2): p. 157-164.

2. Becker, J.S., *Mass spectrometry of long-lived radionuclides*. Spectrochimica Acta Part B, 2003. **58**: p. 1757–1784.

3. Becker, J.S., *Recent developments in isotope analysis by advanced mass spectrometric techniques*. Journal of Analytical Atomic Spectrometry, 2005. **20**(11): p. 1173-1184.

4. Houk, R.S., et al., *Inductively coupled argon plasma as an ion source for mass spectrometric determination of trace elements*. Analytical Chemistry, 1980. **52**(14): p. 2283-2289.

5. Papastefanou, C. and C. Papastefanou, *Radioactive nuclides as tracers of environmental processes*. Journal of Radioanalytical and Nuclear Chemistry, 2006. **267**(2): p. 315-320.

6. IAEA. *Isotopes in Hydrology, Marine Ecosystems and Climate Change Studies Vol.1*. 2011. Monaco: International Atomic Energy Agency.

7. IAEA. *Isotopes in Hydrology, Marine Ecosystems and Climate Change Studies Vol.2*. 2011. Monaco: International Atomic Energy Agency.

8. Y. Igarashi, C.K.K., Y. Takaku, M. Yamamoto, N. Ikeda, K. Shiraishi, *Application of Inductively Coupled Plasma Mass Spectrometry to the Measurement of Long-Lived Radionuclides in Environmental Samples A Review*. Analytical Sciences, 1990. **6**: p. 157-164.

9. Dominic Lariviere, V.F.T., R. Douglas Evans, R. Jack Cornett, *Radionuclide determination in environmental samples by inductively coupled plasma mass spectrometry*. Spectrochimica Acta Part B, 2006. **61**: p. 877–904.

10. Luo, M., et al., *Simultaneous determination of actinides and 90Sr in large-size soil and sediment samples*. Journal of Environmental Radioactivity, 2022. **247**: p. 106854.

11. Bu, W., et al., *Development and application of mass spectrometric techniques for ultra-trace determination of 236U in environmental samples-A review*. Analytica Chimica Acta, 2017. **995**: p. 1-20.

12. Dalencourt, C., et al., *A rapid sequential chromatographic separation of U- and Th-decay series radionuclides in water samples*. Talanta, 2020. **207**: p. 120282.

13. Shareef, A.-R., et al., *Rapid detection of enriched uranium in food*. Applied Radiation and Isotopes, 2017. **126**: p. 76-78.

14. Boulyga, S.F., *Mass spectrometric analysis of long-lived radionuclides in bio-assays*. International Journal of Mass Spectrometry, 2011. **307**(200-210).

15. Vanhaecke, F., M. Resano, and L. Moens, *Electrothermal vaporisation ICP-mass spectrometry (ETV-ICP-MS) for the determination and speciation of trace elements in solid samples – A review of real-life applications from the author's lab*. Analytical and Bioanalytical Chemistry, 2002. **374**(2): p. 188-195.

16. Sugiyama, N. and M. Omori, *Quantitative analysis of high purity metals using laser ablation coupled to an Agilent 7900 ICP-MS*. 2015, Agilent Technologies.

17. Wang, Z., B. Hattendorf, and D. Günther, *Analyte Response in Laser Ablation Inductively Coupled Plasma Mass Spectrometry.* Journal of the American Society for Mass Spectrometry, 2006. **17**(5): p. 641-651.

18. Koch, J. and D. Günther, *Review of the state-of-the-art of laser ablation inductively coupled plasma mass spectrometry.* Applied Spectroscopy, 2011. **65**(5): p. 155A-162A.

19. Sharp, B.L., *Pneumatic nebulisers and spray chambers for inductively coupled plasma spectrometry. A review. Part 1. Nebulisers.* Journal of Analytical Atomic Spectrometry, 1988. **3**(5): p. 613-652.

20. B'Hymer, C. and J.A. Caruso, *Chapter 7 Nebulizer sample introduction for elemental speciation*, in *Comprehensive Analytical Chemistry*. 2000, Elsevier. p. 213-226.

21. José L. Todolí, J.M.M., *Sample introduction systems for the analysis of liquid microsamplesby ICP-AES and ICP-MS* Spectrochimica Acta Part B, 2006. **61**: p. 239-283.

22. Sharp, B.L., *Pneumatic nebulisers and spray chambers for inductively coupled plasma spectrometry. A review. Part 2. Spray chambers.* Journal of Analytical Atomic Spectrometry, 1988. **3**(7): p. 939-963.

23. Jorabchi, K., et al., *High efficiency nebulization for helium inductively coupled plasma mass spectrometry.* Spectrochimica Acta Part B: Atomic Spectroscopy, 2006. **61**(8): p. 945-950.

24. Chan, S.K., R.L. Van Hoven, and A. Montaser, *Generation of a helium inductively coupled plasma in a low-gas-flow torch.* Analytical Chemistry, 1986. **58**(11): p. 2342-2343.

25. Petrović, Z., *The Contribution of Nikola Tesla to Plasma Physics and Current Status of Plasmas that He Studied*. Serbian Journal of Electrical Engineering, 2006. **3**: p. 203-216.

26. Gray, A.L., *Mass-spectrometric analysis of solutions using an atmospheric pressure ion source.* Analyst, 1975. **100**(1190): p. 289-299.

27. Graham, W.G., *1 - The physics and chemistry of plasmas for processing textiles and other materials*, in *Plasma Technologies for Textiles*, R. Shishoo, Editor. 2007, Woodhead Publishing. p. 3-24.

28. Leyh, B., *Ion Dissociation Kinetics, Mass Spectrometry*, in *Encyclopedia of Spectroscopy and Spectrometry*, J.C. Lindon, Editor. 1999, Elsevier: Oxford. p. 963-971.

29. Ramendik, G.I., et al., *New Approach to the Calculation of Relative Sensitivity Factors in Inductively Coupled Plasma Mass Spectrometry.* Journal of Analytical Chemistry, 2001. **56**(6): p. 500-506.

30. Lariviere, D., et al., *Radionuclide determination in environmental samples by inductively coupled plasma mass spectrometry.* Spectrochimica Acta Part B: Atomic Spectroscopy, 2006. **61**(8): p. 877-904.

31. Frank-Kamenetskii, D., *Plasma: The Fourth State of Matter*. 2012: Springer US.

32. Tanner, S.D., *Characterization of ionization and matrix suppression in inductively coupled 'cold' plasma mass spectrometry.* Journal of Analytical Atomic Spectrometry, 1995. **10**(11): p. 905-921.

33. Christian Agatemor, D.B., *Matrix effects in inductively coupled plasma mass spectrometry: A review*. Analytica Chimica Acta, 2011. **706**: p. 66-83.

34. Farnsworth, P.B. and R.L. Spencer, *Ion sampling and transport in Inductively Coupled Plasma Mass Spectrometry*. Spectrochimica Acta Part B: Atomic Spectroscopy, 2017. **134**: p. 105-122.

35. Beauchemin, D., *Inductively Coupled Plasma Mass Spectrometry Methods*, in *Encyclopedia of Spectroscopy and Spectrometry (Third Edition)*, J.C. Lindon, G.E. Tranter, and D.W. Koppenaal, Editors. 2017, Academic Press: Oxford. p. 236-245.

36. Tanner, S.D., V.I. Baranov, and D.R. Bandura, *Reaction cells and collision cells for ICP-MS: a tutorial review*. Spectrochimica Acta Part B: Atomic Spectroscopy, 2002. **57**(9): p. 1361-1452.

37. Bandura, D.R., V.I. Baranov, and S.D. Tanner, *Reaction chemistry and collisional processes in multipole devices for resolving isobaric interferences in ICP–MS*. Fresenius' Journal of Analytical Chemistry, 2001. **370**(5): p. 454-470.

38. David W. Koppenaal, G.C.E., Charles J. Barinaga, *Collision and reaction cells in atomic mass spectrometry: development, status, and applications*. J. Anal. At. Spectrom., 2004. **19**: p. 561-700.

39. Gray, P.J. and J.W. Olesik, *Ion-neutral gas reactions in a collision/reaction cell in inductively coupled plasma mass spectrometry: Correlation of ion signal decrease to kinetic rate constants*. Spectrochimica Acta Part B: Atomic Spectroscopy, 2015. **105**: p. 60-70.

40. Tanner, S.D. and V.I. Baranov, *Theory, design, and operation of a dynamic reaction cell for ICP-MS*. Atomic Spectroscopy, 1999. **20**: p. 45-52.

41. Eiden, G.C., C.J. Barinaga, and D.W. Koppenaal, *Communication. Selective removal of plasma matrix ions in plasma source mass spectrometry*. Journal of Analytical Atomic Spectrometry, 1996. **11**(4): p. 317-322.

42. Du, Z. and R.S. Houk, *Attenuation of metal oxide ions in inductively coupled plasma mass spectrometry with hydrogen in a hexapole collision cell*. Journal of Analytical Atomic Spectrometry, 2000. **15**(4): p. 383-388.

43. Amr, M.A., *The collision/reaction cell and its application in inductively coupled plasma mass spectrometry for the determination of radioisotopes: A literature review*. Advances in Applied Science Research, 2012. **3**: p. 2179-2191.

44. de Hoffman, E. and V. Stroobant, *Mass Spectrometry: Principles and Applications*. Third Edition ed. 2007: Wiley.

45. Miller, P.E. and M.B. Denton, *The quadrupole mass filter: basic operating concepts*. Journal of chemical education, 1986. **63**(7): p. 617.

46. Du, Z., D. J. Douglas, and N. Konenkov, *Elemental analysis with quadrupole mass filters operated in higher stability regions*. Journal of Analytical Atomic Spectrometry, 1999. **14**(8): p. 1111-1119.

47. Nelms, M.S., *Inductively Coupled Plasma Mass Spectrometry Handbook*. 2005: Blackwell Publishing Ltd. 1-497.

48. Henchman, M. and C. Steel, *Understanding the Quadrupole Mass Filter through Computer Simulation*. Journal of Chemical Education, 1998. **75**(8): p. 1049.

49. March, R.E. and J.F.J. Todd, *The Development of the Quadrupole Mass Filter and Quadrupole Ion Trap*, in *The Encyclopedia of Mass Spectrometry*, M.L. Gross and R.M. Caprioli, Editors. 2016, Elsevier: Boston. p. 43-60.

50. March, R.E. and J.F.J. Todd, *Quadrupole ion trap mass spectrometry*. Second Edition ed, ed. J.D. Winefordener. Vol. 165. 2005: John Wiley & Sons.

51. Montaser, A., *Inductively coupled plasma mass spectrometry*. 1998: John Wiley & Sons.

52. Nageswaran, G., Y.S. Choudhary, and S. Jagannathan, *Chapter 8 - Inductively Coupled Plasma Mass Spectrometry*, in *Spectroscopic Methods for Nanomaterials Characterization*, S. Thomas, et al., Editors. 2017, Elsevier. p. 163-194.

53. Wieser, M.E. and W.A. Brand, *Isotope Ratio Studies Using Mass Spectrometry*, in *Encyclopedia of Spectroscopy and Spectrometry (Third Edition)*, J.C. Lindon, G.E. Tranter, and D.W. Koppenaal, Editors. 2017, Academic Press: Oxford. p. 488-500.

54. Ian W. Croudace, B.C.R., Phil W. Warwick, *Plasma source mass spectrometry for radioactive waste characterisation in support of nuclear decommissioning: a review.* J. Anal. At. Spectrom., 2016: p. 1-33.

55. E. Hywel Evans, J.J.G., *Interferences in Inductively Coupled Plasma Mass Spectrometry A Review.* Journal of Analytical Atomic Spectrometry, 1993. **8**: p. 1-18.

56. Dams, R.F.J., J. Goossens, and L. Moens, *Spectral and non-spectral interferences in inductively coupled plasma mass-spectrometry.* Microchimica Acta, 1995. **119**(3): p. 277-286.

57. Thomas W. May, R.H.W., *A Table of Polyatomic Interferences in ICP-MS.* Atomic Spectroscopy, 1998. **5**: p. 150-155.

58. Pupyshev, A.A. and E.V. Semenova, *Formation of doubly charged atomic ions in the inductively coupled plasma.* Spectrochimica Acta Part B: Atomic Spectroscopy, 2001. **56**(12): p. 2397-2418.

59. Thomas, R., *A Review of Interferences.* Spectroscopy, 2002. **17**: p. 24-31.

60. Hattendorf, B., et al., *Abundance and Impact of Doubly Charged Polyatomic Argon Interferences in ICPMS Spectra.* Analytical Chemistry, 2016. **88**(14): p. 7281-7288.

61. Raut, N.M., et al., *Mathematical Correction for Polyatomic Isobaric Spectral Interferences in Determination of Lanthanides by Inductively Coupled Plasma Mass Spectrometry.* Journal of the Chinese Chemical Society, 2005. **52**(4): p. 589-597.

62. Laborda, F., et al., *Mathematical correction for polyatomic interferences in the speciation of chromium by liquid chromatography–inductively coupled plasma quadrupole mass spectrometry.* Spectrochimica Acta Part B: Atomic Spectroscopy, 2006. **61**(4): p. 433-437.

63. Lum, T.-S. and K. Sze-Yin Leung, *Strategies to overcome spectral interference in ICP-MS detection.* Journal of Analytical Atomic Spectrometry, 2016. **31**(5): p. 1078-1088.

64. Taylor, H.E., *Chapter 9 - Optimization*, in *Inductively Coupled Plasma-Mass Spectrometry*, H.E. Taylor, Editor. 2001, Academic Press: San Diego. p. 143-148.

65. Amais, R.S., et al., *Tandem mass spectrometry (ICP-MS/MS) for overcoming molybdenum oxide interferences on Cd determination in milk.* Microchemical Journal, 2015. **120**: p. 64-68.

66. Böting, K., et al., *First experimental proof of asymmetric charge transfer in ICP-MS/MS (ICP-QQQ-MS) through isotopically enriched oxygen as cell gas.* Journal of Analytical Atomic Spectrometry, 2014. **29**(3): p. 578-582.

67. Ohno, T., et al., *Determination of ultratrace 129I in soil samples by Triple Quadrupole ICP-MS and its application to Fukushima soil samples.* Journal of Analytical Atomic Spectrometry, 2013. **28**(8): p. 1283-1287.

68. Ohno, T., et al., *Determination of strontium 90 in environmental samples by triple quadrupole ICP-MS and its application to Fukushima soil samples.* Journal of Analytical Atomic Spectrometry, 2018. **33**(6): p. 1081-1085.

69. Amaral, C.D.B., et al., *A novel strategy to determine As, Cr, Hg and V in drinking water by ICP-MS/MS.* Analytical Methods, 2015. **7**(3): p. 1215-1220.

70. Tanimizu, M., et al., *Determination of ultra-low 236U/238U isotope ratios by tandem quadrupole ICP-MS/MS.* Journal of Analytical Atomic Spectrometry, 2013. **28**(9): p. 1372-1376.

71. P. E. Warwick, B.C.R., I. W. Croudace, Z. Zacharauskas, *Evaluation of inductively coupled plasma tandem mass spectrometry for radionuclide assay in nuclear waste characterisation.* J. Anal. At. Spectrom., 2019.

72. Russell, B.C., et al., *Development of a single method for direct measurement of multiple radionuclides using ICP-MS/MS.* Journal of Analytical Atomic Spectrometry, 2023. **38**(1): p. 97-110.

73. Suárez-Oubiña, C., et al., *Single-particle inductively coupled plasma mass spectrometry using ammonia reaction gas as a reliable and free-interference determination of metallic nanoparticles.* Talanta, 2022. **242**: p. 123286.

74. D'Ilio, S., et al., *Dynamic reaction cell ICP-MS for determination of total As, Cr, Se and V in complex matrices: Still a challenge? A review.* Analytica Chimica Acta, 2011. **698**(1): p. 6-13.

75. D'Ilio, S., et al., *Determination of trace elements in serum by dynamic reaction cell inductively coupled plasma mass spectrometry. Developing of a method with a desolvating system nebulizer.* Analytica Chimica Acta, 2006. **573-574**: p. 432-438.

76. Fu, L., et al., *Analysis of impurity elements in high purity cobalt powder by inductively coupled plasma tandem mass spectrometry.* Microchemical Journal, 2018. **139**: p. 236-241.

77. Singh, S., M.R. Mucalo, and M.N.C. Grainger, *Analysis of sulfur in soil and plant digests using methane as a reaction gas for ICP-MS.* Talanta, 2025. **281**: p. 126797.

78. Zhu, X., et al., *Detection of intermediates for diatomic [TaO]+ catalyzed gas-phase reaction of methane coupling to ethane and ethylene by ICP-MS/MS.* Microchemical Journal, 2021. **161**: p. 105762.

79. He, Q., et al., *Rapid screening of gaseous catalysts in methane activation using ICP-QQQ-MS.* Journal of Analytical Atomic Spectrometry, 2018. **33**(4): p. 563-568.

80. Russell, B., et al., *Applications of hydrogen as a collision and reaction cell gas for enhanced measurement capability applied to low level stable and radioactive isotope detection using ICP-MS/MS.* Journal of Analytical Atomic Spectrometry, 2021. **36**(12): p. 2704-2714.

81. Jackson, B.P., A. Liba, and J. Nelson, *Advantages of reaction cell ICP-MS on doubly charged interferences for arsenic and selenium analysis in foods*. Journal of Analytical Atomic Spectrometry, 2015. **30**(5): p. 1179-1183.

82. Makishima, A. and E. Nakamura, *Suppression of Matrix Effects in ICP-MS by High Power Operation of ICP: Application to Precise Determination of Rb, Sr, Y, Cs, Ba, REE, Pb, Th and U at ng g-1 Levels in Milligram Silicate Samples*. Geostandards Newsletter, 1997. **21**(2): p. 307-319.

83. Wilschefski, S.C. and M.R. Baxter, *Inductively Coupled Plasma Mass Spectrometry: Introduction to Analytical Aspects*. The Clinical biochemist. Reviews, 2019. **40**(3): p. 115-133.

84. Rodushkin, I., et al., *Assessment of the natural variability of B, Cd, Cu, Fe, Pb, Sr, Tl and Zn concentrations and isotopic compositions in leaves, needles and mushrooms using single sample digestion and two-column matrix separation*. Journal of Analytical Atomic Spectrometry, 2016. **31**(1): p. 220-233.

85. Elmer, P., *Measurement of 90Sr by Preconcentration/Matrix Separation and Reaction Cell ICP-MS*. 2014.

86. Wysocka, I. and E. Vassileva, *Determination of ultra-trace level of 232Th in seawater by ICP-SFMS after matrix separation and preconcentration*. Analytica Chimica Acta, 2018. **1000**: p. 144-154.

87. Ni, Y., et al., *Trace impurity analysis in uranium materials by rapid separation and ICP-MS/MS measurement with matrix matched external calibration*. Microchemical Journal, 2021. **169**: p. 106615.

88. Bürger, S., L.R. Riciputi, and D.A. Bostick, *Determination of impurities in uranium matrices by time-of-flight ICP-MS using matrix-matched method*. Journal of Radioanalytical and Nuclear Chemistry, 2007. **274**(3): p. 491-505.

89. Carter, J.A., et al., *Traditional Calibration Methods in Atomic Spectrometry and New Calibration Strategies for Inductively Coupled Plasma Mass Spectrometry*. Frontiers in Chemistry, 2018. **Volume 6 - 2018**.

90. Becker, J.S., et al., *Ultratrace and Isotope Analysis of Long-Lived Radionuclides by Inductively Coupled Plasma Quadrupole Mass Spectrometry Using a Direct Injection High Efficiency Nebulizer*. Analytical Chemistry, 1999. **71**(15): p. 3077-3084.

91. Zacharauskas, Ž., et al., *Development of an optimised method for measurement of iodine-129 in decommissioning wastes using ICP-MS/MS*. Journal of Analytical Atomic Spectrometry, 2023.

92. Valković, V., *Chapter 11 Determination of radionuclides in environmental samples*, in *Techniques and Instrumentation in Analytical Chemistry*, D. BarcelÓ, Editor. 2000, Elsevier. p. 457-535.

93. Dasch, E.J., *Strontium isotopes in weathering profiles, deep-sea sediments, and sedimentary rocks*. Geochimica et Cosmochimica Acta, 1969. **33**(12): p. 1521-1552.

94. Crowley, B.E., J.H. Miller, and C.P. Bataille, *Strontium isotopes (87Sr/86Sr) in terrestrial ecological and palaeoecological research: empirical efforts and recent advances in continental-scale models*. Biological Reviews, 2017. **92**(1): p. 43-59.

95. Nielsen, S.P., *The biological role of strontium*. Bone, 2004. **35**: p. 583– 588.

96. Clarke, B.L., *Strontium*, in *Encyclopedia of Bone Biology*. 2019, Elsevier Inc.

97. Capo, R.C., B.W. Stewart, and O.A. Chadwick, *Strontium isotopes as tracers of ecosystem processes: theory and methods*. Geoderma, 1998. **82**(1): p. 197-225.

98. Bentley, R.A., *Strontium Isotopes from the Earth to the Archaeological Skeleton: A Review*. Journal of Archaeological Method and Theory, 2006. **13**: p. 135-187.

99. Price, D. and H. Gestsdóttir, *The first settlers of Iceland: An isotopic approach to colonisation*. Antiquity, 2006. **80**: p. 130-144.

100. Douglas Price, T., V. Tiesler, and J.H. Burton, *Early African diaspora in colonial Campeche, Mexico: Strontium isotopic evidence*. American Journal of Physical Anthropology, 2006. **130**(4): p. 485-490.

101. Shaw, H., et al., *Identifying migrants in Roman London using lead and strontium stable isotopes*. Journal of Archaeological Science, 2016. **66**: p. 57-68.

102. Petrini, R., et al., *The 87Sr/86Sr strontium isotopic systematics applied to Glera vineyards: A tracer for the geographical origin of the Prosecco*. Food Chemistry, 2015. **170**: p. 138-144.

103. Tescione, I., et al., *87Sr/86Sr isotopes in grapes of different cultivars: A geochemical tool for geographic traceability of agriculture products*. Food Chemistry, 2018. **258**: p. 374-380.

104. Goitom Asfaha, D., et al., *Combining isotopic signatures of n(87Sr)/n(86Sr) and light stable elements (C, N, O, S) with multi-elemental profiling for the authentication of provenance of European cereal samples*. Journal of Cereal Science, 2011. **53**(2): p. 170-177.

105. Medini, S., et al., *Methodological development for 87Sr/86Sr measurement in olive oil and preliminary discussion of its use for geographical traceability of PDO Nîmes (France)*. Food Chemistry, 2015. **171**: p. 78-83.

106. Martın Resano, F.V., *Forensic Applications*.

107. DeBord, J., et al., *Profiling of heroin and assignment of provenance by 87Sr/86Sr isotope ratio analysis*. Inorganica Chimica Acta, 2017. **468**: p. 294-299.

108. Stewart, B.W., R.C. Capo, and O.A. Chadwick, *Quantitative strontium isotope models for weathering, pedogenesis and biogeochemical cycling*. Geoderma, 1998. **82**(1): p. 173-195.

109. Smichowski, P. and D. Gómez, *Chapter 8 - Spectroscopic and Chromatographic Techniques and Methodologies for the Determination of Metals, Metalloids and Ions in Atmospheric Aerosols*, in *Comprehensive Analytical Chemistry*, P.B.C. Forbes, Editor. 2015, Elsevier. p. 239-266.

110. Furr, A.K., et al., *National survey of elements and radioactivity in fly ashes. Absorption of elements by cabbage grown in fly ash-soil mixtures*. Environmental Science & Technology, 1977. **11**(13): p. 1194-1201.

111. Senesi, N., M. Polemio, and L. Lorusso, *Evaluation of barium, rubidium and strontium contents in commercial fertilizers*. Fertilizer research, 1983. **4**(2): p. 135-144.

112. Ondov, J.M., et al., *Atmospheric behavior of trace elements on particles emitted from a coal-fired power plant*. Atmospheric Environment (1967), 1989. **23**(10): p. 2193-2204.

113. Lee, R.E. and D.J. von Lehmden, *Trace Metal Pollution in the Environment*. Journal of the Air Pollution Control Association, 1973. **23**(10): p. 853-857.

114. Raven, K.P. and R.H. Loeppert, *Trace Element Composition of Fertilizers and Soil Amendments*. Journal of Environmental Quality, 1997. **26**(2): p. 551-557.

115. Sadek, R., et al., *Spectrally adapted red flare tracers with superior spectral performance*. Defence Technology, 2017. **13**(6): p. 406-412.

116. Sillen, A. and M. Kavanagh, *Strontium and paleodietary research: A review*. American Journal of Physical Anthropology, 1982. **25**(S3): p. 67-90.

117. Blum, J.D., et al., *Changes in Sr/Ca, Ba/Ca and 87Sr/86Sr ratios between trophic levels in two forest ecosystems in the northeastern U.S.A.* Biogeochemistry, 2000. **49**(1): p. 87-101.

118. Hutchin, M.E. and B.E. Vaughan, *Relation Between Simultaneous Ca and Sr Transport Rates in Isolated Segments of Vetch, Barley, and Pine Roots*. Plant Physiology, 1968. **43**(12): p. 1913-1918.

119. Bowen, H.J.M. and J.A. Dymond, *The Uptake of Calcium and Strontium by Plants from Soils and Nutrient Solutions*. Journal of Experimental Botany, 1956. **7**(20): p. 264-272.

120. Veresoglou, D.S., et al., *Transfer factors for Sr as influenced by species Ca uptake and soil Ca availability*. Plant and Soil, 1995. **175**(2): p. 225-232.

121. Smith, J.T., et al., *A review and test of predictive models for the bioaccumulation of radiostrontium in fish*. Journal of Environmental Radioactivity, 2009. **100**(11): p. 950-954.

122. Chowdhury, M.J. and R. Blust, *7 - Strontium*, in *Fish Physiology*, C.M. Wood, A.P. Farrell, and C.J. Brauner, Editors. 2011, Academic Press. p. 351-390.

123. Bronner, F., et al., *Strontium and its relation to calcium metabolism*. The Journal of clinical investigation, 1963. **42**(7): p. 1095-1104.

124. Dolphin, G.W. and I.S. Eve, *The Metabolism of Strontium in Adult Humans*. Physics in Medicine and Biology, 1963. **8**(2): p. 193-203.

125. Spencer, H., D. Laszlo, and M. Brothers, *Strontium-85 and calcium-45 metabolism in Man*. The Journal of Clinical Investigation, 1957. **36**(5): p. 680-688.

126. M. Pilmane, K.S.-A., D. Loca b, J. Locs, L. Berzina-Cimdina, *Strontium and strontium ranelate: Historical review of some of their functions*. Materials Science and Engineering C, 2017. **78**: p. 1222-1230.

127. Parker, A.M. and M. Thoennessen, *Discovery of rubidium, strontium, molybdenum, and rhodium isotopes*. Atomic Data and Nuclear Data Tables, 2012. **98**(4): p. 812-831.

128. Semenishchev, V.S. and A.V. Voronina, *Isotopes of Strontium: Properties and Applications*, in *Strontium Contamination in the Environment*, P. Pathak and D.K. Gupta, Editors. 2020, Springer International Publishing: Cham. p. 25-42.

129. Alvarez-Diez, T.M., et al., *Manufacture of strontium-82/rubidium-82 generators and quality control of rubidium-82 chloride for myocardial perfusion imaging in patients using positron emission tomography*. Applied Radiation and Isotopes, 1999. **50**(6): p. 1015-1023.

130. IAEA, *Production of Long Lived Parent Radionuclides for Generators: 68Ge, 82Sr, 90Sr and 188W*. 2010, Vienna: International Atomic Energy Agency.

131. Klein, R., et al., *Precision-controlled elution of a 82Sr/82Rb generator for cardiac perfusion imaging with positron emission tomography.* Physics in Medicine and Biology, 2007. **52**(3): p. 659-673.

132. Yoshinaga, K., R. Klein, and N. Tamaki, *Generator-produced rubidium-82 positron emission tomography myocardial perfusion imaging—From basic aspects to clinical applications.* Journal of Cardiology, 2010. **55**(2): p. 163-173.

133. Ziadi, M.C., et al., *Chapter 19 - Diagnosis and Prognosis in Cardiac Disease Using Cardiac PET Perfusion Imaging*, in *Clinical Nuclear Cardiology (Fourth Edition)*, B.L. Zaret and G.A. Beller, Editors. 2010, Mosby: Philadelphia. p. 309-331.

134. Ghotbi, A.A., A. Kjaer, and P. Hasbak, *Review: comparison of PET rubidium-82 with conventional SPECT myocardial perfusion imaging.* Clinical physiology and functional imaging, 2014. **34**(3): p. 163-170.

135. Giammarile, F., et al., *Bone pain palliation with 85Sr therapy.* Journal of nuclear medicine : official publication, Society of Nuclear Medicine, 1999. **40**: p. 585-90.

136. DeNardo, G.L. and J.A. Volpe, *Detection of bone lesions with the strontium-85 scintiscan.* Journal of Nuclear Medicine, 1966. **7**(3): p. 219-236.

137. Parsons, V., et al., *Strontium-85 scanning of suspected bone disease.* British medical journal, 1969. **1**(5635): p. 19-23.

138. Malmberg, I., et al., *Painful bone metastases in hormone-refractory prostate cancer: economic costs of strontium-89 and/or external radiotherapy.* Urology, 1997. **50**(5): p. 747-753.

139. Coursey, B.M., et al., *Measurement standards for strontium-89 for use in bone palliation.* Applied radiation and isotopes, 1998. **49**(4): p. 335-344.

140. Storto, G., et al., *Combined therapy of Sr-89 and zoledronic acid in patients with painful bone metastases.* Bone, 2006. **39**(1): p. 35-41.

141. Bauman, G., et al., *Radiopharmaceuticals for the palliation of painful bone metastases—a systematic review.* Radiotherapy and Oncology, 2005. **75**(3): p. 258.E1-258.E13.

142. Bączyk, M., et al., *Efficacy of samarium 153 and strontium 89 treatment for bone metastases in prostate cancer patients: monotherapy vs. treatment combined with external beam radiotherapy. Preliminary report.* Reports of Practical Oncology & Radiotherapy, 2007. **12**(4): p. 211-216.

143. Marx, D., et al., *A review of the latest insights into the mechanism of action of strontium in bone.* Bone Reports, 2020. **12**: p. 100273.

144. Liepe, K., I. Murray, and G. Flux, *Dosimetry of Bone Seeking Beta Emitters for Bone Pain Palliation Metastases.* Seminars in Nuclear Medicine, 2022. **52**(2): p. 178-190.

145. Teo, J.-Y., et al., *A systematic review of contralateral liver lobe hypertrophy after unilobar selective internal radiation therapy with Y90.* HPB, 2016. **18**(1): p. 7-12.

146. Zalutsky, M.R., *Targeted radiotherapy of brain tumours.* British Journal of Cancer, 2004. **90**(8): p. 1469-1473.

147. DeNardo, S.J. and G.L. DeNardo, *Targeted radionuclide therapy for solid tumors: An overview.* International Journal of Radiation Oncology • Biology • Physics, 2006. **66**(2): p. S89-S95.

148. Ojovan, M.I., W.E. Lee, and S.N. Kalmykov, *Chapter 6 - Power Utilisation of Nuclear Energy*, in *An Introduction to Nuclear Waste Immobilisation (Third Edition)*, M.I. Ojovan, W.E. Lee, and S.N. Kalmykov, Editors. 2019, Elsevier. p. 57-70.

149. O'Brien, R.C., et al., *Safe radioisotope thermoelectric generators and heat sources for space applications*. Journal of Nuclear Materials, 2008. **377**(3): p. 506-521.

150. Wang, X., et al., *Critical design features of thermal-based radioisotope generators: A review of the power solution for polar regions and space*. Renewable and Sustainable Energy Reviews, 2020. **119**: p. 109572.

151. England, T.R. and B.F. Rider, *Evaluation and compilation of fission product yields 1993*. 1995: United States.

152. Murray, R.L. and K.E. Holbert, *Chapter 6 - Fission*, in *Nuclear Energy (Eighth Edition)*, R.L. Murray and K.E. Holbert, Editors. 2020, Butterworth-Heinemann. p. 101-114.

153. Organization, W.H., *Strontium and Strontium Compounds*. 2010: p. 1-66.

154. Synhaeve, N., et al., *Chronic exposure to low concentrations of strontium 90 affects bone physiology but not the hematopoietic system in mice*. Journal of Applied Toxicology, 2014. **34**(1): p. 76-86.

155. Musilli, S., et al., *DNA damage induced by Strontium-90 exposure at low concentrations in mesenchymal stromal cells: the functional consequences*. Scientific reports, 2017. **7**: p. 41580-41580.

156. Commission, U.S.A.E., *Worldwide effects of atomic weapons. Project Sunshine*. 1953, ; RAND Corp., Santa Monica, Calif. p. Medium: ED; Size: Pages: 105.

157. Martell, E.A., *Stronitium-90 concentration data for biological materials, soils, waters, and air filters. Project Sunshine Bulletin No. 11*. 1957, ; Univ. of Chicago, IL (United States). Enrico Fermi Inst. for Nuclear Studies. p. Medium: ED; Size: 67 p.

158. T. R. Fehner, F.G.G., *Atmospheric Nuclear Weapons Testing, 1951-1963. Battlefield of the Cold War: The Nevada Test Site, Volume I* 2006, Department of Energy: Washington, D.C. p. 244.

159. B. L. Larson, K.E.E., *Significance of Strontium-90 in Milk. A review*. 1958.

160. Garland, J.A. and R. Wakeford, *Atmospheric emissions from the Windscale accident of October 1957*. Atmospheric Environment, 2007. **41**(18): p. 3904-3920.

161. Chamberlain, A.C., *Environmental impact of particles emitted from windscale piles, 1954–1957*. Science of The Total Environment, 1987. **63**: p. 139-160.

162. Chamberlain, A.C. and H.J. Dunster, *Deposition of Radioactivity in North-West England from the Accident at Windscale*. Nature, 1958. **182**(4636): p. 629-630.

163. Bryant, F.J. and J.F. Loutit, *The entry of strontium-90 into human bone*. Proceedings of the Royal Society of London. Series B. Biological Sciences, 1964. **159**(976): p. 449-465.

164. Office, H.M.S., *The Accident at Windscale on October 10, 1957*. Nature, 1958. **182**(4636): p. 635-635.

165. Loutit, J.F., W.G. Marley, and R.S. Russell, *The nuclear reactor accident at Windscale - October, 1957: Environmental aspects*. 1960: International Atomic Energy Agency (IAEA). p. 129-139.

166. Crick, M.J. and G.S. Linsley, *An Assessment of the Radiological Impact of the Windscale Reactor Fire, October 1957.* International Journal of Radiation Biology and Related Studies in Physics, Chemistry and Medicine, 1984. **46**(5): p. 479-506.

167. Nelson, N., K.P. Kitchen, and R.H. Maryon, *A study of the movement of radioactive material discharged during the windscale fire in October 1957.* Atmospheric Environment, 2006. **40**(1): p. 58-75.

168. Smith, A.D., et al., *A review of irradiated fuel particle releases from the Windscale Piles, 1950–1957.* Journal of Radiological Protection, 2007. **27**(2): p. 115-145.

169. Dunster, H.J., H. Howells, and W.L. Templeton, *District Surveys following the Windscale Incident, October 1957.* Journal of Radiological Protection, 2007. **27**(3): p. 217-230.

170. Penney, W., et al., *Report on the accident at Windscale No. 1 Pile on 10 October 1957.* Journal of Radiological Protection, 2017. **37**(3): p. 780-796.

171. UNSCEAR, *Sources, Effects and Risks of Ionizing Radiation.* 1988, United Nations Scientific Committee on the Effects of Atomic Radiation: New York.

172. Bennett, B.G. and A. Bouville, *Radiation doses in countries of the northern hemisphere from the chernobyl nuclear reactor accident.* Environment International, 1988. **14**(2): p. 75-82.

173. Mishra, U.C., *Comparison of radionuclides levels from the Chernobyl reactor accident and from global fallout.* Journal of Radioanalytical and Nuclear Chemistry, 1990. **138**(1): p. 119-125.

174. Feely, H.W., et al., *Fallout in the New York metropolitan area following the chernobyl accident.* Journal of Environmental Radioactivity, 1988. **7**(2): p. 177-191.

175. Higuchi, H., et al., *Radioactivity in surface air and precipitation in Japan after the Chernobyl accident.* Journal of Environmental Radioactivity, 1988. **6**(2): p. 131-144.

176. Ministry of Ukraine of, E. and K. Affairs of population protection from the consequences of Chornobyl Catastrophe, *20 years after Chernobyl Accident Future outlook National Report of Ukraine*. 2006, Atika: Ukraine. p. 225.

177. IAEA, *Environmental Consequences of the Chernobyl Accident and their Remediation: Twenty Years of Experience*. 2006, Vienna: International Atomic Energy Agency

178. UNSCEAR, *Sources and effects of ionizing radiation. Volume 1 and 2*. 2000, United Nations Scientific Committee on the Effects of Atomic Radiation.

179. Thakur, P., S. Ballard, and R. Nelson, *An overview of Fukushima radionuclides measured in the northern hemisphere.* Science of The Total Environment, 2013. **458-460**: p. 577-613.

180. Morino, Y., T. Ohara, and M. Nishizawa, *Atmospheric behavior, deposition, and budget of radioactive materials from the Fukushima Daiichi nuclear power plant in March 2011*. Geophysical Research Letters, 2011. **38**(7).

181. Miyasaka, M., *Chapter 11 - Lessons from the Fukushima Daiichi Nuclear Disaster*, in *Radioactivity in the Environment*, D. Oughton and S.O. Hansson, Editors. 2013, Elsevier. p. 177-195.

182. Nobuyuki Hamada, H.O., *Food safety regulations: what we learned from the Fukushima nuclear accident.* Journal of Environmental Radioactivity, 2012. **111**: p. 83-99.

183. UNSCEAR, *Levels and Effects of Radiation Exposure Due to the Nuclear Accident after the 2011 Great East-Japan Earthquake and Tsunami*. 2014. p. 321.

184. Masson, O., et al., *Tracking of airborne radionuclides from the damaged Fukushima Dai-ichi nuclear reactors by European networks*. Environmental Science & Technology, 2011. **45**(18): p. 7670-7677.

185. Leon, J.D., et al., *Arrival time and magnitude of airborne fission products from the Fukushima, Japan, reactor incident as measured in Seattle, WA, USA*. Journal of Environmental Radioactivity, 2011. **102**(11): p. 1032-1038.

186. Bolsunovsky, A. and D. Dementyev, *Evidence of the radioactive fallout in the center of Asia (Russia) following the Fukushima Nuclear Accident*. Journal of Environmental Radioactivity, 2011. **102**(11): p. 1062-1064.

187. Casacuberta, N., et al., *90Sr and 89Sr in seawater off Japan as a consequence of the Fukushima Dai-ichi nuclear accident*. Biogeosciences, 2013. **10**(6): p. 3649-3659.

188. Povinec, P.P., et al., *Dispersion of Fukushima radionuclides in the global atmosphere and the ocean*. Applied Radiation and Isotopes, 2013. **81**: p. 383-392.

189. Loveland, D.W., D.J. Morrissey, and G.T. Seaborg, *Radiochemical Techniques*, in *Modern Nuclear Chemistry*. 2017. p. 625-662.

190. Nora Vajda, C.K.K., *Determination of radiostrontium isotopes: A review of analytical methodology*. Applied Radiation and Isotopes, 2010. **68**: p. 2306-2326.

191. C.K. Kim, A.A.-H., A. Torvenyi, G. Kis-Benedek, U. Sansone, *Validation of rapid methods for the determination of radiostrontium in milk*. Applied Radiation and Isotopes, 2009. **67**: p. 786-793.

192. Harvey R. B., I.R.D., Lovett M.B., Williams K. J., *Analytical procedures for the determination of strontium radionuclides in environmental materials*. 1989.

193. Maeck, W., R. Abernathey, and J. Rein, *Burnup determination of nuclear fuels. Project Report for the Quarter, October 1-December 31, 1965*. 1966, Phillips Petroleum Co., Idaho Falls, Idaho. Atomic Energy Div.

194. Anderson, E.C., et al., *Barium-140 Radioactivity in Foods*. Science, 1958. **127**(3293): p. 283-284.

195. Garner, R.J., H.G. Jones, and B.F. Sansom, *Fission products and the dairy cow. 2. Some aspects of the metabolism of the alkaline-earth elements calcium, strontium and barium*. The Biochemical journal, 1960. **76**(3): p. 572-579.

196. Motojima, K., et al., *Separation of Zirconium-95, 97 and Niobium-95, 97 from Fission Product-Mixtures and Irradiated Uranium by an Extraction Method using 8-Quinolinol*. Journal of Nuclear Science and Technology, 1966. **3**(8): p. 326-332.

197. Pallson, W. and R.H. Springborn, *Estimation of fission-product gas pressure in uranium dioxide ceramic fuel elements*. 1968.

198. Reynolds, S.A. and J.S. Eldridge, *Investigation of Cerenkov counting of environmental strontium-90*. Conference: International conference on liquid scintillation counting--recent applications and development, San Francisco, CA, USA, 21 Aug 1979. 1979: ; Oak Ridge National Lab., TN (USA). Medium: ED; Size: Pages: 9.

199. Larsen, I.L., *Strontium-90 determinations by Cerenkov radiation counting for well monitoring at Oak Ridge National Laboratory*. 1981: United States. p. 24.

200. Sunderman, D.N. and C.W. Townley, *The radiochemistry of barium, calciuim and strontium*. 1960, National Research Council. Committee on Nuclear Science; Battelle Memorial Inst. p. Medium: ED; Size: Pages: 123.

201. D. N. Sunderman, W.W.M., *Evaluation of Radiochemical Separation Procedures*. Analytical Chemistry, 1957. **29**: p. 1578-1589.

202. Coryell, C.D. and N. Sugarman, *Radiochemical studies: the fission products*. National nuclear energy series. Manhattan Project technical section. Division IV: Plutonium Project record,v. 9. 1951, New York: McGraw-Hill. 3 v. (xxx, 2086 p.).

203. L. Popov, G.M., I. Hristova, P. Dimitrova, R. Tzibranski, V. Avramov, I. Naidenov, B. Stoenelova, *Separation of strontium from calcium by the use of sodium hydroxide and its application for the determination of long-term background activity concentrations of 90 Sr in 100 km area around Kozloduy Nuclear Power Plant (Bulgaria).* Journal of Radioanalytical and Nuclear Chemistry, 2009. **279**: p. 49-64.

204. David Tait, A.W., Gerhard Haase, *Binding of Sr from milk by solid phase extraction with cryptand C222 sorbed on silica gel, cation exchange, chelating or adsorbent resins for simplified 90Sr analysis.* The Science of the Total Environment, 1995. **173/174**: p. 159-167.

205. Shabana, E.I., K.A. Al-Hussan, and Q.K. Al-Jaseem, *Adaptation of a radioanalytical method for strontium-90 to different kinds of environmental samples and its application for the investigation of some samples in the Riyadh region.* Journal of Radioanalytical and Nuclear Chemistry, 1996. **212**(3): p. 229-240.

206. Bjørnstad, H.E., et al., *Determination of 90Sr in environmental and biological materials with combined HDEHP solvent extraction-low liquid scintillation counting technique*. Journal of Radioanalytical and Nuclear Chemistry, 1992. **156**(1): p. 165-173.

207. Stéphane Brun, Y.K., Bernadette Boursier, Jean-Marc Fremy, Françoise Janin, *Methodology for determination of radiostrontium in milk: a review.* Le Lait, 2003. **83**: p. 1-15.

208. Philip Horwitz, E.C., Renato Dietz, Mark L., *A novel strontium-selective extraction chromatographic resin.* Solvent Extraction and Ion Exchange, 1992. **10**(2): p. 313-336.

209. IAEA, *Rapid Simultaneous Determination of 89Sr and 90Sr in Milk using Cerenkov and Scintillation Counting*. 2013, International Atomic Energy Agency. p. 66.

210. Tieh-Chii Chu, J.-J.W., Yu-Ming Lin, *Radiostrontium Analytical Method using Crown-ether Compound and Cerenkov Counting and Its Applications in Environmental Monitoring*. Appl. Radiat. Isot., 1998. **49**: p. 1671-1675.

211. Željko Grahek, M.R.M., *Isolation of iron and strontium from liquid samples and determination of 55Fe and 89,90Sr in liquid radioactive waste.* Analytica Chimica Acta, 2004. **511**: p. 339–348.

212. Rožle Jakopič, L.B., *Tracer Studies on Sr Resin and Determination of 90Sr in Environmental Samples*. Acta Chim. Slov, 2005. **52**: p. 297–302.

213. Zeljko Grahek, M.R.M., *Determination of radioactive strontium in seawater.* Analytica Chimica Acta, 2005. **534**: p. 271-279.

214. Claudia Landstetter, G.W., *Determination of strontium-90 in deer bones by liquid scintillation spectrometry after separation on Sr-specific ion exchange columns*. Journal of Environmental Radioactivity, 2006. **87**: p. 315-324.

215. Eliane S. C. Temba, A.S.R.J., Raquel M. Mingote, Roberto P. G. Monteiro, *Determination of 90Sr in low-level radioactive wastes using extraction chromatography and LSC* 2009 International Nuclear Atlantic Conference - INAC 2009, 2009.

216. Eliane S. C. Temba, Â.M.A., Aluísio S. Reis Júnior, Roberto P. G. Monteiro, *Determination of 90Sr in food using extraction chromatography and LSC.* 2013 International Nuclear Atlantic Conference - INAC 2013, 2013.

217. Eva Kabai, B.S., Isabell Mehlsam, Angela Poppitz-Spuhler, *Combined method for the fast determination of pure beta emitting radioisotopes in food samples.* J Radioanal Nucl Chem, 2017: p. 1401-1408.

218. Nicolas Guerin, R.R., Ray Rao, Sheila Kramer-Tremblay, Xiongxin Dai, *An improved method for the rapid determination of 90Sr in cow's milk.* Journal of Environmental Radioactivity, 2017(175-176): p. 115-119.

219. J.N. Sharma, P.N.K., P.S. Dhami, Poonam Jagasia, V. Tessy, C.P. Kaushik, *Separation of strontium-90 from a highly saline high level liquid waste solution using 4,4'(5')-[di-tert-butyldicyclohexano]-18-crown-6+isodecyl alcohol/n-dodecane solvent.* Separation and Purification Technology, 2019(229): p. 1-6.

220. Jelley, J.V., *Cerenkov radiation and its applications.* British Journal of Applied Physics, 1955. **6**(7): p. 227-232.

221. Jelley, J.V., *Cerenkov radiation and its applications*. 1958: Pergamon Press.

222. Ross, H.H., *Measurement of beta-emitting nuclides using Cerenkov radiation.* Analytical Chemistry, 1969. **41**(10): p. 1260-1265.

223. Ross, H.H., *Theory and application of Cerenkov counting*, in *Liquid Scintillation*, A.A. Noujaim, C. Ediss, and L.I. Weibe, Editors. 1976, Academic Press. p. 79-91.

224. L'Annunziata, M.F., *Chapter 16 - Cherenkov Radiation*, in *Radioactivity (Second Edition)*, M.F. L'Annunziata, Editor. 2016, Elsevier: Boston. p. 547-581.

225. Wypych, G., *Production methods, properties, and main applications*, in *Handbook of Solvents (Third Edition)*, G. Wypych, Editor. 2019, ChemTec Publishing. p. 79-132.

226. Kessler, M.J., *Liquid Scintillation Analysis*. 2015: PerkinElmer.

227. Prasannakumar, S., S. Krishnaveni, and T.K. Umesh, *Determination of rest mass energy of the electron by a Compton scattering experiment.* European Journal of Physics, 2011. **33**(1): p. 65-72.

228. Kulcsár, F., D. Teherani, and H. Altmann, *Study of the spectrum of cherenkov light.* Journal of radioanalytical chemistry, 1982. **68**(1): p. 161-168.

229. Claus, R., et al., *A waveshifter light collector for a water Cherenkov detector.* Nuclear Instruments and Methods in Physics Research Section A: Accelerators, Spectrometers, Detectors and Associated Equipment, 1987. **261**(3): p. 540-542.

230. Walter, K., N. Trautmann, and G. Herrmann, *Simultaneous Determination of Strontium-90 and Strontium-89 by Cerenkov-Radiation and Liquid-Scintillation Counting: a Re-Evaluation for Low-Level Counting.* 1993. **62**(4): p. 207.

231. Chang, T.-M., et al., *Rapid and accurate determination of 89/90Sr in radioactive samples by Cerenkov counting.* Journal of Radioanalytical and Nuclear Chemistry, 1996. **204**(2): p. 339-347.

232. Todorović, N., et al., *90Sr determination in water samples using Čerenkov radiation*. Journal of Environmental Radioactivity, 2017. **169-170**: p. 197-202.

233. Günther, K., S. Lange, and M. Veit, *A rapid method for determining 89Sr and 90Sr by Cerenkov counting*. Applied Radiation and Isotopes, 2009. **67**(5): p. 781-785.

234. Grau Carles, A. and A. Grau Malonda, *Radionuclide standardization by Cherenkov counting*. Applied Radiation and Isotopes, 1995. **46**(8): p. 799-803.

235. Bunnenberg, C., K. Kraul, and W. Kühn, *Analysis of beta-nuclides by Cherenkov-spectrometry*. Nuclear Instruments and Methods in Physics Research Section A: Accelerators, Spectrometers, Detectors and Associated Equipment, 1987. **255**(1): p. 346-350.

236. Stamoulis, K.C., et al., *Rapid screening of 90Sr activity in water and milk samples using Cherenkov radiation*. Journal of Environmental Radioactivity, 2007. **93**(3): p. 144-156.

237. L'Annunziata, M.F. and C.J. Passo, *Cherenkov counting of yttrium-90 in the dry state; correlations with phosphorus-32 Cherenkov counting data*. Applied Radiation and Isotopes, 2002. **56**(6): p. 907-916.

238. L'Annunziata, M.F., *Chapter 18 - Radionuclide Decay, Radioactivity Units, and Radionuclide Mass*, in *Radioactivity (Second Edition)*, M.F. L'Annunziata, Editor. 2016, Elsevier: Boston. p. 621-638.

239. L'Annunziata, M.F., *Birth of a unique parent-daughter relation. Secular equilibrium. An experiment in radioisotope techniques*. Journal of Chemical Education, 1971. **48**(10): p. 700.

240. Steinhauser, G. and K. Buchtela, *Chapter 3 - Gas Ionization Detectors*, in *Handbook of Radioactivity Analysis (Third Edition)*, M.F. L'Annunziata, Editor. 2012, Academic Press: Amsterdam. p. 191-231.

241. Habibi, A., et al., *A rapid sequential separation of actinides and radiostrontium coupled to ICP-MS and gas proportional counting*. Journal of Radioanalytical and Nuclear Chemistry, 2016. **310**(1): p. 217-227.

242. Maxwell, S., B. Culligan, and G. Noyes, *Rapid separation of actinides and radiostrontium in vegetation samples*. Journal of radioanalytical and nuclear chemistry, 2010. **286**(1): p. 273-282.

243. Maxwell, S.L., Culligan, B.K., Shaw, P.J., , *Rapid determination of radiostrontium in large soil samples*. J. Radioanal. Nucl. Chem. , 2013. **295**: p. 965-971.

244. L'Annunziata, M.F. and M.J. Kessler, *Chapter 7 - Liquid Scintillation Analysis: Principles and Practice*, in *Handbook of Radioactivity Analysis (Third Edition)*, M.F. L'Annunziata, Editor. 2012, Academic Press: Amsterdam. p. 423-573.

245. Wang, J.-J., *A quick liquid scintillation counting technique for analysis of 90Sr in environmental samples*. Applied Radiation and Isotopes, 2013. **81**: p. 169-174.

246. Uesugi, M., et al., *Rapid method for determination of 90Sr in seawater by liquid scintillation counting with an extractive scintillator*. Talanta, 2018. **178**: p. 339-347.

247. Choonshik Shin, H.C., Hye-Min Kwon, Hye-Jin Jo, Hye-Jeong Kim, Hae-Jung Yoon,Dong-Sul Kim, Gil-Jin Kang, *Determination of plutonium isotopes (238,239,240Pu) and strontium (90Sr) in seafood using alpha spectrometry and liquid scintillation spectrometry*. Journal of Environmental Radioactivity, 2017(177): p. 151-157.

248. Xiaolin Hou, P.R., *Critical comparison of radiometric and mass spectrometric methods for the determination of radionuclides in environmental, biological and nuclear waste samples*. Analytica Chimica Acta, 2008. **608**: p. 105-139.

249. Taylor, V.F., Evans,R.D.,Cornett,R.J.,, *Determination of 90Sr in contaminated samples by tuneable band pass dynamic reaction cell ICP-MS*. Anal.Bioanal. Chem. , 2007. **387**: p. 343–350.

250. Feuerstein, J., *Determination of 90Sr in soil samples using inductively coupled plasma mass spectrometry equipped with dynamic reaction cell ICP-DRC-MS*, in *Department of Chemistry*. 2007, University of Natural Resources and Applied Life Sciences, Vienna. p. 109.

251. Amr, M.A., et al., *Ultra-trace determination of 90Sr, 137Cs, 238Pu, 239Pu, and 240Pu by triple quadruple collision/reaction cell-ICP-MS/MS: Establishing a baseline for global fallout in Qatar soil and sediments*. Journal of Environmental Radioactivity, 2016. **153**: p. 73-87.

252. Tomita, J. and E. Takeuchi, *Rapid analytical method of 90Sr in urine sample: Rapid separation of Sr by phosphate co-precipitation and extraction chromatography, followed by determination by triple quadrupole inductively coupled plasma mass spectrometry (ICP-MS/MS)*. Applied Radiation and Isotopes, 2019. **150**: p. 103-109.

253. Fujiwara, K., K. Yanagisawa, and K. Iijima, *Rapid Determination of Sr-90 in Environmental Matrices by SPE-ICP-MS for Emergency Monitoring*, in *Environmental Radiochemical Analysis VI*. 2020, The Royal Society of Chemistry. p. 89-96.

254. Zhou, Z., et al., *Recent Development on Determination of Low-Level 90Sr in Environmental and Biological Samples: A Review*. Molecules, 2023. **28**(1): p. 90.

255. Russell, B., M. García-Miranda, and P. Ivanov, *Development of an optimised method for analysis of 90Sr in decommissioning wastes by triple quadrupole inductively coupled plasma mass spectrometry*. Applied Radiation and Isotopes, 2017. **126**: p. 35-39.

256. Feuerstein, J., et al., *Determination of 90Sr in soil samples using inductively coupled plasma mass spectrometry equipped with dynamic reaction cell (ICP-DRC-MS)*. Journal of environmental radioactivity, 2008. **99**(11): p. 1764-1769.

257. Takagai, Y., et al., *Sequential inductively coupled plasma quadrupole mass-spectrometric quantification of radioactive strontium-90 incorporating cascade separation steps for radioactive contamination rapid survey*. Analytical Methods, 2014. **6**(2): p. 355-362.

258. Taylor, V.F., R.D. Evans, and R.J. Cornett, *Determination of 90Sr in contaminated environmental samples by tuneable bandpass dynamic reaction cell ICP–MS*. Analytical and Bioanalytical Chemistry, 2007. **387**(1): p. 343-350.

259. G.C. Eiden, J.B., D.W.Koppenaal, *Beneficial Ion/Molecule Reactions in Elemental Mass Spectrometry*. Rapid communications in mass spectrometry, 1997. **11**: p. 34-42.

260. H. Isnard, M.A., P. Blanchet, R. Brennetot, F. Chartier, V. Geertsen, F. Manuguerra, *Determination of 90Sr / 238U ratio by double isotope dilution inductively coupled plasma mass spectrometer with multiple collection in spent nuclear fuel samples with in situ 90Sr / 90Zr separation in a collision-reaction cell*. Spectrochimica Acta Part B, 2006. **61**: p. 150-156.

261. Gregory K. Koyanagi, D.C., Voislav Blagojevic, and Diethard K. Bohme, *Gas-Phase Reactions of Transition-Metal Ions with Molecular Oxygen: Room-Temperature Kinetics and Periodicities in Reactivity*. J. Phys. Chem. A, 2002. **106**: p. 4581-4590.

262. Scott D. Tanner, V.I.B., Dmitry R. Bandura, *Reaction cells and collision cells for ICP-MS: a tutorial review*. Spectrochimica Acta Part B, 2002. **57**: p. 1361–1452.

263. Georges Favre, R.B., Frederic Chartier, Pierre Vitorge, *Understanding reactions with O2 for 90Sr measurements by ICP-MS with collision-reaction cell*. International Journal of Mass Spectrometry, 2007. **265**: p. 15-22.

264. Narukawa, T. and K. Chiba, *Oxygenation Mechanism of Ions in Dynamic Reaction Cell ICP-MS*. Analytical Sciences, 2013. **29**(7): p. 747-752.

265. Mayes, R.W., *The quantification of dietary intake, digestion and metabolism in farm livestock and its relevance to the study of radionuclide uptake*. Science of The Total Environment, 1989. **85**: p. 29-51.

266. Howard, B.J., et al., *A review of current knowledge of the transfer of radiostrontium to milk and possible countermeasures. Final report*. 1995, NERC/Institute of Terrestrial Ecology. p. 65.

267. Howard, B.J., et al., *The use of dietary calcium intake of dairy ruminants to predict the transfer coefficient of radiostrontium to milk*. Radiation and Environmental Biophysics, 1997. **36**(1): p. 39-43.

268. Anderson, R.R., *Comparison of Trace Elements In Milk of Four Species*. Journal of Dairy Science, 1992. **75**(11): p. 3050-3055.

269. N. Herwig, K.S., U. Panne, W. Pritzkow, J. Vogl, *Multi-element screening in milk and feed by SF-ICP-MS*. Food Chemistry, 2011. **124**: p. 1223–1230.

270. Bowen, H.J.M., *Strontium and barium in sea water and marine organisms*. Journal of the Marine Biological Association of the United Kingdom, 1956. **35**(3): p. 451-460.

271. Hummel, R.W. and A.A. Smales, *Determination of strontium in sea water by using both radioactive and stable isotopes*. Analyst, 1956. **81**(959): p. 110-113.

272. Qi, Y., et al., *Iodine cycling in the subarctic Pacific Ocean: Insights from 129I*. Geochimica et Cosmochimica Acta, 2023. **344**: p. 12-23.

273. Köhrle, J., *Selenium, Iodine and Iron-Essential Trace Elements for Thyroid Hormone Synthesis and Metabolism*. Int J Mol Sci, 2023. **24**(4).

274. de Benoist, B., E. McLean, and M. Andersson, *Chapter 48 - Iodine Deficiency: The Extent of the Problem*, in *Comprehensive Handbook of Iodine*, V.R. Preedy, G.N. Burrow, and R. Watson, Editors. 2009, Academic Press: San Diego. p. 459-467.

275. Tran, H.A., *Chapter 72 - Iodine, Thyroid Diseases and Neuromuscular Dysfunction*, in *Comprehensive Handbook of Iodine*, V.R. Preedy, G.N. Burrow, and R. Watson, Editors. 2009, Academic Press: San Diego. p. 701-711.

276. Lin, C.C. and J.H. Chao, *Chapter 17 - Radiochemistry of Iodine: Relevance to Health and Disease*, in *Comprehensive Handbook of Iodine*, V.R. Preedy, G.N. Burrow, and R. Watson, Editors. 2009, Academic Press: San Diego. p. 171-182.

277. Osterc, A., V. Stibilj, and P. Raspor, *Iodine in the Environment*, in *Encyclopedia of Environmental Health (Second Edition)*, J. Nriagu, Editor. 2011, Elsevier: Oxford. p. 701-707.

278. Raisbeck, G.M. and F. Yiou, *129I in the oceans: origins and applications*. Science of The Total Environment, 1999. **237-238**: p. 31-41.

279. Muramatsu, Y., et al., *Studies with natural and anthropogenic iodine isotopes: iodine distribution and cycling in the global environment*. Journal of Environmental Radioactivity, 2004. **74**(1): p. 221-232.

280. He, P., et al., *Iodine isotopes species fingerprinting environmental conditions in surface water along the northeastern Atlantic Ocean*. Scientific Reports, 2013. **3**(1): p. 2685.

281. He, P., et al., *A summary of global 129I in marine waters*. Nuclear Instruments and Methods in Physics Research Section B: Beam Interactions with Materials and Atoms, 2013. **294**: p. 537-541.

282. López-Gutiérrez, J.M., et al., *Relative influence of 129I sources in a sediment core from the Kattegat area*. Science of The Total Environment, 2004. **323**(1): p. 195-210.

283. Database, E.C.R.D. *RADD*. 2023.

284. Raisbeck, G.M., et al., *129I from nuclear fuel reprocessing facilities at Sellafield (U.K.) and La Hague (France); potential as an oceanographie tracer*. Journal of Marine Systems, 1995. **6**(5): p. 561-570.

285. Fréchou, C. and D. Calmet, *129I in the environment of the La Hague nuclear fuel reprocessing plant—from sea to land*. Journal of Environmental Radioactivity, 2003. **70**(1): p. 43-59.

286. Xiaolin Hou, V.H., Ala Aldahan, Göran Possnert, Ole Christian Lind, Galina Lujaniene, *A review on speciation of iodine-129 in the environmental and biological samples*. Analytica Chimica Acta, 2009. **632**: p. 181-196.

287. Handl, J. and A. Pfau, *Long-term transfer of I-129 into the food chain*. Science of The Total Environment, 1989. **85**: p. 245-252.

288. Muramatsu, Y. and S. Yoshida, *Determination of129I and127I in environmental samples by neutron activation analysis (NAA) and inductively coupled plasma mass spectrometry (ICP-MS)*. Journal of Radioanalytical and Nuclear Chemistry, 1995. **197**(1): p. 149-159.

289. Handl, J., A. Pfau, and F.W. Huth, *Measurements of 129I in human and bovine thyroids in Europe--transfer of 129I into the food chain*. Health Phys, 1990. **58**(5): p. 609-18.

290. Seki, R., et al., *Distribution and behavior of long-lived radioiodine in soil*. Journal of Radioanalytical and Nuclear Chemistry, 1990. **138**(1): p. 17-31.

291. Doshi, G.R., S.N. Joshi, and K.C. Pillai, *129I in soil and grass samples around a nuclear reprocessing plant*. Journal of Radioanalytical and Nuclear Chemistry, 1991. **155**(2): p. 115-127.

292. Schmitz, K. and D.C. Aumann, *A study on the association of two iodine isotopes, of natural127I and of the fission product129I, with soil components using a sequential extraction procedure*. Journal of Radioanalytical and Nuclear Chemistry, 1995. **198**(1): p. 229-236.

293. Environment Agency, F.S.A., Food Standards Scotland, Natural Resources Wales, Northern Ireland Environment Agency, Scottish Environment Protection Agency. *RIFE 28 Summary, Radioactivity in food and the environment, 2022*. 2023.

294. Frechou, C. and D. Calmet, *Variations of iodine-129 activities in various seaweed collected on the French channel coast.* Czechoslovak Journal of Physics, 2003. **53**(1): p. A83-A90.

295. Lefèvre, O., et al., *Self-absorption correction factor applied to 129I measurement by direct gamma–X spectrometry for Fucus serratus samples.* Nuclear Instruments and Methods in Physics Research Section A: Accelerators, Spectrometers, Detectors and Associated Equipment, 2003. **506**(1): p. 173-185.

296. Cutshall, N.H., I.L. Larsen, and C.R. Olsen, *Direct analysis of 210Pb in sediment samples: Self-absorption corrections.* Nuclear Instruments and Methods in Physics Research, 1983. **206**(1): p. 309-312.

297. Galloway, R.B., *Correction for sample self-absorption in activity determination by gamma spectrometry.* Nuclear Instruments and Methods in Physics Research Section A: Accelerators, Spectrometers, Detectors and Associated Equipment, 1991. **300**(2): p. 367-373.

298. Hou, X., et al., *A review on speciation of iodine-129 in the environmental and biological samples.* Analytica Chimica Acta, 2009. **632**(2): p. 181-196.

299. Hou, X., et al., *Determination of Chemical Species of Iodine in Seawater by Radiochemical Neutron Activation Analysis Combined with Ion-Exchange Preseparation.* Analytical Chemistry, 1999. **71**(14): p. 2745-2750.

300. Hou, X., et al., *Determination of 129I in seawater and some environmental materials by neutron activation analysis.* Analyst, 1999. **124**(7): p. 1109-1114.

301. Frechou, C., et al., *129 I and 129 I/ 127 I ratio measurements in environmental samples by RNAA, AMS and direct γ -X spectrometry. Intercomparison exercises.* Radioprotection, 2002. **37**.

302. Takashi Suzuki, S.B., Toshikatsu Kitamura, Shoji Kabuto, Keisuke Isogai, Hikaru Amano, *Determination of 129I in environmental samples by AMS and NAA using an anion exchange resin disk.* Nuclear Instruments and Methods in Physics Research B, 2007. **259**: p. 370-373.

303. J.M. Gómez-Guzmán, S.M.E.-B., A.R. Pinto-Gómez, J.M. Abril-Hernández, *Microwave-based digestion method for extraction of 127I and 129I from solid material for measurements by AMS and ICP-MS.* International Journal of Mass Spectrometry, 2011. **303**: p. 103-108.

304. Rugel, G., et al., *The first four years of the AMS-facility DREAMS: Status and developments for more accurate radionuclide data.* Nuclear Instruments and Methods in Physics Research Section B: Beam Interactions with Materials and Atoms, 2016. **370**: p. 94-100.

305. Victoria, L.-T., et al., *129I in sediment cores from the Celtic Sea by AMS through a microwave digestion process.* Nuclear Instruments and Methods in Physics Research Section B: Beam Interactions with Materials and Atoms, 2022. **529**: p. 61-67.

306. Jacobsen, G.E., et al., *AMS measurement of 129I, 36Cl and 14C in underground waters from Mururoa and Fangataufa atolls.* Nuclear Instruments and Methods in Physics Research Section B: Beam Interactions with Materials and Atoms, 2000. **172**(1): p. 666-671.

307. Kutschera, W., et al., *Atom counting with accelerator mass spectrometry.* Reviews of Modern Physics, 2023. **95**(3): p. 035006.

308. Suárez, J.A., A.G. Espartero, and M. Rodríguez, *Radiochemical analysis of 129I in radioactive waste streams*. Nuclear Instruments and Methods in Physics Research Section A: Accelerators, Spectrometers, Detectors and Associated Equipment, 1996. **369**(2): p. 407-410.

309. Izmer, A.V., S.F. Boulyga, and J.S. Becker, *Determination of 129I/127I isotope ratios in liquid solutions and environmental soil samples by ICP-MS with hexapole collision cell*. Journal of Analytical Atomic Spectrometry, 2003. **18**(11): p. 1339-1345.

310. Izmer, A.V., et al., *Improvement of the detection limit for determination of 129I in sediments by quadrupole inductively coupled plasma mass spectrometer with collision cell*. Journal of Analytical Atomic Spectrometry, 2004. **19**(9): p. 1278-1280.

311. Yang, G., H. Tazoe, and M. Yamada, *Improved approach for routine monitoring of 129I activity and 129I/127I atom ratio in environmental samples using TMAH extraction and ICP-MS/MS*. Analytica Chimica Acta, 2018. **1008**: p. 66-73.

312. Kim, J., et al., *Review of the development in determination of 129I amount and the isotope ratio of 129I/127I using mass spectrometric measurements*. Microchemical Journal, 2021. **169**: p. 106476.

313. Coralie, C., et al., *Mass-shift mode to quantify low level 129I in environmental samples by ICP-MS/MS*. Journal of Analytical Atomic Spectrometry, 2022. **37**(6): p. 1309-1317.

314. Carrier, C., et al., *Determination of environmental gaseous 129I trapped in charcoal cartridges by ICP-MS/MS*. Journal of Radioanalytical and Nuclear Chemistry, 2023. **332**(6): p. 2003-2015.

315. Williams, R., et al., *Iodine-129 Analysis of NTS Near-Field Groundwater Samples on the Multi-Collector ICP-MS*. 2005, Lawrence Livermore National Lab., Livermore, CA (US): United States.

316. Gómez-Guzmán, J.M., et al., *Pre- and post-Chernobyl accident levels of 129I and 137Cs in the Southern Baltic Sea by brown seaweed Fucus vesiculosus*. Journal of Environmental Radioactivity, 2013. **115**: p. 134-142.

317. Hou, X. and X. Yan, *Study on the concentration and seasonal variation of inorganic elements in 35 species of marine algae*. Science of The Total Environment, 1998. **222**(3): p. 141-156.

318. Brown, C.F., K.N. Geiszler, and T.S. Vickerman, *Extraction and Quantitative Analysis of Iodine in Solid and Solution Matrixes*. Analytical Chemistry, 2005. **77**(21): p. 7062-7066.

319. Hou, X. and Y. Wang, *Determination of ultra-low level 129I in vegetation using pyrolysis for iodine separation and accelerator mass spectrometry measurements*. Journal of Analytical Atomic Spectrometry, 2016. **31**(6): p. 1298-1310.

320. A. Schmidt, C.S., J. Handl, D. Jakob, R. Michela, H.-A. Synal, J.M. Lopez, M. Suter, *On the analysis of iodine-129 and iodine-127 in environmental materials by accelerator mass spectrometry and ion chromatography*. The Science of the Total Environment, 1998. **223**: p. 131-156.

321. Hou, X., et al., *Determination of Ultralow Level 129I/127I in Natural Samples by Separation of Microgram Carrier Free Iodine and Accelerator Mass Spectrometry Detection*. Analytical Chemistry, 2010. **82**(18): p. 7713-7721.

322. Tanner, S.D., *Space charge in ICP-MS: calculation and implications*. Spectrochimica Acta Part B: Atomic Spectroscopy, 1992. **47**(6): p. 809-823.

323. Lehn, S.A., et al., *Effect of sample matrix on the fundamental properties of the inductively coupled plasma*. Spectrochimica Acta Part B: Atomic Spectroscopy, 2003. **58**(10): p. 1785-1806.

324. Zhang, M., et al., *Rapid analysis of129I in natural water samples using accelerator mass spectrometry*. Atomic Spectroscopy, 2021. **42**(4): p. 190-196.

325. Fujiwara, H., et al., *Determination of 129I in soil samples by DRC-ICP-MS*. Journal of Analytical Atomic Spectrometry, 2011. **26**(12): p. 2528-2533.

326. Hou, X., *Liquid scintillation counting for determination of radionuclides in environmental and nuclear application*. Journal of Radioanalytical and Nuclear Chemistry, 2018.

327. Mazeron, J.-J. and A. Gerbaulet, *The centenary of discovery of radium*. Radiotherapy and Oncology, 1998. **49**(3): p. 205-216.

328. IAEA, *The Environmental Behaviour of Radium: Revised Edition*. 2014, Vienna: INTERNATIONAL ATOMIC ENERGY AGENCY.

329. Fry, C. and M. Thoennessen, *Discovery of actinium, thorium, protactinium, and uranium isotopes*. Atomic Data and Nuclear Data Tables, 2013. **99**(3): p. 345-364.

330. Kónya, J. and N.M. Nagy, *Chapter 4 - Radioactive Decay*, in *Nuclear and Radiochemistry (Second Edition)*, J. Kónya and N.M. Nagy, Editors. 2018, Elsevier. p. 49-84.

331. Roberts, W.C., *Facts and ideas from anywhere*. Proc (Bayl Univ Med Cent), 2017. **30**(4): p. 481-490.

332. Ropp, R.C., *Chapter 1 - The Alkaline Earths as Metals*, in *Encyclopedia of the Alkaline Earth Compounds*, R.C. Ropp, Editor. 2013, Elsevier: Amsterdam. p. 1-23.

333. Silva, C.M., et al., *226Ra in milk of the dairy cattle from the rural region of Pernambuco, Brazil*. Journal of Radioanalytical and Nuclear Chemistry, 2006. **270**(1): p. 237-241.

334. Szerbin, P. and D.K. Popov, *Transfer of radium-228, thorium-228 and radium-226 from forage to cattle and reindeer*. Journal of Environmental Radioactivity, 1988. **8**(2): p. 129-141.

335. Simon, S.L. and S.A. Ibrahim, *Biological uptake of radium by terrestrial plants*. 1990, International Atomic Energy Agency (IAEA): IAEA.

336. Khalid AL Nabhani, F.K., Ming Yang, *Technologically Enhanced Naturally Occurring Radioactive Materials in oil and gas production: A silent killer*. Process Safety and Environmental Protection, 2016. **99**: p. 237-247.

337. Ahmad, F., et al., *Fate of radium on the discharge of oil and gas produced water to the marine environment*. Chemosphere, 2021. **273**: p. 129550.

338. IAEA, *Radiation Protection and Management of NORM Residues in the Phosphate Industry*. 2013, Vienna: International Atomic Energy Agency.

339. Ali, M.M.M., et al., *Concentrations of TENORMs in the petroleum industry and their environmental and health effects*. RSC Advances, 2019. **9**(67): p. 39201-39229.

340. Al Nabhani, K., F. Khan, and M. Yang, *Technologically Enhanced Naturally Occurring Radioactive Materials in oil and gas production: A silent killer*. Process Safety and Environmental Protection, 2016. **99**: p. 237-247.

341. Al Nabhani, K. and F. Khan, *Chapter Two - Fundamentals of technologically enhanced naturally occurring nuclear radioactive materials in the oil and gas industry*, in *Nuclear Radioactive Materials in the Oil and Gas Industry*, K. Al Nabhani and F. Khan, Editors. 2020, Elsevier. p. 51-90.

342. Al Nabhani, K. and F. Khan, *Chapter Three - Risk assessment and management of TENORM waste disposal options in the oil and gas industry*, in *Nuclear Radioactive Materials in the Oil and Gas Industry*, K. Al Nabhani and F. Khan, Editors. 2020, Elsevier. p. 91-123.

343. E. Fonollosa, A.N., A. Penalver, C. Aguilar, F. Borrull, *Presence of radionuclides in sludge from conventional drinking water treatment plants. A review.* Journal of Environmental Radioactivity, 2015. **141**: p. 24-31.

344. IAEA, *Analytical Methodology for the Determination of Radium Isotopes in Environmental Samples*. 2011, Vienna: INTERNATIONAL ATOMIC ENERGY AGENCY.

345. Panahifar, A., et al., *Biodistribution of strontium and barium in the developing and mature skeleton of rats.* Journal of Bone and Mineral Metabolism, 2019. **37**(3): p. 385-398.

346. Franchi, S., et al., *The Curies' element: state of the art and perspectives on the use of radium in nuclear medicine.* EJNMMI Radiopharmacy and Chemistry, 2023. **8**(1): p. 38.

347. Jia, G. and G. Torri, *Estimation of radiation doses to members of the public in Italy from intakes of some important naturally occurring radionuclides (238U, 234U, 235U, 226Ra, 228Ra, 224Ra and 210Po) in drinking water.* Applied Radiation and Isotopes, 2007. **65**(7): p. 849-857.

348. Mears, C., et al., *Using 226Ra and 228Ra isotopes to distinguish water mass distribution in the Canadian Arctic Archipelago.* Biogeosciences, 2020. **17**(20): p. 4937-4959.

349. Paradis, S., et al., *Organic matter contents and degradation in a highly trawled area during fresh particle inputs (Gulf of Castellammare, southwestern Mediterranean).* Biogeosciences, 2019. **16**(21): p. 4307-4320.

350. Jia, G., et al., *Determination of radium isotopes in mineral water samples by α-spectrometry.* International Congress Series, 2005. **1276**: p. 412-414.

351. Jia, G., et al., *Determination of radium isotopes in mineral and environmental water samples by alpha-spectrometry.* Journal of Radioanalytical and Nuclear Chemistry, 2006. **267**(3): p. 505-514.

352. Waska, H., et al., *An efficient and simple method for measuring 226Ra using the scintillation cell in a delayed coincidence counting system (RaDeCC).* Journal of Environmental Radioactivity, 2008. **99**(12): p. 1859-1862.

353. Sethy, N.K., et al., *A simple method for calibration of Lucas scintillation cell counting system for measurement of 226Ra and 222Rn.* Journal of Radiation Research and Applied Sciences, 2014. **7**(4): p. 472-477.

354. Liu, M., H.W. Lee, and A.B. McDonald, *222Rn emanation into vacuum.* Nuclear Instruments and Methods in Physics Research Section A: Accelerators, Spectrometers, Detectors and Associated Equipment, 1993. **329**(1): p. 291-298.

355. Dowdall, M. and A. Lepland, *Elevated levels of radium-226 and radium-228 in marine sediments of the Norwegian Trench ("Norskrenna") and Skagerrak.* Marine Pollution Bulletin, 2012. **64**(10): p. 2069-2076.

356. Cooper, E.L., R.M. Brown, and G.M. Milton, *Determination of 222Rn and 226Ra in environmental waters by liquid scintillation counting.* Environment International, 1988. **14**(4): p. 335-340.

357. Lagacé, F., et al., *Quantification of 226Ra at environmental relevant levels in natural waters by ICP-MS: Optimization, validation and limitations of an extraction and preconcentration approach.* Talanta, 2017. **167**: p. 658-665.

358. Dever, L. and C. Hillaire-Marcel. *226Ra measurement by thermal ionisation mass spectrometry: Use of 226Ra and 14C for groundwater dating*. in *Second international conference on isotopes Conference proceedings*. 1997. Australia.

359. Andrews, A., et al., *Application of an ion-exchange separation technique and thermal ionization mass spectrometry to 226Ra for radiometric age determination of long-lived fishes.* Canadian Journal of Fisheries and Aquatic Sciences, 1999. **56**: p. 1329-1338.

360. Zhou, Z., X. Zhao, and R.J. Cornett, *An AMS method for measurement of Radium-226 in drinking water.* Nuclear Instruments and Methods in Physics Research Section B: Beam Interactions with Materials and Atoms, 2019. **455**: p. 271-275.

361. Jia, G. and J. Jia, *Determination of radium isotopes in environmental samples by gamma spectrometry, liquid scintillation counting and alpha spectrometry: a review of analytical methodology.* Journal of Environmental Radioactivity, 2012. **106**: p. 98-119.

362. Abbasi, A., *A review of the analytical methodology to determine Radium-226 and Radium-228 in drinking waters.* Radiochimica Acta, 2018. **106**(10): p. 819-829.

363. Thakur, P., A.L. Ward, and A.M. González-Delgado, *Optimal methods for preparation, separation, and determination of radium isotopes in environmental and biological samples.* Journal of Environmental Radioactivity, 2021. **228**: p. 106522.

364. Al-Hamarneh, I.F. and F.I. Almasoud, *A comparative study of different radiometric methodologies for the determination of 226Ra in water.* Nuclear Engineering and Technology, 2018. **50**(1): p. 159-164.

365. Köhler, M., et al., *Comparison of methods for the analysis of 226Ra in water samples.* Applied Radiation and Isotopes, 2002. **56**(1): p. 387-392.

366. Epov, V.N., et al., *Direct determination of 226Ra in environmental matrices using collision cell inductively coupled plasma mass-spectrometry.* Journal of Radioanalytical and Nuclear Chemistry, 2003. **256**(1): p. 53-60.

367. Varga, Z., *Ultratrace-level radium-226 determination in seawater samples by isotope dilution inductively coupled plasma mass spectrometry.* Analytical and Bioanalytical Chemistry, 2008. **390**(2): p. 511-519.

368. Bourquin, M., et al., *Determination of 226Ra concentrations in seawater and suspended particles (NW Pacific) using MC-ICP-MS.* Marine Chemistry, 2011. **126**(1): p. 132-138.

369. Tolmachev, S., K. Tagami, and S. Uchida. *Determination of 226Ra in surface waters using high-resoultion inductively coupled plasma mass spectrometry after selective extraction*. in *Proceedings of the 2nd International Conference on Radioactivity in the Environment, 592–596,(Nice, France, 2–6 October 2005)*. 2005.

370. Copia, L., et al., *Low-level 226Ra determination in groundwater by SF-ICP-MS: optimization of separation and pre-concentration methods.* Journal of Analytical Science and Technology, 2015. **6**(1): p. 22.

371. Joannon, S. and C. Pin, *Ultra-trace determination of 226Ra in thermal waters by high sensitivity quadrupole ICP-mass spectrometry following selective extraction and concentration using radium-specific membrane disks*. Journal of Analytical Atomic Spectrometry, 2001. **16**(1): p. 32-36.

372. Larivière, D., et al., *Determination of 226Ra in sediments by ICP-MS: A comparative study of three sample preparation approaches*. Journal of Radioanalytical and Nuclear Chemistry, 2007. **273**(2): p. 337-344.

373. Yang, G., et al., *Simple and sensitive determination of radium-226 in river water by single column-chromatographic separation coupled to SF-ICP-MS analysis in medium resolution mode*. Journal of Environmental Radioactivity, 2020. **220-221**: p. 106305.

374. Dalencourt, C., et al., *Rapid, versatile and sensitive method for the quantification of radium in environmental samples through cationic extraction and inductively coupled plasma mass spectrometry*. Journal of Analytical Atomic Spectrometry, 2018. **33**(6): p. 1031-1040.

375. van Es, E.M., et al., *Development of a method for rapid analysis of Ra-226 in groundwater and discharge water samples by ICP-QQQ-MS*. Applied Radiation and Isotopes, 2017. **126**: p. 31-34.

376. Vesterbacka, P., et al., *Activity concentrations of 226Ra and 228Ra in drilled well water in Finland*. Radiat Prot Dosimetry, 2006. **121**(4): p. 406-12.

377. Lauria, D.C. and J.M. Godoy, *Abnormal high natural radium concentration in surface waters*. Journal of Environmental Radioactivity, 2002. **61**(2): p. 159-168.

378. Cozzella, M.L., A. Leila, and R.S. Hernandez, *Determination of 226Ra in urine samples by Q-ICP-MS: A method for routine analyses*. Radiation Measurements, 2011. **46**(1): p. 109-111.

379. Shivakumara, B.C., et al., *Studies on 226Ra and 222Rn concentration in drinking water of Mandya region, Karnataka State, India*. Journal of Radiation Research and Applied Sciences, 2014. **7**(4): p. 491-498.

380. Hou, X. and P. Povinec, *Chromatographic Separation Methods for Preparation of Iodine-129 and Plutonium Targets in AMS Measurements*. Acto Physica Universitatis Comenianae, 2016. **LIII**: p. 101-109.

381. Zulauf, A., et al., *Characterization of an extraction chromatographic resin for the separation and determination of 36Cl and 129I*. Journal of Radioanalytical and Nuclear Chemistry, 2010. **286**(2): p. 539-546.